Multi-faced study for the development of enhanced transfection systems

Laura Balcells García

UNIVERSITAT RAMON LLULL

DOCTORAL THESIS

Title	Multi-faced study for the development of enhanced transfection systems
Presented by	Laura Balcells Garcia
Centre	IQS School of Engineering
Department	Bioengineering
Directed by	Dr. Anna Cascante Cirera Dr. Salvador Borrós Gómez

A la meva família

“What you learn from a life in science is the vastness of our ignorance”

David Eagleman

Acknowledgments

En primer lloc vull agrair als meus directors de tesi, el Dr. Salvador Borrós i la Dra. Anna Cascante, la confiança dipositada en mi i l'oportunitat que m'han donat de realitzar aquesta tesi doctoral. Moltes gràcies Salvador per haver-me permès viure aquests anys a GEMAT, on he estat molt feliç. Gràcies per obrir-me la porta i haver-me tingut sempre en tan bona consideració. Per mi ha estat un aprenentatge continu treballar amb tu, tant en el vessant professional com en el personal i un orgull formar part d'aquest gran grup. Admiro el teu optimisme, la teva manera de veure oportunitats en tots els problemes i el teu entusiasme per la feina que fas. Gràcies de tot cor, Chicho. També vull agrair molt especialment a la Dra. Anna Cascante tota l'ajuda i recolzament durant aquests anys. Gràcies per tots els consells, per orientar-me al llarg de tota la tesi i per dedicar-te tan a fons a les correccions. He après molt al vostre costat durant aquest temps. Gràcies per haver estat els meus pares científics, formeu un gran tàndem!

I am very grateful to Prof. Kimberly Hamad-Schifferli for welcoming me in her Nanobiointerfaces Lab at UMAss Boston to share and work together in this project. Thanks Kim for your passion for science. It was a pleasure working with you those months and getting to know you. I had a great time at UMASS and learnt so much from you. My acknowledgements also to all the Hamadlings, specially to Dr. Hristov and Alyssa. Thank you guys for making my time in Boston so funny.

I seguint per l'aventura de Boston, vull agrair a tots els que em vau acompanyar durant aquells mesos a l'altra banda de l'Atlàntic: Marta, Elena sou genials, gràcies per totes les estones compartides (inclús les més doloroses..!); Mire, Ferran, Gonzalo, Roger i companyia, moltes gràcies. I molt especialment vull donar les gràcies a dues persones que em van cuidar com una filla adoptiva i amb qui vaig compartir grans estones: Cris i Fer. Sempre us estaré agraïda per tot el que vau fer per mi durant la meva estada a Boston. Cris, va ser una gran sort treballar amb tu durant aquells mesos i compartir tota mena d'aventures. Admiro la Cris responsable, divertida i eco-friendly en què t'has convertit. Quant vaig aprendre amb tu dins i fora el lab..! Gràcies per tot. Fer, ¡qué gran descubrimiento haberte conocido! Viva las IPAs, NEIPAs y el homebrewing. Gracias por tanto. Amb vosaltres vaig guanyar dos grans amics.

Em sento també molt afortunada d'haver fet la tesi a GEMAT. Som més que un grup, som una família a la que ja començo a trobar a faltar abans d'haver marxat. I marxo amb la sensació d'haver viscut una època daurada del grup on el dia a dia al lab i també *firasus*, cases rurals i torretes quedaran per la posteritat. Gràcies a tots els que n'heu format part durant el meu pas, perquè de tots m'emporto grans coses.

Gràcies Núria i Marina pel tracte rebut tots aquests anys; estic segura que el CTPTI està en les millors mans possibles! Gràcies també a tots els "Sagetos" per tot el que hem compartit: Irene, Elena i Miguel Ángel.

Gràcies Dra. Cristina Fornaguera per tota l'ajuda i consells durant tots aquests anys. Ha estat una sort compartir amb tu el temps al laboratori. Amb tu, GEMAT ha guanyat una investigadora incansable i jo he guanyat una gran amiga. Gràcies de tot cor! Gràcies també al Dr. Victor Ramos per tota l'ajuda proporcionada durant els meus inicis a GEMAT. I gràcies al grup del Jerónimo Blanco del CSIC, per la col·laboració en el projecte del que ha derivat la meva tesi, i per haver-me permès conèixer a la Marta Guerra. El món de la investigació necessita més gent com tu! Gràcies per tot! Gràcies Pau Brugada per haver estat "el meu doctorand" quan vaig arribar a GEMAT i per cuidar-me tant. Gràcies Gemma per introduir-me a GEMAT.

Robert, gràcies per portar l'alegria cada dia a GEMAT i contagiar als demés. Per fer-m'ho tan fàcil per integrar-me, per tots els grans moments i per haver-me cuidat i ajudat sempre que ho he necessitat. Un laboratori sense tu és molt més avorrit. Ets un *cabrón* adorable. Joan, gràcies per ser el meu tècnic de Mac personal. Espero que amb mi hagis après a no preguntar "què et passa?" quan vegis a venir un drama. Gràcies per tot! AnnaMas! Peça irreemplaçable de GEMAT. Passaran els anys i els gematos seguiran referint-se a tu. Gràcies per haver estat un exemple a seguir de com treballar i fer funcionar un laboratori. I gràcies també per estar tan tarada i haver estat un dels grans descobriments personals d'aquesta etapa. Periii!! Gràcies per ser tan noble. El món necessita més persones com tu. Gràcies per tot el compartit aquí i a Boston, i sobretot per ser tan i tan bo! Visca Bor!! Recién doctortitooo no hay gracias sin bbq! German, estàs com una cabra, però fas la vida més divertida. Gràcies per totes les estones compartides! Mario gracias por las clases exprés de orgánica y por las microsiestas en bares compartidas. Cris gracias por tu vitalidad y por enseñarme que nos preocupamos por tonterías mientras la vida se nos pasa. Ha sido una suerte coincidir contigo estos años. Y gracias también Manu por ser como eres; has sido un gran descubrimiento! Nunu, gràcies per tots aquests anys. He gaudit moltíssim treballant amb tu al lab, a la saleta, fora d'IQS,... M'enduc grans records i vivències compartides i alguna frase lapidària per la posteritat: "ets un raig de llum". Pooool! Gràcies per tot el que hem compartit. Ha estat un plaer coincidir en aquesta etapa amb tu i compartir aficions esportives, salseos i *afterworks*. I a la Mireia, que és la nòvia del Pol (no he pogut evitar-ho), gràcies per ser la Antonia més gran. M'ho he passat increïblement bé amb tu des del Màster i tant de bo per molts anys més. Sou molt grans. Antoniooo!! Me ha encantado coincidir contigo estos años. Gracias por todas las risas y memes compartidos (no puedo ser más específica). ¡Que sean muchos más! I gràcies també Patri per tots els moments divertits que hem compartit durant aquests anys. Oiane, Anna els mesos al CTPTI han estat breus però intensos, gràcies!; Beba, ha sido un placer coincidir contigo, mucha suerte en el futuro y gracias por estos meses!

Generacions de TFMs n'he conegut unes quantes i vull agrair especialment a l'Anna Lopez i l'Aricookies pel gran any que ens van regalar. I a la nova fornada de PhDs – Glòria, Laura O. i Mònica – dir-vos que estic tranquil·la perquè amb vosaltres el futur de GEMAT està en bones mans. Gràcies per aquest tram final de la meva tesi que hem compartit i molta sort en el futur. Coral, a ti no sé si meterte en Tractivus, en nuevas PhDs o en la categoria "foreign students" (*racihmo*!). Gracias por este tiempo, eres un gran fichaje para GEMAT y estoy muy muy contenta de haberte conocido. I Elena, ara com a Tracti-girl, em vaig alegrar molt quan em van dir que estaries per GEMAT; mantingues a ratlla als Tracti-boys i gràcies per ser com ets. Gràcies també Alejandro, Benjamí, Dulsat, Cate, Sejin, C.Castells, pels moments compartits i el bon tracte rebut. Gràcies també a la Luna i al David, "els meus estudiants", per tota la feina ben feta.

Un agraïment també molt sincer als del lab del costat, els *biochos*. Gràcies pel vostre bon rotllo i per contribuir a que la gent dels dos grups siguem a dia d'avui no només companys sinó amics. Pascu, ets un gran, gràcies per tots els grans moments des del màster fins aquí. Núria, Laia, gràcies per passar de ser les millors auxiliars a les millors veïnes de lab, sou genials. Bernat, Marc, Álvaro i companyia un plaer tenir-vos de veïns i compartir estones dins i fora d'IQS. I gràcies als meus companys de Màster per dos anys meravellosos i amistats que han perdurat.

Victor, quin gran descobriment. Serà que els "bordes" ens hem de donar una oportunitat? Ets un gran amic i estic molt contenta que formis part de la nostra vida. Gràcies per tot! Raül, gràcies pels anys de "Vilapici" i per tots els bons moments viscuts. I Gabi gràcies per estar sempre disposat a ajudar! I acabant el *tour* per IQS, no vull oblidar-me de tota la gent que m'ha tractat molt bé aquests anys i m'ha ajudat en algun moment: Albert G., Magda, David S., Eli B., Ari V., Chema, David, Yolanda, Cristian...moltes gràcies.

I el més especial que m'enduc de la tesi, sens dubte, és com un raig de llum. Gracias por llegar a mi vida en mi peor momento y recordarme cada día desde entonces lo que significa ser feliz. Gracias por

ser la mejor compañera de laboratorio y de vida que podría tener. Gracias por tu alegría contagiosa, por cuidarme y apoyarme siempre y por ponerme en valor las pequeñas y más importantes cosas de la vida. Ojala pueda escucharte inventarte la letra de todas las canciones toda la vida. Buena parte de esta tesis es tuya.

Y gracias por traer contigo unos amigos tan leales como lo son Marc y Mire. Gracias, petardos, por ser como sois y por haberme aceptado tal y como soy, con mi gran perder incluido. Es una suerte contar con vuestra amistad. Sois geniales. Gràcies també Jaume i Puxi per tots els grans moments compartits...i que en siguin molts més!

I ja fora d'IQS, volia agrair molt especialment als *Bio-botiflers* per ser un grup tan ben parit. Celebrarem aquesta tesi, les demés i algun aniversari fora de data aviat. Gràcies per ser com sou. Aini, carrera+màster juntes es diu aviat. Tot i les dificultats, sempre t'he considerat una amiga i una gran companya. Gràcies per tants moments únics, per tots els riures i en definitiva per tots aquests anys. David, gràcies per ser com ets. Un plaer haver compartit tants moments. Gràcies, *nenes*, per ser-hi des de sempre i seguir formant aquest grup tan divers i incomprensible com especial i indispensable. Teta, què fort que surts ja a dues tesis, eh? Gràcies per ser com una germana per mi i per entendre'm només mirar-me. Ens queda molt camí(no) per compartir. Gràcies també Anna i Maria per la vostra amistat durant tants anys. I gràcies a la gent del món del bàsquet que m'ha ajudat a créixer i fer-me qui sóc avui.

Gracias a mi familia política por hacerme la vida más divertida. Muchas gracias Sita – ahora que no puedes decirme que no te las dé –, Carlos, Sara y Oscar por acogerme como una más. Por muchos más momentos felices juntos, pronto siendo uno más. Gracias también a toda la extensión de esta familia y amigos de la misma por el cariño recibido.

Gràcies a tota la meva família, en especial als meus avis per haver-me ensenyat tant. Avi, yaya, la vostra *baloncestista* i *puturru de fuá* ja és gairebé doctora. Yaya, me gustaría que te acordaras de los logros de tu nieta, y de otras muchas cosas, pero yo te prometo que me acordaré siempre de cuando eras tú. Y gracias yayo por ser un ejemplo para mí. Estoy segura que si la vida te hubiera tratado mejor, hubieras sido por lo menos catedrático y doctor *honoris causa*. Yo, de mayor, quiero ser como tú. Os quiero y os llevaré siempre conmigo.

Gràcies també a les meves tietes i cosins. I moltes gràcies al club del 5 de setembre (i als seus fruits) per ser el millor club d'amics del món. Per mi sou la meva família i us estimo molt a tots!

Sandra, gràcies per ser la millor germana que podria tenir. Ets un exemple de perseverança, autoexigència i humilitat. Tant de bo sabessis tot el que vals..! Gràcies per cuidar-me sempre i per tot el que fas per mi. És un orgull immens ser la teva germana. T'estimo molt. I gràcies, Àngel, per ser com un germà gran per mi i per la paciència, el tracte i el carinyo rebuts.

I per últim, papes, m'agradaria donar-vos les gràcies per fer-me la persona que sóc avui. Gràcies per haver-me acompanyat, cuidat, guiat i estimat sempre i haver-me permès arribar on he arribat. Gràcies pels valors que m'heu inculcat, per ser els meus referents i per haver format la família meravellosa on m'he criat. Gràcies mama per estimar-me incondicionalment, per inspirar-me i motivar-me a donar sempre el millor de mi mateixa. Gràcies papa per aconsellar-me sempre el millor per mi, per ser un mirall del que vull ser i per haver confiat sempre en mi. Mai us arribaré a agrair l'esforç i sacrifici que heu fet perquè pugui ser aquí ni us podré tornar tot el que heu fet per mi, però sempre us ho agrairé. Per tot això i més, aquesta tesi és vostra. Us estimo.

Laura Balcells Garcia, 2 de setembre de 2020.

This thesis has been funded by the Programa Estatal de I+D+i Orientada a los RETOS de la sociedad (RTI2018-094734-B-C22) from the Ministerio de Ciencia e Innovación

This thesis has also been made thanks to the fellowship grant for the doctorate degree of IQS School of Engineering (2017).

Abstract

Multi-faced study for the development of enhanced transfection systems

The current transfer of knowledge from a research laboratory scale to pharmaceutical products and human therapies is limited, among other reasons, due to the perception of cells as black boxes, where there are inputs and outputs but little attention is devoted to the inner cell processes governing the overall results. This doctoral thesis proposes a method to study the cellular mechanisms involved in cell uptake and transfection that often remain unnoticed. That is, through the development of a new class of multicomponent nanoparticles derived from a well-performing polymeric type gene delivery system, it is here projected an inspection from inside the cells that will allow not only a better understanding of cell experiment results, but also setting the basis for an innovative and improved cell therapy platform.

First, the intracellular mechanisms of autophagy and exosomes production will be studied using OM-pBAE polyplexes in combination with metallic nanoparticles. The role of both the polymeric and the metallic component of the system will be investigated in these two cell mechanisms that are induced upon cell transfection. Also, the intracellular location assessment of the complexes will be monitored. Then, the interactions of these gene delivery systems with the proteins present in any given biological medium will be analyzed, since they have a great impact in cellular internalization. And finally, with the knowledge on both the cellular mechanisms behind cell transfection and the effect of protein corona on the cell uptake profiles of different nanoparticles, it will be proposed the application of our gene delivery systems to a more challenging purpose: the modification of mesenchymal stem cells for further use as cell therapy strategies.

In conclusion, in this thesis, multicomponent nanoparticles have been employed to perform a thorough study of the cellular mechanisms induced upon cell transfection. Gene delivery systems composed of polyplexes made of OM-pBAEs and pDNA and a metallic component being either gold nanoparticles or SPIONs have been used to unbox cells and analyze the intra and intercellular processes that dictate the fate of internalized vectors – namely autophagy and exosomes production –, study their interaction with proteins and demonstrate that this phenomenon is key for their cellular uptake, and finally apply the knowledge of their properties and abilities to genetically modify reluctant to transfection cells that are used for cell therapy strategies.

Resumen

Multi-faced study for the development of enhanced transfection systems

La actual transferencia de conocimientos desde la escala de laboratorio de investigación a los productos farmacéuticos y las terapias humanas es limitada, entre otras razones, debido a la percepción de las células como cajas negras, en las que hay entradas y salidas pero se presta poca atención a los procesos celulares internos que rigen los resultados generales. Esta tesis doctoral propone un método para estudiar los mecanismos celulares que intervienen en la internalización de NPs y la transfección de células, que a menudo pasan desapercibidos. Es decir, mediante el desarrollo de una nueva clase de nanopartículas multicomponentes derivadas de un sistema polimérico de *gene delivery* de buen rendimiento, se proyecta aquí una inspección desde el interior de las células que permitirá no sólo comprender mejor los resultados de los experimentos celulares, sino también sentar las bases de una plataforma de terapia celular innovadora y mejorada.

En primer lugar, se estudiarán los mecanismos intracelulares de autofagia y producción exosomas utilizando poliplejos OM-pBAE en combinación con nanopartículas metálicas. Se investigará el papel del componente polimérico y metálico del sistema en estos dos mecanismos celulares que se inducen con la transfección celular. También se supervisará la evaluación de la ubicación intracelular de los complejos. A continuación, se analizarán las interacciones de estos sistemas de *gene delivery* con las proteínas presentes en el medio biológico, ya que tienen un gran impacto en la internalización celular. Y, por último, con el conocimiento tanto de los mecanismos celulares que subyacen a la transfección celular como del efecto de la corona proteínica en los perfiles de internalización celular de las diferentes nanopartículas, se propondrá la aplicación de nuestros sistemas de *gene delivery* a un propósito más desafiante: la modificación de las células madre mesenquimales para su posterior uso como estrategias de terapia celular.

En conclusión, en esta tesis se han empleado nanopartículas multicomponentes para realizar un estudio exhaustivo de los mecanismos celulares inducidos en la transfección celular. Se han utilizado sistemas de entrega de genes compuestos de poliplejos hechos de OM-pBAE y pDNA y un componente metálico que son nanopartículas de oro o SPIONs para abrir las células y analizar los procesos intra e intercelulares que dictan el destino de los vectores internalizados - la autofagia y la producción de exosomas -, estudiar su interacción con las proteínas y demostrar que este fenómeno es clave para su absorción celular y, por último, aplicar el conocimiento de sus propiedades y capacidades para modificar

genéticamente las células reacias a la transfección que se utilizan para las estrategias de terapia celular.

Resum

Multi-faced study for the development of enhanced transfection systems

L'actual transferència de coneixements des de l'escala de laboratori d'investigació als productes farmacèutics i les teràpies humanes és limitada, entre altres raons, a causa de la percepció de les cèl·lules com caixes negres, en què hi ha entrades i sortides però es presta poca atenció als processos cel·lulars interns que regeixen els resultats generals. Aquesta tesi doctoral proposa un mètode per estudiar els mecanismes cel·lulars que intervenen en la internalització NPs i la transfecció de cèl·lules, que sovint passen desapercebuts. És a dir, mitjançant el desenvolupament d'una nova classe de nanopartícules multicomponents derivades d'un sistema polimèric de *gene delivery* de bon rendiment, es projecta aquí una inspecció des de l'interior de les cèl·lules que permetrà no només comprendre millor els resultats dels experiments cel·lulars, sinó també establir les bases d'una plataforma de teràpia cel·lular innovadora i millorada.

En primer lloc, s'estudiaran els mecanismes intracel·lulars d'autofàgia i producció exosomes utilitzant poliplexes OM-pBAE en combinació amb nanopartícules metàl·liques. S'investigarà el paper del component polimèric i metàl·lic de sistema en aquests dos mecanismes cel·lulars que es indueixen amb la transfecció cel·lular. També es supervisarà l'avaluació de la ubicació intracel·lular dels complexos. A continuació, s'analitzaran les interaccions d'aquests sistemes de *gene delivery* amb les proteïnes presents en el medi biològic, ja que tenen un gran impacte en la internalització cel·lular. I, finalment, amb el coneixement tant dels mecanismes cel·lulars subjacents a la transfecció cel·lular com de l'efecte de la corona proteica en els perfils d'internalització cel·lular de les diferents nanopartícules, es proposarà l'aplicació dels nostres sistemes de *gene delivery* a un propòsit més desafiant: la modificació de les cèl·lules mare mesenquimals per al seu posterior ús com a estratègies de teràpia cel·lular.

En conclusió, en aquesta tesi s'han emprat nanopartícules multicomponents per realitzar un estudi exhaustiu dels mecanismes cel·lulars induïts en la transfecció cel·lular. S'han utilitzat sistemes de lliurament de gens compostos de poliplexes fets d'OM-pBAE i pDNA i un component metàl·lic que són nanopartícules d'or o SPIONs per obrir les cèl·lules i analitzar els processos intra i intercel·lulars que dicten el destí dels vectors internalitzats - la autofàgia i la producció de exosomes -, estudiar la seva interacció amb les proteïnes i demostrar que aquest fenomen és clau per a la seva absorció cel·lular i, finalment, aplicar el coneixement de

les seves propietats i capacitats per modificar genèticament les cèl·lules reticents a la transfecció que s'utilitzen per a les estratègies de teràpia cel·lular.

Table of Contents

Acknowledgments ..... **I**

Abstract ..... **VII**

Resumen ..... **IX**

Resum ..... **XI**

Table of Contents ..... **XIII**

Index of Figures ..... **XV**

Index of Tables ..... **XVII**

List of Abbreviations ..... **XVIII**

Chapter I. Motivation and objectives **21**
1.1 Content of this dissertation **32**
1.2 References **33**

Chapter II. Autophagy and exosomes: tracking intracellular fate of nanoparticles **39**
2.1 Introduction **41**
2.2 Aims **49**
2.3 Materials and Methods **51**
2.3.1 Materials 51
2.3.2 Synthesis of spherical gold nanoparticles 51
2.3.3 Synthesis of C6-pBAE nanoparticles 51
2.3.4 Manufacturing of SPION and AuNP-containing pBAE NPs 53
2.3.5 NP characterization 53
2.3.6 In vitro experiments for confocal imaging 54
2.3.6.1 HeLa cells 54
2.3.6.2 Cell transfection 54
2.3.6.3 Immunostaining procedure for confocal imaging 55
2.3.6.4 Confocal imaging and image processing 56
2.4 Results and Discussion **57**
2.4.1 Nanoparticle synthesis and characterization 57
2.4.2 Basal autophagy and exosomes production levels in HeLa cells 59
2.4.3 Assessing exosomes production and autophagy in HeLa cells 60
2.4.4 Overall view of cell transfection 66
2.5 Concluding remarks **70**
2.6 References **72**

Chapter III. The nanoparticle journey: from synthesis to inside the cell **81**
3.1 Introduction **83**
3.2 Aims **87**
3.3 Materials and Methods **88**
3.3.1 Materials 88
3.3.2 Synthesis of Gold nanorods (AuNR) 88
3.3.3 Gold NR characterization 88
3.3.4 Cell culture 89
3.3.5 MTT and MTS cytotoxicity assays 89
3.3.6 NPs cell uptake 90
3.3.6.1 ICP-OES 90
3.3.6.2 ICP-MS 90
3.3.6.3 Single cell ICP-MS 90

3.3.7 Transfection Efficacy 91
3.3.8 nanoDSC for protein corona characterization 91
3.3.9 Protein Isolation for MS 91
3.3.10 Proteomic studies: Inductively Coupled Plasma – Mass Spectrometry (ICP-MS) 92
3.4 Results and discussion 94
3.4.1 SPION or AuNP–containing polyplexes do not impair cell viability 94
3.4.2 Cells internalize more metallic nanoparticles when they are complexed with OM-pBAE-NPs 95
3.4.2.1 Uptake of SPIONs in HeLa cells 95
3.4.2.2 Uptake of complexed SPIONs and spherical AuNPs in PANC-1 cells 97
3.4.3 Gold NPs are internalized in a shape-dependent manner 98
3.4.3.1 Gold nanorods synthesis and characterization 98
3.4.3.2 Single cell ICP-MS 99
3.4.4 Transfection efficiency does not correlate with NP uptake 102
3.4.5 Protein corona modulates uptake and transfection 103
3.4.5.1 Preliminary protein corona characterization 104
3.4.5.2 Proteomics studies of PC 106
3.5 Concluding remarks 111
3.6 References 113

Chapter IV. Designing an enhanced transfection system for mesenchymal stem cells 121
4.1 Introduction 123
4.2 Aims 127
4.3 Materials and Methods 128
4.3.1 Materials 128
4.3.2 pBAE synthesis and modification with oligopeptides 128
4.3.4 Gel retardation assays 130
4.3.5 Biophysical characterization of SPION-containing nanoparticles 130
4.3.5.1 Dynamic Light Scattering 130
4.3.6 In vitro experiments 131
4.3.6.2 Cell transfection 131
4.3.7 Magnetic cell sorting 132
4.3.8 Statistical analysis 132
4.4 Results and Discussion 133
4.4.1 Manufacturing of multicomponent nanoparticles 133
4.4.3 Transfection screening of the different SPION-containing nanoparticles 137
4.4.4 SPIONs improve cell transfection of OM-pBAE/pDNA polyplexes 138
4.4.5 SPIONs allow the selection of effectively transfected cells 141
4.4.6 AMSCs transfection with multicomponent nanoparticles 144
4.4.6.1 Basal autophagy and exosomes production levels in AMSC cells 145
4.4.6.2 Assessing exosomes production and autophagy in AMSC cells transfected with OM-PBAEs-based gene delivery systems 146
4.5 Concluding remarks 151
4.6 References 153

Chapter V. Conclusions 157
Conclusions 159

Index of Figures

Figure 1. Formation of the NP-biomolecule corona[22]. 25
Figure 2. The gene delivery process of cationic polymers.....27
Figure 3. Biomedical applications of (A) SPIONs[75] and (B) gold nanoparticles[76] 30
Figure 4. A schematic summary of pBAE-based materials and their applications[90].....41
Figure 5. Schematic autophagic progression[101].....44
Figure 6. Scheme of the endocytic pathway, autophagy and exosome biogenesis[41].....48
Figure 7. Schematic representation of the cell processes with an impact on cell transfection. 49
Figure 8. Chemical structure of C32CR3 and C6CR3 OM-pBAEs, indicating the C32 and C6 initial polymers reacting with the CR3 peptide.....52
Figure 9. Schematic representation of the mounting procedure.....56
Figure 10. Characterization of the nanoparticles used in Chapter II.....58
Figure 11. Basal levels of exosomes production and autophagy in HeLa cells at different timepoints. 60
Figure 12. Exosomes production in HeLa cells in response to different nanoparticles at different timepoints. 62
Figure 13. Autophagy in HeLa cells in response to different nanoparticles at different timepoints. 63
Figure 14. Schematic representation of the variations in the intra and intercellular processes with an impact on cell transfection.....65
Figure 15. Confocal images of HeLa cells transfected with different polyplexes.....66
Figure 16. Confocal images of HeLa cells transfected with different polyplexes.....67
Figure 17. Confocal images of HeLa cells using different channel merges.....69
Figure 18. Entry pathways for mammalian cells. 84
Figure 19. Schematic illustration of the proton sponge effect leading to endosomal escape for cationic nanoparticles. 85
Figure 20. HeLa and PANC-1 cell viability when incubated with OM-pBAE-NPs.....94
Figure 21. HeLa and PANC-1 cell viability when incubated with metallic NPs. 95
Figure 22. HeLa iron content after incubation with nanoparticles.....96
Figure 23. PANC-1 iron and gold content after incubation with nanoparticles. 98
Figure 24. Characterization of gold nanorods.....99
Figure 25. Single cell ICP-MS analysis of HeLa cells.....100
Figure 26. Transfection efficacy of the complexes on PANC1 cells. 102
Figure 27. Thermograms of gold nanoparticles and nanorods incubated with BSA.....105

Figure 28. Schematic representation of the BSA deposition on gold nanospheres and nanorods. *106*
Figure 30. Mass spectrometry data for the different NPs used. *108*
Figure 31. DMSA coating of SPIONs *125*
Figure 32. Scheme of the different structures hypothesized for SPION-containing nanoparticles *129*
Figure 33. Manufacturing and characterization of SPION-containing nanoparticles. *134*
Figure 34. FACS analysis regarding the transfection efficiency screening of different SPIONs concentrations into C32-CR3:pGFP(50:1) T nanoparticles. *136*
Figure 35. Transfection screenings of the different nanoparticles. *137*
Figure 36. Transfection efficiency results *139*
Figure 37. Magnetic cell sorting. *142*
Figure 38. Schematic summary of transfection and magnetic sorting results[149] *144*
Figure 39. Basal levels of exosomes production and autophagy in AMSC cells at different timepoints. *146*
Figure 40. Exosomes production in AMSCs in response to different nanoparticles at different timepoints. *147*
Figure 41. Autophagy in AMSCs in response to different nanoparticles at different timepoints. *148*

Index of Tables

Table 1. Primary antibodies used for confocal imaging *56*
Table 2. Secondary antibodies used for confocal imaging *56*
Table 3. Polidispersity Index (PDI) values for the complexes used in chapter II *59*
Table 4. Samples incubated in HeLa cells *61*
Table 5. Single cell ICP-MS results *101*

List of Abbreviations

AcONa	Sodium acetate
ag	Attogram
AMSC	Adipose-derived Mesenchymal Stem Cell
AR	Aspect ratio
Arg	Arginine
Au	Gold
AuNP	Gold Nanoparticle
AuNR	Gold Nanorod
BCA	Bicinchoninic acid assay
BI	Biological identity
BSA	Bovine Serum Albumin
ºC	Celsius Degrees
CD9	Cluster of Differentiation 9
Cos-7	African green monkey kidney fibroblast-like cell line
CryoTEM	Cryogenic Transmission Electron Microscopy
CTAB	Cetyltrimethylammonium bromide
Cys	Cysteine
Cy5	Cyanine 5
DAPI	4',6 – Diamino-2-phenylindole dihydrochloride
D_H	Hydrodynamic diameter
DLS	Dynamic Light Scattering
DMEM	Dulbecco's Modified Eagle Medium
DMSA	Dimercaptosuccinic Acid
DMSO	Dimethyl Sulfoxide
DNA	Deoxyribonucleic Acid
DTT	Dithiothreitol
EDTA	Ethylenediaminetetraacetic acid
emPAI	Exponentially Modified Protein Abundance Index
EMSA	Electrophoretic Mobility Shift Assay
FACS	Fluorescence-Activated Cell Sorting
FBS	Fetal Bovine Serum
Fe	Iron
Fe_3O_4	Iron (IV) oxide or magnetite
Fe_2O_3	Iron (III) oxide
g	Gram
GFP	Green Fluorescent Protein
HeLa	Henrietta Lacks - Human Cervical Carcinomal Cell Line

ICP-MS	Inductively Coupled Plasma Mass Spectrometry
ICP-OES	Inductively Coupled Plasma Optical Emission Spectrometry
kV	kilovolt
LbI	Layer by layer
LC-MS	Liquid chromatography–mass spectrometry
LC3	Light Chain 3
LSPR	Longitudinal SPR
mg	milligram
min	Minute
mL	Millilitre
mmol	millimolar
MNP	Magnetic Nanoparticle
MRI	Magnetic Resonance Imaging
mRNA	Messenger RNA
ms	Millisecond
MSC	Mesenchymal Stem Cell
mTOR	Mammalian Target of Rapamycin
MTS	3-(4,5-dimethylthiazol-2-yl)-5-(3-carboxymethoxyphenyl)-2-(4-sulfophenyl)-2H-tetrazolium
MTT	3-(4,5-dimethylthiazol-2-yl)-2,5-diphenyltetrazolium bromide
mV	Millivolts
MVB	Multivesicular Bodies
mW	milliwatt
NanoDSC	Nano Differential Scanning Calorimeter
nL	Nanoliter
nm	Nanometer
NP	Nanoparticle
OM-pBAEs	Oligopeptide modified Poly(β-aminoester)s
PANC-1	Human pancreatic epithelioid carcinoma-like cell line
pBAEs	Poly(β-aminoester)s
PBS	Phosphate Buffered Saline
PC	Protein Corona
PdI	Polydispersity Index
pDNA	Plasmid DNA
pg	picogram
pGFP	Plasmid encoding GFP
pKa	Acid dissociation constant
RNA	Ribonucleic Acid
SC-ICP-MS	Single Cell-ICP-MS
SD	Standard deviation

SDS-Page	Sodium Dodecyl Sulphate Polyacrylamide Gel Electrophoresis
SI	Synthetic Identity
SPION	Superparamagnetic Iron Oxide Nanoparticle
SPR	Surface Plasmon Resonance
TEM	Transmission Electron Microscopy
T_m	Transition midpoint
U-87 MG	Human glioblastoma-like cell line
UV-Vis	Ultraviolet Visible
v/v	Volume/volume fraction
w/v	Weight/volume fraction
w/w	Mass fraction (weight/weight)
µl	Microlitre
µm	Micrometre

Chapter I. Motivation and objectives

This page left blank intentionally

Introduction: Cellular trafficking of polyplexes

A limitation of the current transfer of knowledge from research to pharmaceutical products arises from the perception of cells as black boxes, where there are inputs and outputs but little attention is devoted to the inner cell processes governing the overall results. This doctoral thesis proposes a method to study the cellular mechanisms involved in cell uptake and transfection that are often overlooked. Through the development of a new class of multicomponent nanoparticles derived from a well-performing polymeric type gene delivery system, it is here projected an inspection from inside the cells that will allow not only a better understanding of cell experiment results, but also setting the basis for an innovative and improved cell therapy platform.

Gene therapy emerged as a pioneering technique to treat or improve the health condition of patients by modifying their cells genetically. Although it aroused huge expectations, the number of gene therapeutic products in the market is limited and does not correlate with numerous lab-scale research studies concerning them[1–4]: marketed nanomedicine products only represent one-tenth of nanomedicines reported in literature[5]. The major historical problem is the development of efficient and safe systems for the delivery of therapeutic genes into the target cells. However, the main reason of this gap between research labs and industries is not the design of improved gene delivery vectors but the lack of wide and systematic studies regarding the intracellular and intercellular mechanisms involved in cell uptake and transfection of such systems. That is, many research devotes efforts to developing gene delivery systems that might overcome the current barriers of gene therapy without considering the cell mechanisms that rule the nanoparticles' fate. Eventually, if transferring *in vitro* experiments to *in vivo* ones, the whole physiological environment would be another hurdle for the system to generate any desired effect. So, in order to have a whole approach when developing gene delivery systems, other factors besides the design and synthesis of the nanoparticles have to be considered.

This absence of studies focusing on the cell processes involved in cell uptake and transfection limits the transfer from novel designed nanosystems at a research laboratory scale to real human therapies. In other words, when using cells for therapeutic purposes, they are often perceived as black boxes. Even when using well-studied cell lines and well-stablished gene delivery systems, the intra and intercellular mechanisms are overlooked. Much of the attention is focused on either the preparation of the nanocarrier

– input – or on the result obtained from cells (e.g. cell viability or cell transfection efficiency) – output – but less importance is given to what is actually happening inside cells. As it is well known, cells are complex, and thousands of processes take place simultaneously inside them. Thus, identifying the key processes that have an impact on cell modifications when using gene delivery systems is of major importance to better understand any obtained result. That is, starting by comprehending the cellular mechanisms that guide intra and intercellular trafficking will allow us to give insight not only on the cellular outcomes but also on the gene delivery systems' design and development.

To study these processes, a well-performing gene delivery system is needed. This way, it will be possible to test different conditions and aisle the factors to be analyzed. For this purpose, polyplexes based on poly(beta-amino ester)s (pBAEs) will be used. These cationic, biodegradable polymers have been developed as promising nucleic acid delivery systems[6,7]. pBAEs possess a high transfection efficacy *in vitro* and *in vivo*, together with a low toxicity and the possibility to incorporate targeting moieties to mediate ligand-specific uptake. Their capacity to efficiently complex nucleic acids into discrete nanoparticles and transfer genetic material to target cells make them suitable as gene delivery vectors for cell therapy applications[8]. Furthermore, our group has developed a family of poly(ß-amino ester) polymers with oligopeptide-modified termini (OM-pBAEs) that proved increased transfection efficiency and excellent biocompatibility. These previous results have demonstrated that tailored formulations of different cationic OM-pBAE polymers are capable of rendering nanoparticles with specific features, such as cell specificity or intracellular localization[9]. All these advantages, specially the suitability and well-known use of pBAEs as gene delivery vectors for cell modification and their versatility in terms of cell localization, makes them an appropriate system for the study of intra and intercellular mechanisms related with cell transfection. That is, pBAE-NPs will be the tool that will be here used to unbox cells.

Moving to one step before the gene delivery system is already inside the cell, we find the cellular internalization or uptake. Endocytosis is the energy-dependent process through which cells internalize ions and biomolecules[10]. And the first step for the internalization of a NP is its interaction with cell membranes. This interaction, and consequently, NP uptake, depends on multiple properties of both, NP and cell membranes[11–16]. Importantly, the type of interaction of the NP with the cellular membrane will determine the cell penetration route, and this interaction can be completely different depending on the physicochemical properties of the NPs[17–19]. The NPs' factors can be

summarized as size, surface charge, shape and NP composition; and the cell factors, as if they are polarized or not, cancerous or healthy and the cell cycle phase at which they are[20]. However, the most important factor that will guide the fate of the gene delivery system is classified as a NP factor but is not a physicochemical property resulting from its synthesis: it is the interaction of the NP with the biological medium. When nanoparticles are incubated in a biological fluid their surface is modified by selective adsorption of biomolecules (such as proteins and lipids) forming what is known as the protein corona (PC). This PC can be thought as a biomolecular interface composed of a "soft" and a "hard" corona with "short" and "long" typical exchange times, respectively[21] (Figure 1).

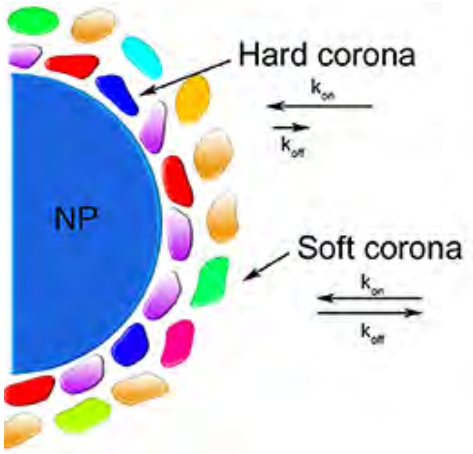

Figure 1. Formation of the NP-biomolecule corona[22]. Upon exposure to physiological fluids, NPs become coated with a variety of proteins and other biomolecules. The hard corona is comprised of lower abundance, high affinity biomolecules with almost negligible exchange rates. The soft corona is comprised of more abundant, lesser affinity biomolecules with faster exchange rates.

This biomolecules adsorption can modify the physicochemical properties of NPs, conferring a new biological identity to NPs. The interaction of nanoparticles with macromolecules present in biological media has been proved to be determinant in the cellular uptake, intracellular fate and biodistribution of nanoparticles, hence determining the physiological response[23–25].Therefore, before transferring any novel designed nanosystem to pharmaceutical industries and after the characterization of its physicochemical properties, a deep study of the interaction of such nanosystem with biological components is required to ensure its safety and to assess its behavior in physiological conditions[26]. So, what will be recognized by the cell and will therefore alter its intra and intercellular processes is not the gene delivery system that was designed and synthetized, but the interaction of this system with the biological milieu. By controlling

differences in the PC formation, we will be able to study its influence on intracellular fate of the nanoparticles.

Once inside the cell, these gene delivery systems are usually delivered to the early endosome (EE) via vesicular or tubular intermediates that are derived from the plasma membrane[27]. Then, in order to cause any cellular effect, they have to escape the regular endosomal route, which ends up in the degrading vesicles called lysosomes, and they need to be released to the cytosol[28] (see Figure 2). Polyplexes have often the inherent ability to escape from endosomes – the so-called endosomal escape capacity – and release their cargo to the cytoplasm. It is the case of pBAEs, the titratable tertiary amines from their structure provide pBAE-based NPs with a mechanism of endosomal escape (the “proton sponge” effect) that will be detailed in the following chapters. Plasmid DNA can then travel through the cytoskeletal network before reaching the nuclear membrane[29,30], where it must either wait for cell division or be specifically transported through the nuclear pore complex, in order to reach the nucleoplasm where it can be transcribed[31].Next, the transcribed messenger RNA will be transported into the cytosol, and will guide protein translation[32,33].

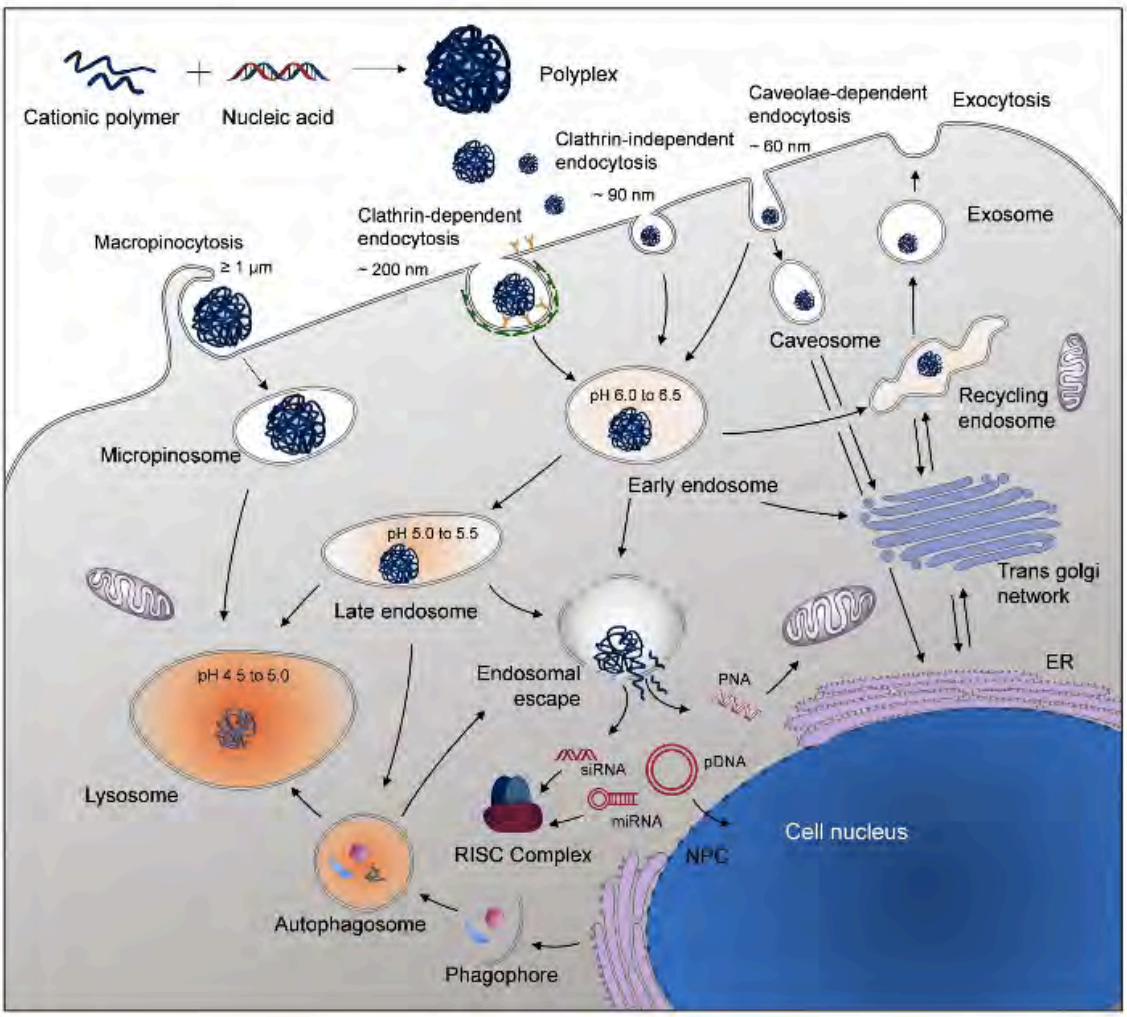

Figure 2. The gene delivery process of cationic polymers. Including polyplex formation, intracellular uptake via various endocytosis pathways, intracellular polyplex trafficking, endosomal escape into the cytoplasm, release of the cargo from the polymer and transport to the site of action. Depending on the type of nucleic acid, the site of action is either located within the cytoplasm or in the nucleus. ER: Endoplasmic reticulum; NPC: Nuclear pore complex[34].

However, besides the regular intracellular trafficking and subsequent degradation of the polyplexes, other cellular processes have also an impact on *in vitro* and *in vivo* results. In this context, the two main cell mechanisms that have raised as indispensable to understand gene delivery processes are autophagy and exosomes production.

The past decade has witnessed an explosion of research on the fundamental cell biology pathway called autophagy (Greek for “self-eating”)[35] that may alter not only intracellular trafficking but also cell viability and cell-to-cell communication. Autophagy is an intracellular stress response that is enhanced under starvation conditions, and also when the cellular components are damaged[36]. This process is widely studied during analysis of nanoparticle/cell interactions due to its two-way regulation. First, autophagy induction is a cellular protection reaction toward NPs. For instance, autophagy can

promote cell survival through eliminating stress factors caused by foreign NPs and accelerate digesting abnormally accumulated protein in degenerated cells[37–39]. Second, autophagy triggered by NPs can lead to autophagic cell death, also known as type II programmed cell death (PCD). This type II PCD is characterized by the accumulation of autophagic vesicles (autophagosomes and autophagolysosomes) and is often observed when massive cell elimination is demanded or when phagocytes do not have easy access to the dying cells[40]. Thus, autophagy might act as a double-edge sword all along cell transfection. Its understanding and its modulation might be key to control not only cell transfection efficacy but also cell viability after pBAE-NPs transfection.

Recent studies have revealed shared molecular machinery as well as substantial crosstalk between autophagy and another key cellular process called exosome biogenesis[41]. Cells communicate and exchange information by different means such as small molecular mediators, cell-to-cell adhesion molecules and tunnelling nanotubes[42–45]. However, in the past few years research focus has been redirected to extracellular vesicles[46–48] such as exosomes as a way of cell-to-cell communication, a mechanism that for many years has remained unnoticed[49]. Exosomes are bilayer nano-sized membrane vesicles (30–120 nm in size) released by almost every mammalian cell type including dendritic cells (DC), B cells, T cells, mast cells, epithelial cells and tumor cells[50–53] and are unique to the cell of origin. Therefore, they exhibit biomarker profiles specific to the cell they are derived from[54]. Exosomes have recently emerged as promising tools for theragnostic purposes and as drug and gene delivery systems with low immunogenicity, high biocompatibility, and high efficacy of delivery[55–57]. As exosomes are small and native to animals, they are able to avoid phagocytosis, fuse with the cell membrane, and bypass the engulfment by lysosomes[58]. And since they naturally carry genetic material between cells, it has been speculated that this property might be useful in gene therapy[59–61]. Also, the rising function of exosomes as means of alleviating intracellular stress conditions by secreting harmful or unwanted material outside the cell and in coordination with the autophagy-lysosomal pathway, has been found an essential mechanism to preserve intracellular homeostasis[62]. Therefore, studies on exosome production in relation with pBAE-based nanoparticles have been here conducted to better estimate the potential of naturally produced exosomes as a gene delivery platform and to provide insight into the impact of exosomes production in cell transfection efficiency.

As mentioned before, a way to study and monitor both autophagy and exosomes production without using chemicals could be altering these processes through slight

modifications of the gene delivery system. These modifications could include changes in the synthesis of the gene carrier that would lead to changes in its interaction with biomolecules and cells, and that would finally regulate the intracellular processes. For instance, modifications on the pBAE-NPs synthesis will be used in the present work to study differences in the protein corona formation, in the cellular uptake and transfection, and in the autophagy and exosomes production processes. More specifically, the addition of a metallic component to the pBAE-NPs will be exploited. In particular, metallic nanoparticles based on iron and gold will be used.

On the one hand, superparamagnetic iron oxide nanoparticles (SPIONs) are excellent MRI contrast agents used for imaging of cancer, cardiovascular and inflammatory diseases in both research and clinical applications[63]. Increased cell uptake of SPIONs has been reported[64,65]. They have been also used for magnetofection, which is a transfection technique that uses magnetic fields to attract particles containing magnetic nanoparticles into cells[66–68]. Here, SPIONs were combined in different ways with pBAE-NPs to render multicomponent nanoparticles. Their initial intended use was to perform magnetic selection of cells after they were transfected.

On the other hand, gold nanosystems are perhaps the most mature and well-developed metallic nanoparticles and have been undergoing continuous exploration over several decades for various applications including sensing, imaging, catalysis, therapeutics, diagnostics, and drug delivery, to mention but a few[69–72]. In the present work, AuNPs and AuNRs were used for different studies in combination with pBAEs, plasmid DNA and proteins due to their unique chemical and physical properties that imply their major advantages being, first, that the gold core is essentially inert and non-toxic[73]; and second the ease and shape-versatility of their synthesis[74]. Thus, the synthesis of pBAE-based multicomponent nanoparticles containing metallic nanoparticles will be employed in the present work for the study of cellular processes regarding cell uptake and transfection.

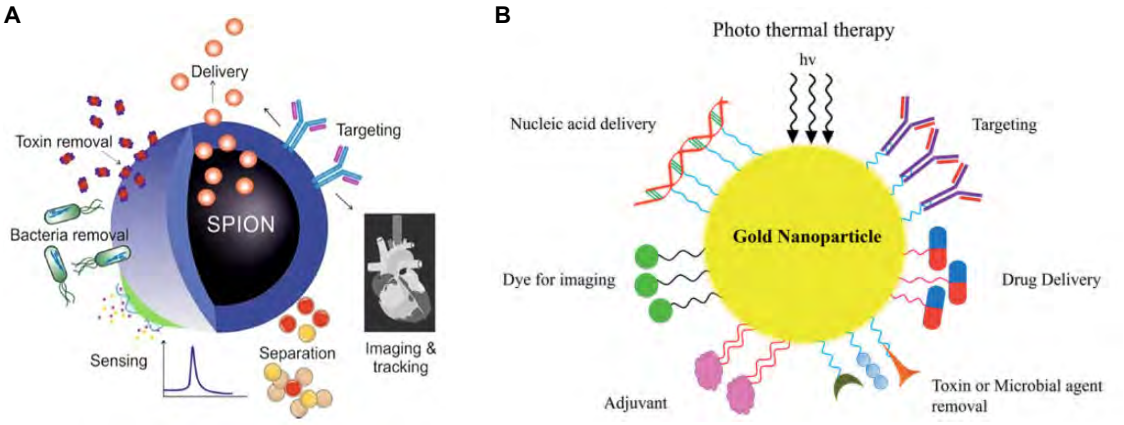

Figure 3. Biomedical applications of (A) SPIONs[75] and (B) gold nanoparticles[76]

Finally, once the cell mechanisms that drive the fate of nanoparticles in a cell transfection procedure are understood and the previous step of cell uptake is controlled, the work presented here opens the door to an additional use of the systems composed of pBAE polyplexes and a metallic component. These multicomponent nanoparticles could be used in cells that are difficult to modify genetically. This is the case of adipose-derived mesenchymal stem cells (AMSCs), which show poor results of *in vitro* transfection using non-viral gene delivery vectors[77]. Stem cells are often used for cell therapy approaches such as bone engineering[78], articular cartilage lesions[79] or cancer treatment[80]. Most of these cell therapy applications require a selection of successfully modified cells to increase the probabilities of achieving a final beneficial effect and, therefore, the enrichment and selection of genetically modified cells becomes a key issue[81]. At this point, and given the current growing interest in the combination of both gene and cell therapy strategies, a system allowing first the genetic modification of cells and later their selection for *in vivo* implantation would be of great relevance. In addition, since cell therapy relies on the delivery of cells to the target site, monitoring and tracking these cells to ensure tissue delivery and engraftment becomes a key issue in stabilizing clinical safety and therapeutic efficacy[64]. This could be possible with these innovative SPION-containing nanoparticles. Thus, understanding the cell mechanisms behind cell transfection will allow for the development of improved gene delivery systems that could broaden the uses of gene therapy and boost the efficiency of current applications.

In the light of the current needs for new insights on the cellular mechanisms that govern cellular outcomes, this doctoral thesis focuses on the study of different intra and

intercellular processes, namely autophagy and exosomes production, and their impact on cell uptake and transfection through the modification of the well-performing pBAE-NPs by adding metallic nanoparticles to them. The analysis of the different resulting nanoparticles in terms of synthetic and biological identities (protein corona) will shed light on the understanding of the cell mechanisms behind cell uptake and transfection. These multicomponent nanoparticles will also provide a proof of concept of a platform for genetic modification of stem cells for further cell therapy applications.

1.1 Content of this dissertation

The main objective of this thesis is the development of gene delivery systems with enhanced transfection efficiencies that could be used to overcome the huge challenge of transfecting stem cells. To do so, it is here proposed an inspection from inside the cells that will allow both a better understanding of cell experiment results, and setting the basis for an innovative and improved cell therapy platform.

First, the intracellular mechanisms of autophagy and exosomes production using OM-pBAE polyplexes in combination with metallic nanoparticles will be studied (**Chapter II**). It will be elucidated the role of each component of the system in these two cell mechanisms that are induced upon cell transfection. Also, the intracellular location of the complexes will be monitored.

Then, the interactions of our gene delivery systems with the proteins present in the medium will be analyzed, and these interactions will be related with the nanosystems' cellular internalization profiles (**Chapter III**).

Finally, the use of our gene delivery systems will be transferred to the challenging modification of mesenchymal stem cells that might be later employed in further cell therapy strategies (**Chapter IV**).

1.2 References

1. Ge, Y., Li, S., Wang, S. & Moore, R. *Nanomedicine - Principles of Nanomedicine*. (2014).
2. Venkatraman, S. Has nanomedicine lived up to its promise? *Nanotechnology* **25**, 3–7 (2014).
3. Venditto, V. J. & Szoka, F. C. Cancer nanomedicines: So many papers and so few drugs! *Adv. Drug Deliv. Rev.* **65**, 80–88 (2013).
4. Mitragotri, S. *et al.* Accelerating the Translation of Nanomaterials in Biomedicine. *ACS Nano* **9**, 6644–6654 (2015).
5. Fornaguera, C. & García-Celma, M. J. Personalized nanomedicine: A revolution at the nanoscale. *J. Pers. Med.* **7**, 14–21 (2017).
6. Kozielski, K. L., Tzeng, S. Y., Hurtado De Mendoza, B. A. & Green, J. J. Bioreducible cationic polymer-based nanoparticles for efficient and environmentally triggered cytoplasmic siRNA delivery to primary human brain cancer cells. *ACS Nano* **8**, 3232–3241 (2014).
7. Tzeng, S. Y. & Green, J. J. Subtle Changes to Polymer Structure and Degradation Mechanism Enable Highly Effective Nanoparticles for siRNA and DNA Delivery to Human Brain Cancer. *Adv. Healthc. Mater.* **2**, 468–480 (2013).
8. Green, J. J., Langer, R. & Anderson, D. G. A combinatorial polymer library approach yields insight into nonviral gene delivery. *Acc. Chem. Res.* **41**, 749–759 (2008).
9. Segovia, N., Dosta, P., Cascante, A., Ramos, V. & Borrós, S. Oligopeptide-terminated poly(ß-amino ester)s for highly efficient gene delivery and intracellular localization. *Acta Biomater.* **10**, 2147–2158 (2014).
10. Iversen, T., Skotland, T. & Sandvig, K. Endocytosis and intracellular transport of nanoparticles : Present knowledge and need for. *Nano Today* **6**, 176–185 (2011).
11. Forest, V. & Pourchez, J. Preferential binding of positive nanoparticles on cell membranes is due to electrostatic interactions: A too simplistic explanation that does not take into account the nanoparticle protein corona. *Mater. Sci. Eng. C* **70**, 889–896 (2017).
12. Harush-Frenkel, O., Debotton, N., Benita, S. & Altschuler, Y. Targeting of nanoparticles to the clathrin-mediated endocytic pathway. *Biochem. Biophys. Res. Commun.* **353**, 26–32 (2007).
13. Nel, A., Xia, T., Mädler, L. & Li, N. Toxic Potential of Materials at the Nanolevel. *Science (80-.).* **311**, 622–627 (2006).

14. Verma, A. & Stellacci, F. Effect of surface properties on nanoparticle-cell interactions. *Small* **6**, 12–21 (2010).
15. Yameen, B. *et al.* Insight into nanoparticle cellular uptake and intracellular targeting. *J. Control. Release* **190**, 485–499 (2014).
16. Park, J. H. & Oh, N. Endocytosis and exocytosis of nanoparticles in mammalian cells. *Int. J. Nanomedicine* 51 (2014). doi:10.2147/ijn.s26592
17. Fröhlich, E. The role of surface charge in cellular uptake and cytotoxicity of medical nanoparticles. *Int. J. Nanomedicine* **7**, 5577–5591 (2012).
18. Li, H., Tsui, T. Y. & Ma, W. Intracellular delivery of molecular cargo using cell-penetrating peptides and the combination strategies. *Int. J. Mol. Sci.* **16**, 19518–19536 (2015).
19. Prabha, S., Zhou, W. Z., Panyam, J. & Labhasetwar, V. Size-dependency of nanoparticle-mediated gene transfection: Studies with fractionated nanoparticles. *Int. J. Pharm.* **244**, 105–115 (2002).
20. Fornaguera, C., Castells-Sala, C. & Borrós, S. Unraveling Polymeric Nanoparticles Cell Uptake Pathways: Two Decades Working to Understand Nanoparticles Journey to Improve Gene Therapy. (2019). doi:10.1007/5584_2019_467
21. Jedlovszky-Hajdú, A., Bombelli, F. B., Monopoli, M. P., Tomb??cz, E. & Dawson, K. A. Surface coatings shape the protein corona of SPIONs with relevance to their application in vivo. *Langmuir* **28**, 14983–14991 (2012).
22. Pearson, R. M., Juettner, V. V. & Hong, S. Biomolecular corona on nanoparticles: A survey of recent literature and its implications in targeted drug delivery. *Front. Chem.* **2**, 1–7 (2014).
23. Lesniak, A. *et al.* Effects of the presence or absence of a protein corona on silica nanoparticle uptake and impact on cells. *ACS Nano* **6**, 5845–5857 (2012).
24. Mahmoudi, M., Bertrand, N., Zope, H. & Farokhzad, O. C. Emerging understanding of the protein corona at the nano-bio interfaces. *Nano Today* **11**, 817–832 (2016).
25. Lazarovits, J., Chen, Y. Y., Sykes, E. A. & Chan, W. C. W. Nanoparticle-blood interactions: The implications on solid tumour targeting. *Chem. Commun.* **51**, 2756–2767 (2015).
26. Fornaguera, C. & Solans, C. Methods for the in vitro characterization of nanomedicines—biological component interaction. *J. Pers. Med.* **7**, (2017).
27. Mayor, S. & Pagano, R. E. Pathways of clathrin-independent endocytosis. *Nat. Rev. Mol. Cell Biol.* **8**, 603–612 (2007).
28. Nguyen, J. & Szoka, F. C. Nucleic acid delivery: The missing pieces of the

puzzle? *Acc. Chem. Res.* **45**, 1153–1162 (2012).

29. Suh, J., Wirtz, D. & Hanes, J. Efficient active transport of gene nanocarriers to the cell nucleus. *Proc. Natl. Acad. Sci. U. S. A.* **100**, 3878–3882 (2003).
30. Vaughan, E. E. & Dean, D. A. Intracellular trafficking of plasmids during transfection is mediated by microtubules. *Mol. Ther.* **13**, 422–428 (2006).
31. Abouzeid, A. H. & Torchilin, V. P. The role of cell cycle in the efficiency and activity of cancer nanomedicines. *Expert Opin. Drug Deliv.* **10**, 775–786 (2013).
32. Hurtley, S. M. Protein kinesis. *Science (80-.).* **271**, 1477 (1996).
33. Zhu, D. *et al.* Detailed investigation on how the protein corona modulates the physicochemical properties and gene delivery of polyethylenimine (PEI) polyplexes. *Biomater. Sci.* **6**, 1800–1817 (2018).
34. Bus, T., Traeger, A. & Schubert, U. S. The great escape: How cationic polyplexes overcome the endosomal barrier. *J. Mater. Chem. B* **6**, 6904–6918 (2018).
35. Mizushima, N., Tamotsu, Y. & Levine, B. Methods in Mammalian Autophagy Research. *Cell* **140**, 2–3 (2010).
36. Kim, H. S., Park, S. Y., Moon, S. H., Lee, J. D. & Kim, S. Autophagy in human skin fibroblasts: Impact of age. *Int. J. Mol. Sci.* **19**, 1–13 (2018).
37. Getts, D. R., Shea, L. D., Miller, S. D. & King, N. J. C. Harnessing nanoparticles for immune modulation. *Trends Immunol.* **36**, 419–427 (2015).
38. Song, W. *et al.* Ceria nanoparticles stabilized by organic surface coatings activate the lysosome-autophagy system and enhance autophagic clearance. *ACS Nano* **8**, 10328–10342 (2014).
39. Wei, P. F. *et al.* Accelerating the clearance of mutant huntingtin protein aggregates through autophagy induction by europium hydroxide nanorods. *Biomaterials* **35**, 899–907 (2014).
40. Shintani, T. & Klionsky, D. J. Autophagy in Health and Disease: A Double-Edged Sword Takahiro. *Science (80-.).* **306**, 990–995 (2004).
41. Xu, J., Camfield, R. & Gorski, S. M. The interplay between exosomes and autophagy - partners in crime. *J. Cell Sci.* **131**, 1–11 (2018).
42. Rustom, A., Saffrich, R., Markovic, I., Walther, P. & Gerdes, H. H. Nanotubular Highways for Intercellular Organelle Transport. *Science (80-.).* **303**, 1007–1010 (2004).
43. Vidulescu, C., Clejan, S. & O'Connor, K. C. Vesicle traffic through intercellular bridges in DU 145 human prostate cancer cells. *J. Cell. Mol. Med.* **8**, 388–396 (2004).
44. Haass, N. K. & Herlyn, M. Normal human melanocyte homeostasis as a

paradigm for understanding melanoma. *J. Investig. Dermatol. Symp. Proc.* **10**, 153–163 (2005).

45. Morel, O., Toti, F., Hugel, B. & Freyssinet, J. M. Cellular microparticles: A disseminated storage pool of bioactive vascular effectors. *Curr. Opin. Hematol.* **11**, 156–164 (2004).
46. Greenwalt, T. J. The how and why of exocytic vesicles. *Transfusion* **46**, 143–152 (2006).
47. Hugel, B., Martínez, M. C., Kunzelmann, C. & Freyssinet, J. M. Membrane microparticles: Two sides of the coin. *Physiology* **20**, 22–27 (2005).
48. Février, B. & Raposo, G. Exosomes: Endosomal-derived vesicles shipping extracellular messages. *Curr. Opin. Cell Biol.* **16**, 415–421 (2004).
49. Ratajczak, J., Wysoczynski, M., Hayek, F., Janowska-Wieczorek, A. & Ratajczak, M. Z. Membrane-derived microvesicles: Important and underappreciated mediators of cell-to-cell communication. *Leukemia* **20**, 1487–1495 (2006).
50. Vlassov, A. V., Magdaleno, S., Setterquist, R. & Conrad, R. Exosomes: Current knowledge of their composition, biological functions, and diagnostic and therapeutic potentials. *Biochim. Biophys. Acta - Gen. Subj.* **1820**, 940–948 (2012).
51. Tan, A., Rajadas, J. & Seifalian, A. M. Exosomes as nano-theranostic delivery platforms for gene therapy. *Adv. Drug Deliv. Rev.* **65**, 357–367 (2013).
52. Rashed, M. H. *et al.* Exosomes: From garbage bins to promising therapeutic targets. *Int. J. Mol. Sci.* **18**, (2017).
53. Mathivanan, S., Ji, H. & Simpson, R. J. Exosomes: Extracellular organelles important in intercellular communication. *J. Proteomics* **73**, 1907–1920 (2010).
54. de la Torre Gomez, C., Goreham, R. V., Bech Serra, J. J., Nann, T. & Kussmann, M. 'Exosomics'-A review of biophysics, biology and biochemistry of exosomes with a focus on human breast milk. *Front. Genet.* **9**, 1–11 (2018).
55. Kim, M. S. *et al.* Engineering macrophage-derived exosomes for targeted paclitaxel delivery to pulmonary metastases: in vitro and in vivo evaluations. *Nanomedicine Nanotechnology, Biol. Med.* **14**, 195–204 (2018).
56. Ha, D., Yang, N. & Nadithe, V. Exosomes as therapeutic drug carriers and delivery vehicles across biological membranes: current perspectives and future challenges. *Acta Pharm. Sin. B* **6**, 287–296 (2016).
57. Aryani, A. & Denecke, B. Exosomes as a Nanodelivery System: a Key to the Future of Neuromedicine? *Mol. Neurobiol.* **53**, 818–834 (2016).
58. Bunggulawa, E. J. *et al.* Recent advancements in the use of exosomes as drug

delivery systems 06 Biological Sciences 0601 Biochemistry and Cell Biology. *J. Nanobiotechnology* **16**, 1–13 (2018).

59. O'Loughlin, A., Woffindale, C. & Wood, M. Exosomes and the Emerging Field of Exosome-Based Gene Therapy. *Curr. Gene Ther.* **12**, 262–274 (2012).
60. Lässer, C. *et al.* Human saliva, plasma and breast milk exosomes contain RNA: Uptake by macrophages. *J. Transl. Med.* **9**, 9 (2011).
61. György, B. *et al.* Membrane vesicles, current state-of-the-art: Emerging role of extracellular vesicles. *Cell. Mol. Life Sci.* **68**, 2667–2688 (2011).
62. Baixauli, F., López-Otín, C. & Mittelbrunn, M. Exosomes and autophagy: Coordinated mechanisms for the maintenance of cellular fitness. *Front. Immunol.* **5**, 1–6 (2014).
63. Jin, R. *et al.* Iron oxide nanoparticles promote macrophage autophagy and inflammatory response through activation of toll-like Receptor-4 signaling. *Biomaterials* **203**, 23–30 (2019).
64. Cortajarena, A. L. *et al.* Engineering Iron Oxide Nanoparticles for Clinical Settings. *Nanobiomedicine* **1**, doi: 10.5772/58841 (2014).
65. Pawelczyk, E., Arbab, A. S., Pandit, S., Hu, E. & Frank, J. A. Expression of transferrin receptor and ferritin following ferumoxides-protamine sulfate labeling of cells: Implications for cellular magnetic resonance imaging. *NMR Biomed.* **19**, 581–592 (2006).
66. Prosen, L. *et al.* Magnetofection: A reproducible method for gene delivery to melanoma cells. *Biomed Res. Int.* **2013**, 6–8 (2013).
67. Kami, D. *et al.* Application of magnetic nanoparticles to gene delivery. *Int. J. Mol. Sci.* **12**, 3705–3722 (2011).
68. Berry, C. C. Progress in functionalization of magnetic nanoparticles for applications in biomedicine. *J. Phys. D. Appl. Phys.* **198**, 224003 (2009).
69. Boisselier, E. & Astruc, D. Gold nanoparticles in nanomedicine: Preparations, imaging, diagnostics, therapies and toxicity. *Chem. Soc. Rev.* **38**, 1759–1782 (2009).
70. De, M., Ghosh, P. S. & Rotello, V. M. Applications of nanoparticles in biology. *Adv. Mater.* **20**, 4225–4241 (2008).
71. Dreaden, E. C., Alkilany, A. M., Huang, X., Murphy, C. J. & El-Sayed, M. A. The golden age: Gold nanoparticles for biomedicine. *Chem. Soc. Rev.* **41**, 2740–2779 (2012).
72. Huang, X., Jain, P. K., El-Sayed, I. H. & El-Sayed, M. A. Gold nanoparticles: Interesting optical properties and recent applications in cancer diagnostics and therapy. *Nanomedicine* **2**, 681–693 (2007).

73. Connor, E. E., Mwamuka, J., Gole, A., Murphy, C. J. & Wyatt, M. D. Gold nanoparticles are taken up by human cells but do not cause acute cytotoxicity. *Small* **1**, 325–327 (2005).
74. De Freitas, L. F., Varca, G. H. C., Batista, J. G. D. S. & Lugão, A. B. An overview of the synthesis of gold nanoparticles using radiation technologies. *Nanomaterials* **8**, (2018).
75. Rahman, M., Saei, A. A., Amiri, H. & Mahmoudi, M. Biomedical Applications of Superparamagnetic Nanoparticles in Molecular Scale. *Curr. Org. Chem.* **19**, 982–990 (2015).
76. Bagheri, S. *et al.* Using gold nanoparticles in diagnosis and treatment of melanoma cancer. *Artif. Cells, Nanomedicine Biotechnol.* **46**, 462–471 (2018).
77. Halim, N., Fakiruddin, K., Ali, S. & Yahaya, B. A Comparative Study of Non-Viral Gene Delivery Techniques to Human Adipose-Derived Mesenchymal Stem Cell. *Int. J. Mol. Sci.* **15**, 15044–15060 (2014).
78. Gómez-Barrena, E. *et al.* Bone regeneration: Stem cell therapies and clinical studies in orthopaedics and traumatology. *J. Cell. Mol. Med.* **15**, 1266–1286 (2011).
79. Im, G.-I. & Shin, K.-J. Epigenetic approaches to regeneration of bone and cartilage from stem cells. *Expert Opin. Biol. Ther.* **15**, 181–93 (2015).
80. Alieva, M. *et al.* Glioblastoma therapy with cytotoxic mesenchymal stromal cells optimized by bioluminescence imaging of tumor and therapeutic cell response. *PLoS One* **7**, 1–11 (2012).
81. Ren, C., Xu, K., Segal, D. J. & Zhang, Z. Strategies for the Enrichment and Selection of Genetically Modified Cells. *Trends Biotechnol.* **xx**, 1–16 (2018).

Chapter II. Autophagy and exosomes: tracking intracellular fate of nanoparticles

This chapter will be published as: Unboxing cells: studying cellular mechanisms behind cell transfection

Authors: L.Balcells, C. Fornaguera, A. Cascante, S. Borrós

This page left blank intentionally

2.1 Introduction

As already discussed in chapter I, a well-performing and widely characterized gene delivery system is required in order to study intra and intercellular processes. One of the most widely used type of non-viral gene vectors are synthetic cationic polymers that are capable of condensing DNA to form nano-sized polyplexes[82]. In our group, there is deep expertise in a class of these cationic polymers known as poly(ß-amino ester)s (pBAEs). Since pBAEs have shown very promising results as genetic material delivery agents[6,7] and have been broadly characterized by our group, they were employed in this work to investigate cell mechanisms.

pBAEs are biodegradable polymers capable of self-assembling with both DNA and RNA. They are easily synthesized by Michael addition of bifunctional amines to diacrylate groups and possess a high transfection efficiency *in vitro* and *in vivo*, together with low toxicity and ability for ligand-specific uptake[9,83]. Moreover, their unique structure allows for the modification and tailoring of their end-termini, thus opening a range of possibilities to design complexes with specific features. pBAEs have already been used successfully for several therapeutic applications including vaccination[84], gene therapy for prostate cancer and ophthalmology[85,86], gene silencing[87] and stem cell modification[88,89].

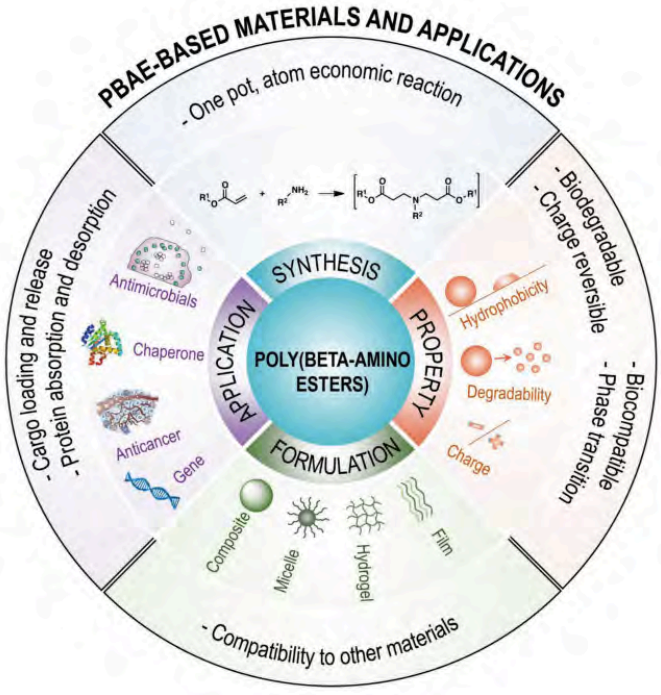

Figure 4. A schematic summary of pBAE-based materials and their applications[90]

Recently, it has been reported by our group that chemical modification at the end-termini of pBAEs with amine-rich oligopeptides is a powerful strategy to develop gene therapy systems that show highly efficient gene delivery and intracellular localization[91]. In particular, it has been shown that pBAE/pDNA nanoparticles made of novel polycations containing terminal oligopeptides, known as Oligopeptide-modified pBAEs (OM-pBAEs) achieve better DNA encapsulation, cellular viability and higher transfection efficacy than other end-modified pBAEs and commercial transfection agents. This led to the use of OM-pBAEs for different applications including: a) to generate human induced pluripotent stem cells (iPS) from human fibroblasts avoiding the use of viral vectors[92]; b) to boost the efficacy of systemic oncolytic adenovirus administration[93] and c) to enable targeting of mRNA to Antigen Presenting Cells (APC) by choosing appropriate end-modifications of the pBAEs[94].

Due to the advantages of OM-pBAEs, specially their suitability and successful use as gene delivery vectors for cell modification and their versatility in terms of cell localization, OM-pBAE-based NPs will be the tool that will be here used to unbox cells. Then, as described in chapter I, the addition of SPIONs or gold nanoparticles to these OM-pBAE-based NPs will be employed to analyze how differences in the structure of the nanoparticles affect intra and inter cellular processes related to cell uptake and transfection. That is, taking advantage of their biocompatibility[69,95], the possibility of functionalizing them[96,97] and their ability to enter cells[98,99], SPIONs and gold nanoparticles will be used as detailed hereinafter to monitor the effect of OM-pBAE-based NPs in autophagy – an intracellular process – and exosomes production – an inter and intracellular one. Once nanoparticles have undergone cell endocytosis (see Chapter III), they find themselves in the complex and constantly changing environment of the inside of a cell. Besides the main intracellular route that endocytosed nanoparticles go through – briefly, the maturation from endosomes that leads to either lysosomal degradation or endosomal escaping and therefore release of their cargo to the cell cytosol – autophagy and exosomes production might shift or disrupt the predetermined course of such particles.

There are three types of autophagy (macroautophagy, microautophagy, and chaperone-mediated autophagy), being macroautophagy the most extensively studied. Macroautophagy (referred to hereafter as autophagy) is a major intracellular degradation pathway essential for cellular and energy homoeostasis. It is involved in the clearance of misfolded proteins and damaged organelles, as well as recycling of cytosolic components during starvation to compensate for nutrient deprivation. Autophagy

pathways are conserved from yeast to mammals and are mediated by a special organelle termed the autophagosome. This process is regulated by mTOR (mammalian target of rapamycin)-dependent and mTOR-independent pathways that are amenable to chemical perturbations[100]. As an essential process to maintain cellular homeostasis and functions, autophagy is responsible for the lysosome-mediated degradation of damaged proteins and organelles, and thus misregulation of autophagy can result in a variety of pathological conditions in human beings. In recent years, an increasing number of studies have shed light on the importance of autophagy in a wide range of physiological processes and human diseases[101].

Autophagy is a genetically regulated and dynamic process associated with the formation of autophagosome, a double-membrane cytoplasmic vesicle that engulfs cellular components. The autophagosome formation starts at phagophore (also known as isolation membrane or sequestering membrane) and requires the conjugation of microtubule-associated protein 1 light chain 3 (LC3), which is the major structural protein of autophagosomes and regulates the phagophore expansion and completion of the sequestering vesicle[102]. This protein, which is a mammalian homolog of yeast Atg8, serves as a marker to follow autophagy in cells[103–105]. The completed autophagosome then fuses with lysosome, becoming autolysosome. Finally, sequestered components are degraded by lysosomal hydrolases and released into the cytosol by lysosomal efflux permeases (Figure 5).

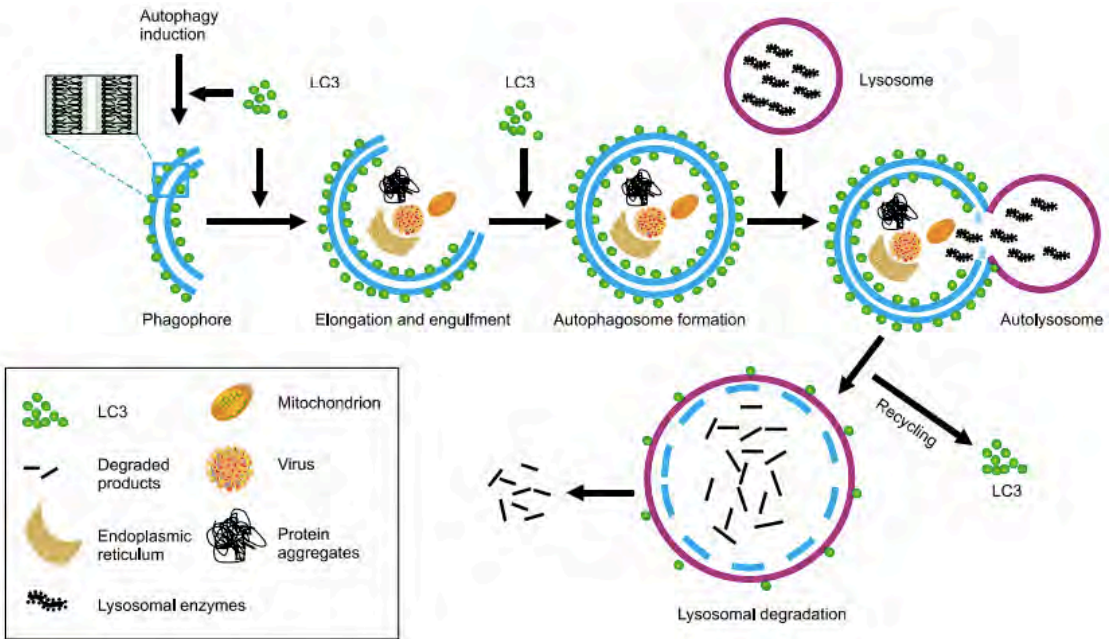

Figure 5. Schematic autophagic progression[101]**.** Upon induction, a small vesicular sac called the isolation membrane or phagophore elongates and subsequently encloses a portion of cytoplasm, which results in the formation of a double-membraned structure, the autophagosome. LC3 conjugates to the sequestering membrane and controls the elongation of phagophore. Then, the outer membrane of the autophagosome fuses with a lysosome to form an autolysosome, leading to the degradation of the enclosed materials together with the inner autophagosomal membrane. Lysosomal hydrolases degrade the cargo together with the inner membrane of autophagosome, and LC3 from the outer membrane as well as the autophagy-derived nutrients are recycled.

Under physiological conditions, autophagy has a number of vital roles such as maintenance of the amino acid pool during starvation, preimplantation development, prevention of neurodegeneration, antiaging, tumor suppression, clearance of intracellular microbes, and regulation of innate and adaptive immunity[106–110]. One of the characteristic features of autophagy is its dynamic regulation; cellular autophagic activity is usually low under basal conditions but can be markedly upregulated by numerous stimuli. The most well-known inducer of autophagy is nutrient starvation, both in cultured cells and in intact organisms, ranging from yeast to mammals. Besides starvation, autophagy can also be activated by other physiological stress stimuli (e.g., hypoxia, energy depletion, endoplasmic reticulum stress, high temperature, and high-density conditions), hormonal stimulation, pharmacological agents (e.g., rapamycin), innate immune signals, and in diseases such as bacterial, viral, and parasitic infections, acute pancreatitis, heart disease, and protein aggregopathies. Conversely, autophagy suppression is often associated with certain diseases, including a subset of cancers, neurodegenerative disorders, infectious diseases, and a decline in autophagy function is a common feature of aging. Given this strong association between autophagy and

different physiological and pathophysiological processes, there is an increasing need for scientific methods in autophagy research that reliably determine (1) whether autophagy is present, upregulated, or suppressed in a given biological context and (2) whether (and how) basal autophagy and/or modified autophagy contribute mechanistically to the physiological or pathophysiological process under investigation[35].

Depending on the different cellular contexts and stimuli, the outcome of autophagy can promote either cell survival or cell death. However, the mechanisms underlying the dual role for autophagy in deciding the destiny of cells remain unclear. On one hand, since autophagy provides cells with nutrients and eliminates damaged organelles, it is primarily believed to function as a protective mechanism for cell survival, particularly under unfavorable conditions. Indeed, cytotoxic drugs often trigger autophagy activation, and autophagy inhibition has been reported to potentiate apoptotic cell death induced by several anticancer drugs[111,112]. Nevertheless, autophagy impairment can also block or delay the development of cell death[113–115], and in some instances, autophagy itself is capable of inducing cell death[116,117].

Recent reports have suggested that some carriers used for gene delivery can activate autophagy, but this has not been studied in detail. These studies have shown that polyplex uptake can increase autophagosome formation in cells, and that polyplexes are sequestered in autophagosomes, a suspected non-productive destination that prevents nuclear transport[103,118,119]. OM-pBAEs could tentatively be sequestered by autophagosomes, thus hindering their efficacy. While the mechanism for this phenomenon has not been determined, the Yang group proposes that mTOR-independent autophagosomes, rather than mTOR-dependent ones, are responsible for polyplex sequestration and reduced transfection efficiency[120]. In addition, cationic polyplexes, such as OM-pBAEs, colocalize with autophagosome markers[121], and autophagosomes can be induced by liposomes[118] and calcium phosphate precipitates used for DNA transfection[122,123]. Similarly, it has been reported that cationic non-viral vectors activate autophagy and generate autophagosomes as they enter cells by endocytosis. The endosomes containing cationic carriers fuse with autophagosomes and generate large tubulovesicular structures containing the autophagosome structural protein, LC3. Importantly, reporter gene expression increased up to 10-fold in cells unable to make autophagosomes. Hence, autophagosome capture can be considered as a new barrier to gene delivery where tubulovesicular autophagosomes, rather than endosomes, slow transfer of nucleic acids to the cytosol[103].

Considering all this knowledge on autophagy, the understanding of nanoparticles' fate might be partially achieved. However, in order to have a full insight into the cellular mechanisms influencing the course of endocytosed nanoparticles, the research on exosomes production is also required.

As mentioned in chapter I, recent studies have reported shared molecular machinery as well as substantial crosstalk between autophagy and exosome biogenesis. In some situations, cells remove their unwanted or damaged material through their release to the extracellular environment as exosomes. Since exosomes can be transferred from one cell to another, secretion of unwanted material to the extracellular environment in exosomes may have an impact, which can be beneficial or detrimental, in neighboring cells[62]. Therefore, besides the degradative route of autophagy, increasing evidence underscores a role for exosomes in the selective secretion of damaged proteins and genetic material and thus in the maintenance of cellular fitness.

Exosomes are small vesicles that are released by almost every cell type to the extracellular environment. Contrary to other types of extracellular vesicles, exosomes have endocytic origin and are formed as intraluminal vesicles (ILVs) by fusion of the limiting membrane of late endosomes or multivesicular bodies (MVBs)[124–126]. Exosome secretion occurs in a constitutive manner although cellular stress or activation signals modulate their secretion[127]. Exosomes carry specific repertoires of proteins and nucleic acids in the form of mRNAs and small non-coding RNAs, including microRNAs, and are considered an unconventional secretory pathway. Exosomes can transfer their content to neighboring cells and regulate at a distance the properties of receptor cells[128]. Consequently, exosomes have been found to play a role in intercellular communication in several physiological processes, and contribute to organism development, immune responses, neuronal communication, and tissue repair[129–132]. However, exosomes may also participate in some pathological disorders, favoring tumor progression[133] or virus spreading[134]. Additionally, given that exosomes carry damaged cellular material targeted for destruction, they facilitate the spreading of toxic forms of aggregated proteins such as α-synuclein, β-amyloid, and prion proteins and thus contribute to the progression of neurodegenerative diseases[48]. Alluding to their nanometric size and inherent biological role[61], compelling evidence indicates that exosomes can be utilized as a novel nanoscale delivery platform for gene therapy[135], as well as a diagnostic tool for biomarkers of disease[136]. This dual functionality of therapeutics and diagnostics is termed "theranostics", and is an emerging field of nanomedicine[51].

According to the most recent findings, these classical exosome markers include the transmembrane protein tetraspanins CD9, CD63 and CD81, and other proteins such as TSG101 and syntenin-1[137]. In the present work, CD9 has been employed as exosomes marker. The transmembrane proteins and ligands on the exosomes surface likely promote tissue-specific endocytosis. In particular, their intrinsic features, such as stability, immunotolerance in circulation systems, capacity to cross natural barriers, and inherent targeting properties, are beneficial for them to work as drug carriers. On the one hand, exosomes derived from certain cell types are intrinsically therapeutic. Mesenchymal stem cell (MSC)-derived exosomes still possess certain functions of the parent MSCs and work through paracrine signaling to promote the repair of damaged tissues, such as skeletal muscle regeneration and brain damage recovery[138,139]. Moreover, exosomes possess better biocompatibility than their progenitor cells. Unlike engrafted stem cells, exosomes circumvent the shortcomings of limited survival and the reduced regenerative capacity caused by immune-mediated rejection[140]. Considering all these features, it will be studied hereafter if the presence of either polyplexes, metallic particles or both elements together upregulate or downregulate the exosome biogenesis and if these gene delivery systems are cleared from cells by exosomes.

The crosstalk between autophagy and exosome biogenesis is largely context dependent. Autophagy and exosome release offer some functional redundancy in eliminating unwanted proteins whereby each route may compensate for a deficiency in the other. Defective MVBs and their contents may be subject to autophagic degradation, and inhibition of autophagy may rescue exosome release from MVBs that would otherwise be degraded[141] (Figure 6). Alternatively, exosome release and autophagy may act in concert to counter cellular stress[142]. Finally, failure to release exosomes can also lead to the redirection of MVBs to autophagic degradation.

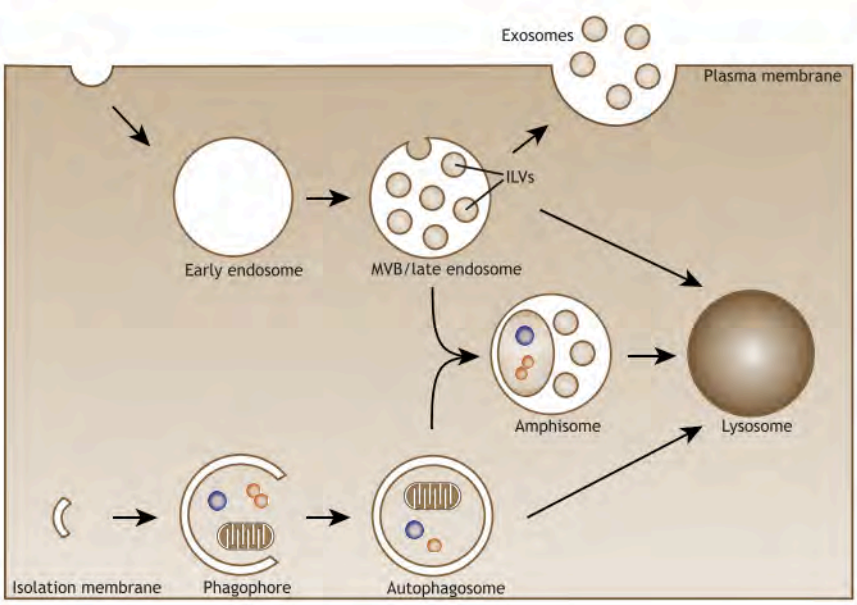

Figure 6. Scheme of the endocytic pathway, autophagy and exosome biogenesis[41]**.** The maturation of early endosomes gives rise to multivesicular bodies (MVBs), late endocytic compartments containing intraluminal vesicles (ILVs). Fusion of MVBs with the plasma membrane results in the release of ILVs into the extracellular space as exosomes. Autophagy starts with the nucleation and expansion of phagophores, which engulf cytoplasmic proteins and organelles. Sealing of the double-membraned phagophores results in the formation of autophagosomes, which subsequently fuse with lysosomes to degrade engulfed contents. Alternatively, autophagosomes can fuse with MVBs to form hybrid organelles termed amphisomes, which are believed to eventually fuse with lysosomes.

Once the importance of both autophagy and exosome release processes has been acknowledged, in the present chapter a monitoring of the expression levels of LC3 and CD9 markers over time is proposed. The effect of OM-pBAE NPs and the role of metallic components as part of these systems in the autophagy and exosomes production processes will be studied using confocal microscopy on HeLa tumoral cells. The aim of this chapter is to give insight into the interplay between autophagy and exosome biogenesis in relationship with cell uptake and transfection.

2.2 Aims

Considering the need for thorough and systematic studies regarding the intracellular and intercellular mechanisms involved in cell uptake and transfection of nanoparticles that has been detailed in the introduction, the main objective of this chapter is to give insight into the effect of exosomes production and autophagy processes on OM-PBAEs-based NPs uptake and transfection. These processes are contextualized in Figure 7.

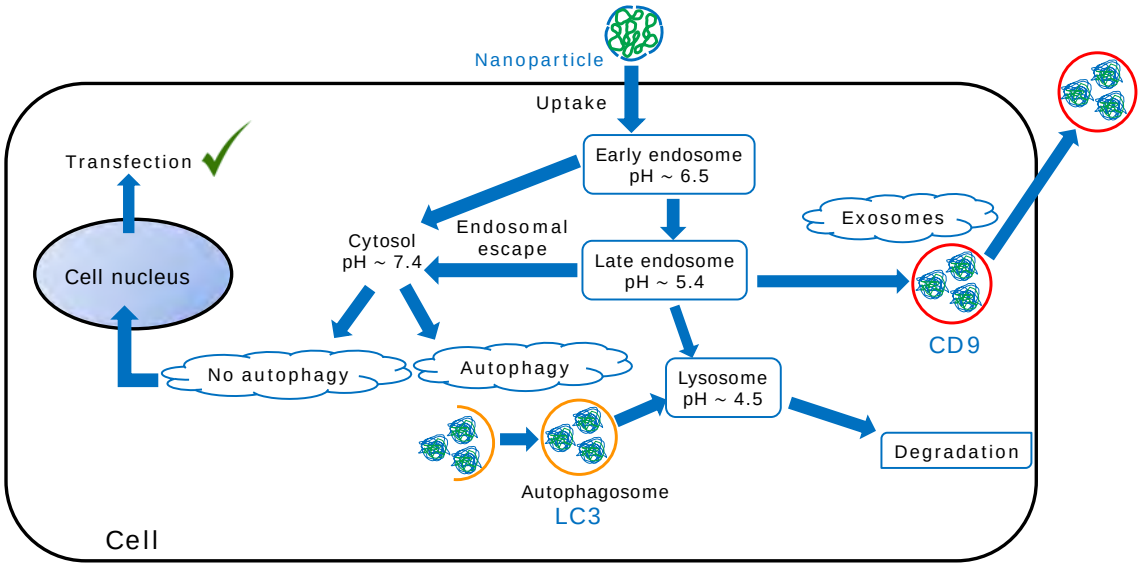

Figure 7. Schematic representation of the cell processes with an impact on cell transfection. After cell uptake, the regular endocytic pathway can lead to the degradation of the gene delivery system. If the nanoparticle is able to escape from endosomes to the cytosol, it can deliver its genetic cargo to the cell nucleus and effectively transfect the cell. However, the alternative maturation of endosomes into exosomes and the degradative route of autophagy can prevent this to happen.

In order to achieve this objective, the following goals were proposed:

- Systemize a feasible method to incorporate metallic particles into OM-pBAE based nanoparticles for cell usage.
- Find a valid methodology to monitor the basal levels of exosomes production and autophagosomes formation in HeLa cells.
- Give insight into the effect caused by nanoparticles on autophagy and exosomes production.
- Use different nanoparticles to analyze changes in the levels of exosomes production and autophagosomes formation in HeLa cells.

- Unravel the relationship between the cell processes of uptake, autophagy exosomes production and cell transfection.

2.3 Materials and Methods

2.3.1 Materials

Reagents and solvents used in the present chapter, including gold chloride trihidrate ($HAuCl_4 \cdot 3H_2O$) and trisodium citrate ($Na_3C_6H_5O_7$), were purchased from Sigma-Aldrich. Plasmid pmaxGFP (3486 bp) was obtained from Amaxa. CR3 (NH2−Cys−Arg−Arg−Arg−COOH) peptide was obtained from GL Biochem Ltd (Shangai). DMSA-coated SPIONs (hydrodynamic size = 45 nm; surface charge = -12 mV; stock SPIONs dispersion, dispersed in water as the dispersant) were performed by Unit 9 of the Plataform of Production of Biomaterials and Nanoparticles of the NANBIOSIS ICTS, by the *Superfícies y Partículas Nanoestructuradas del Instituto de Nanociencia de Aragón* (PI J. Santamaría) group[143,144]. Gold nanoparticles were synthetized as described below. HeLa cells were obtained from the American Type Culture Collection (ATCC, Manassas, VA). Products for cell culture (media, PBS, glutamine, penicillin-streptomycin solution) were obtained from Gibco and Hyclone. Fluoromount^{TM} was obtained from Sigma-Aldrich. Antibodies were obtained from Abcam, Biolegend and Thermo Fisher Scientific, as detailed in Tables Table 1 and Table 2. Glass slides and coverslips for confocal microscopy were purchased from Corning.

2.3.2 Synthesis of spherical gold nanoparticles

Citrate capped Gold NPs (AuNPs) were synthetized as previously described[145]. Briefly, 50 mL of a 0.25 mM solution of $HAuCl_4 \bullet 3H_2O$ was brought to boil with the subsequent addition of 1 mL of trisodium citrate at 6.8 mM. The solution was left to boil for 15 min under vigorous stirring and cooled down until room temperature was reached.

2.3.3 Synthesis of C6-pBAE nanoparticles

Apart from the three different approaches to form SPION-containing nanoparticles that are detailed in following chapters, pDNA/pBAE nanoparticles (without any metallic component) were employed as controls in most of the experiments of this work. First, oligopeptide-modified Poly(β-amino ester)s (OM-pBAEs) were synthesized following a two-step procedure as described by Segovia *et al*.[9]. Then, these polyplexes (also referred to as NPs) were prepared following Dosta et al., protocol[91]. In this chapter, only

C6 backbone was used (see Figure 8) with Cys +3 Arg (referred to as CR3 hereinafter) as terminal peptides in both edges. A mixture of 99% (v/v) C6CR3 and 1% (v/v) of C6CR3 labelled with Cyanine 5 (Cy5) was used for confocal microscopy samples. Polymer characterization is presented in our previous publications[9,91,94]. In brief, NPs were prepared at a 25/1 C6CR3/pDNA weight ratio, by mixing equal volumes of pDNA at 1 mg mL^{-1} with the polymer at 100 mg mL^{-1}, in 25 mM sodium acetate (AcONa) buffer solution. The pDNA was added over the polymer solution and mixed by pipetting, followed by 30 min incubation at 25 ºC. For the formation of discrete structures, this mixture was diluted in a 20-fold volume of serum-free Dulbecco's Modified Eagle Medium (DMEM, 4.5 g glucose mL^{-1} without glutamine, pH = 7.2) prior to each transfection or in a 10-fold volume of Phosphate Buffer Saline (PBS, 1X, pH = 7.4) prior to its physicochemical characterization.

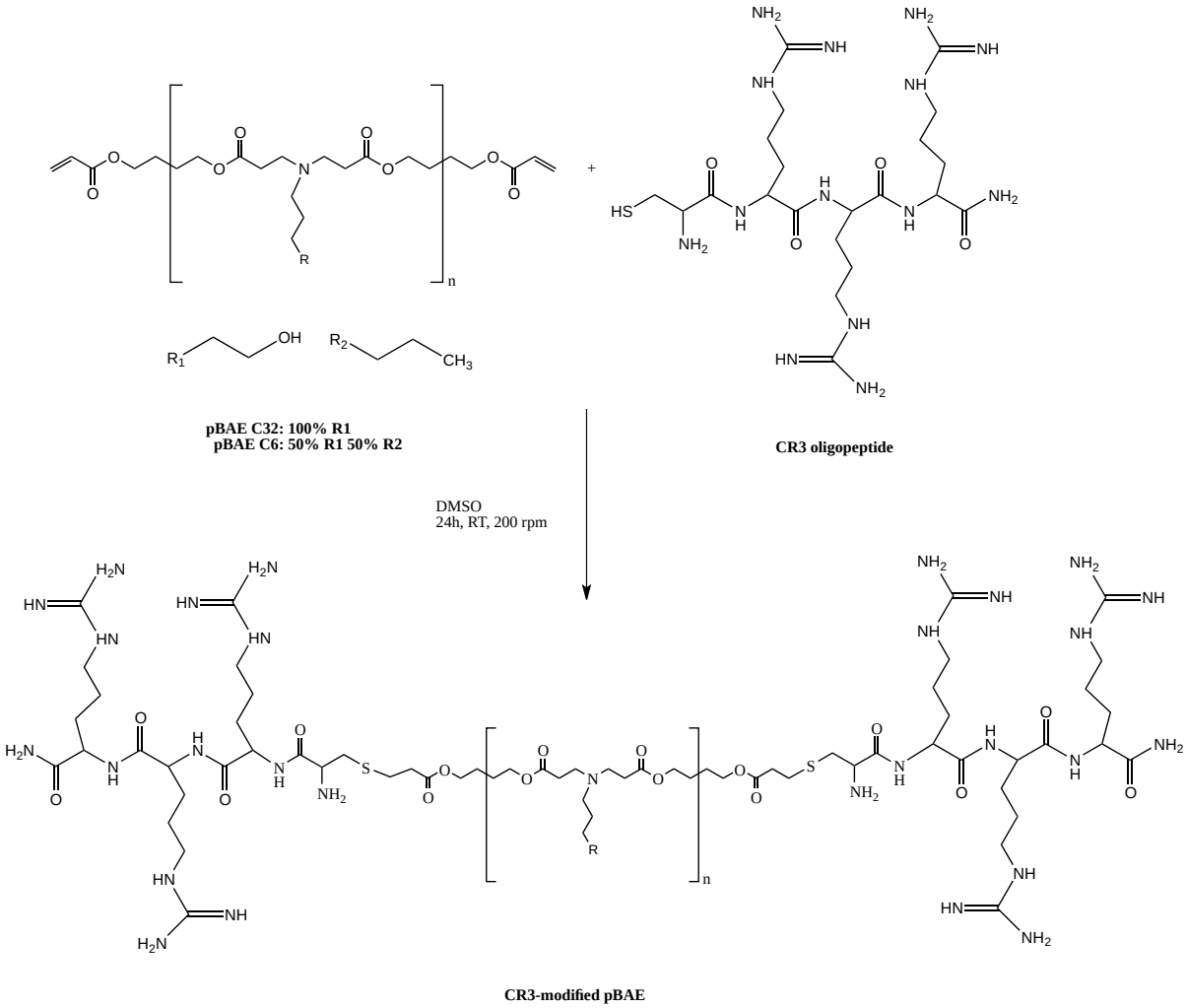

Figure 8. Chemical structure of C32CR3 and C6CR3 OM-pBAEs, indicating the C32 and C6 initial polymers reacting with the CR3 peptide.

2.3.4 Manufacturing of SPION and AuNP-containing pBAE NPs

Three types of SPION-containing nanoparticles have been formed and tested, as detailed in chapter IV. In the present chapter, only nanoparticles where the DNA is encapsulated by the polymer and then SPIONs are added to the solution, named "S" (separated) were used. The same "S"-type OM-pBAE nanoparticles – adding AuNPs to the polyplexes instead of SPIONs – were prepared using spherical gold nanoparticles. These nanoparticles were freshly prepared in sodium acetate buffer solution (25 mM, pH = 5.5) and incubated for 30 minutes at 25 ºC. Then they were nanoprecipitated in serum-free Dulbecco's Modified Eagle Medium (DMEM, 4.5 g glucose mL^{-1} without glutamine, pH = 7.2) prior to each transfection or in Phosphate Buffer Saline (PBS, 1X, pH = 7.4) prior to its DLS analysis. The complexes polymer:DNA:SPIONs or AuNPs were synthetized mixing equal volumes of polymer solution with DNA and/or SPIONs or AuNPs solution at different ratios.

The synthesis of 50 µL of S-type C6-CR3:pGFP (25:1) SPION-containing nanoparticles at 5 µg of SPIONs mL^{-1} is described in detail as an example: One Eppendorf was prepared with 25 µL of pGFP DNA solution in Sodium Acetate buffer 25 mM to get a concentration of $3*10^{-2}$ µg of DNA μL^{-1}. Another Eppendorf was prepared using 0.38 µL of C6-CR3 at 100 mg mL^{-1} diluted in Sodium Acetate buffer 25 mM at 25 µL final volume. The Eppendorf containing the DNA solution was homogenized with a micropipette and its whole volume (25 µL) was added to the polymer solution Eppendorf, which had just been vortexed for 10 seconds. This mixture was incubated at 25 ºC for 30 minutes. Then, nanoparticles were further diluted 10 fold in PBS or DMEM and the necessary volume of SPIONs was added in order to have the final concentration of 5 µg of SPIONs mL^{-1}.

2.3.5 NP characterization

The morphology of AuNPs and SPIONs was determined by TEM (FEI Tecnai G2 at 100 kV) and CryoTEM (JEM-F200 at 200 kV), respectively. ImageJ was used to determine their size.

Characterization of OM-pBAE-metallic NP complexes and PC formation was determined by measuring the hydrodynamic diameter (D_H) with dynamic light scattering (DLS) and zeta (ζ) potential (Malvern Instruments Ltd., United Kingdom, 4-mW laser). All the measurements were performed at 25 °C with 30 s equilibrium time using a laser

wavelength of 633 nm. Correlation functions were collected at a scattering angle of 173°, and Malvern particle sizing software (DTS version 5.03) was used to determine the particle hydrodynamic size. The equipment was set to perform three measures, each of which consists of 10 cycles of measurements. The final size value of each sample was equivalent to the mean of these three measures ± standard deviation. The size distribution was given by the polydispersity index (PDI). The samples to analyze by DLS were prepared by diluting 100 µL of nanoparticle solution (in acetate buffer) in 1 mL of final volume of PBS 1X to simulate the cellular environment. The surface charge (ζ-potential) of the SPIONs/pBAE/DNA polyplexes was determined from the electrophoretic mobility by means of the Smoluchowski equation[146]. The ζ-potential measurements for each sample were performed in triplicates, and every measurement consisted in 20 cycles of an applied electric field. For these measures, 800 µL of the previously diluted nanoparticles was added into a ζ-potential cuvette.

The optical properties of AuNPs and SPIONs were characterized by UV-vis spectroscopy (Agilent Cary 5000 UV-Vis NIR). Starting concentration of the particles was determined by ICP-MS.

2.3.6 In vitro experiments for confocal imaging

2.3.6.1 HeLa cells

HeLa cells (ATCC CCL-2) are derived from a cervical cancer taken from a 31-years-old patient. Cells were thawed and cultured in polystyrene cell culture dishes (Thermo Fisher Scientific, Waltham, MA USA). Culture medium of HeLa cells was DMEM (4.5 g glucose mL^{-1} without glutamine, pH = 7.2) supplemented with 10% Fetal Bovine Serum (FBS, Hyclone, Utah USA), 1% penicillin/streptomycin mixture and the amino acid glutamine (2 mmol L^{-1}). Cells were grown on incubators at 37 ºC with 5% CO_2 atmosphere during successive passages. HeLa cells were always seeded 24 h before starting any experiment. Cells were cultured in 6 or 24 well-plates, using in each well sterile and previously treated with 0.1% gelatin coverslips.

2.3.6.2 Cell transfection

For a 24-well plate, the detailed procedure of transfection was as follows. Cells were seeded on the plate at a concentration of $4x10^4$ cells/cm^2. Seeded cells were incubated

at 37ºC in 5% CO_2 atmosphere for 24 h before transfection. OM-pBAEs/DNA nanoparticles, SPION-containing OM-pBAEs/DNA nanoparticles and AuNP-containing OM-pBAEs/DNA nanoparticles, were prepared as described above using pGFP. Polyplexes were nanoprecipitated and diluted in serum-free DMEM at a final concentration of 1.5 μg pGFP mL^{-1}. Then, cells were washed with PBS and 500 μL of the nanoparticles solution were added to each well at a final pGFP concentration of 1.8 μg/well. Cells were incubated using the different polyplexes or bare SPIONs or gold nanoparticles for different times (0.5, 3, 8 and 48 h, respectively) at 37 ºC in 5% CO_2 atmosphere. A negative control of untreated cells was also prepared for each time-point. Subsequently, transfection medium was removed, cells were washed with PBS 1X and fixed using a solution of formalin 10% for 20 minutes.

2.3.6.3 Immunostaining procedure for confocal imaging

Once cells were fixed, they were washed twice with PBS 1X. Then, they were permeabilized using a solution of 0.1% (v/v) Triton X-100 in PBS for 30 minutes at room temperature with soft shaking. After permeabilization and two PBS washes, the blocking was performed: a solution of 5 % (w/v) non-fat powdered milk in PBS-Tween (0.1%) was added to cells and they were placed in the shaker for 1 h at room temperature. Next, two washes with PBS were performed. Then, samples were incubated with the primary antibodies (Table 1) at a final concentration of 1 μg mL^{-1} in 5 % (w/v) non-fat powdered milk in PBS for 3 hours at room temperature. Next, two PBS washes were performed and samples were incubated in secondary antibodies (Table 2) solutions at a final concentration of 5 μg mL^{-1} in 5 % (w/v) non-fat powdered milk in PBS for 1 hour at room temperature and protected from light. Two washes with PBS 1X were then performed. Next, a DAPI solution at 1 μg mL^{-1} in PBS was added to cells. After 10 min at room temperature and protected from light, samples were gently washed twice using PBS. Finally, the mounting was performed (see Figure 9): a glass slide is prepared for each sample with 10 μL of Fluoromount^{TM}. Using tweezers, each coverslip was transferred from the well to a glass slide facing down. Applying a slight pressure with the tweezers on the coverslip, the excess of Fluoromount^{TM} was discarded. Finally, the edges of the coverslips were sealed using nail polish.

Table 1. Primary antibodies used for confocal imaging

Primary antibodies	*Description*	*Molecular weight*	*Reference*	*Brand*
CD9	Mouse monoclonal to CD9	24 kDa	312102	Biolegend
LC3	Rabbit polyclonal to LC3B	15 kDa	Ab51520	Abcam

Table 2. Secondary antibodies used for confocal imaging

Secondary antibodies	*Fluorescent label*	*Reference*	*Brand*
Rabbit anti-mouse	Alexa Fluor® 555	Ab150114	Abcam
Goat anti-rabbit	Alexa Fluor® 568	A-11011	Thermo Fisher Scientific

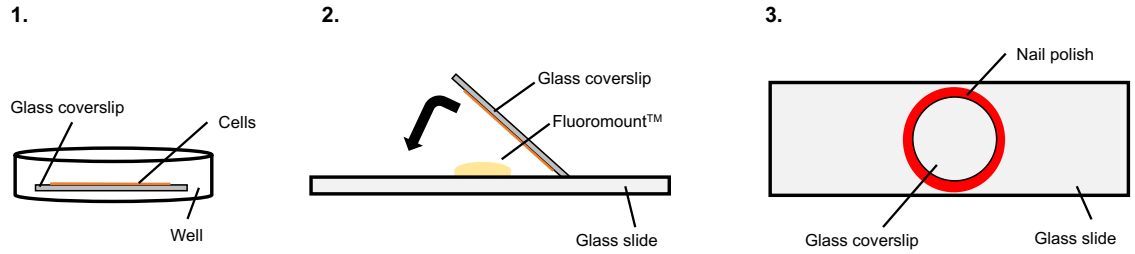

Figure 9. Schematic representation of the mounting procedure

2.3.6.4 Confocal imaging and image processing

Fluorescence confocal microscopy experiments were carried out using a Leica SP8 Lightning resonant-scanning confocal spectral microscope (Leica Microsystems Heidelberg, Manheim, Germany). For visualization of the cells, images were acquired using a HC PL APO CS2 40X/1.3 NA oil objective lens. The system is equipped with 4 long lasting diode lasers (405, 488, 561 and 638 nm) and 4 channel detection, including 2 standard PMT and 2 HyD detectors as well as a transmitted PMT detector for brightfield imaging. The application software for this equipment is LAS X. Images were processed and further analyzed using both LASX and FIJI software from ImageJ. The DAPI staining (excited by the 405 nm laser, maximum emission at 461 nm) was kept in all the images for cell nuclei localization.

2.4 Results and Discussion

2.4.1 Nanoparticle synthesis and characterization

Previous results from our group have shown that a slight increase in the pBAE polymer hydrophobicity (with a backbone called C6) increases its genetic material packaging capacity, stability, and transfection efficiency[147]. Acknowledging the usage and advantageous properties of C6R pBAE NPs from these previous studies, the addition of metallic components to these polyplexes was proposed in order to study differences on intracellular processes. The aim was to slightly modify a well-stablished and performing gene delivery system to investigate the role of each of its components when employed with cells. First, different ways to combine C6R polyplexes with metallic NPs were developed and characterized (described in chapter IV). In the present chapter, either DMSA-SPIONs or spherical gold nanoparticles were added to previously manufactured OM-pBAE NPs. These complexes were denominated S-type NPs.

Initially, the morphology of spherical citrate capped gold NPs (AuNPs) and DMSA-coated SPIONs was determined with TEM. Effective diameters were determined from these images using ImageJ software, resulting in mean hydrodynamic diameters of 18.8 ± 2.5 nm for AuNPs and 9.3 ± 0.9 nm for SPIONs (Figure 10A). The optical properties of the metallic particles were determined by UV-vis spectroscopy (Figure 10B). AuNPs showed a surface plasmon resonance (SPR) peak at 523 nm, which is in accordance with this NP size[148]. SPIONs lacked SPR.

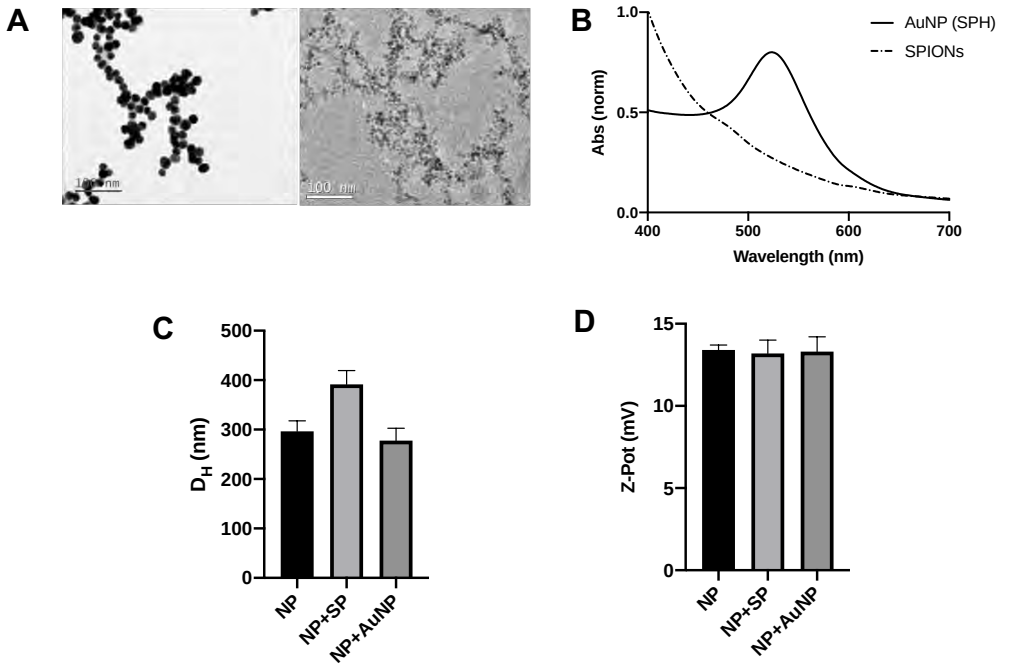

Figure 10. Characterization of the nanoparticles used in Chapter II.TEM images of AuNPs (left) and SPIONs (right). Scalebars = 100 mm.; (B) UV-vis spectra of AuNPs (SPH=spherical) and SPIONs; (C) Size of bare pBAE NPs (NP) and pBAE-NPs complexed with SPIONs (NP+SP) and AuNPs (NP+AuNP); (D) Zeta potential of the same samples.

Also, the polyplexes without metallic components (NP) and containing them (NP+SP and NP+AuNP) were synthetized as described in materials and methods section. Their successful formation was confirmed by DLS, where NPs showed a monodisperse solution with a hydrodynamic diameter (D_H) of 296.5 ± 21.3 nm, NPs with SPIONs of 391.6 ± 27.6 nm and NPs with AuNPs of 277.7 ± 25.1 nm (Figure 10C). Both NP+SP and NP+AuNP maintained a monodisperse NP profile and a constant PDI, confirming the proper formation of NP complexes as previously reported[149] (Table 3). Due to the oligopeptide used in this study (Cys-Arg-Arg-Arg), the OM-pBAE NPs rendered positively charged nanometric polyplexes with a Z-pot value of 13.4 ± 0.3 mV. The complexes of polyplexes and metallic components showed also a positive net charge of 13.2 ± 0.8 and 13.3 ± 0.9 mV for NP-SP and NP-SPH, respectively. This indicates that the addition of SPIONs and spherical gold nanoparticles to the previously formed OM-pBAE NPs is not quantitatively enough to obtain a complete monolayer around the polyplexes. As a consequence, the transfection systems used in this study retained the desired positive charge.

Table 3. Polidispersity Index (PDI) values for the complexes used in chapter II

	PDI
NP	0.209 ± 0.041
NP+SP	0.291 ± 0.021
NP+AuNP	0.150 ± 0.050

2.4.2 Basal autophagy and exosomes production levels in HeLa cells

Once the physicochemical properties of these complexes were proven to be compatible with cell internalization, HeLa cells were incubated with them in order to study alterations on cellular mechanisms. HeLa cells we chosen as they have shown high durability and versatility in research, and have been used for a broad range of applications such as drug discovery, study of viruses, and cancer research. They are the most widely used model cell line for studying human cellular and molecular biology.

Before using the nanoparticles, though, the basal levels of these cellular mechanisms had to be assessed. To do so, HeLa cells were seeded and 24 h later, they were incubated for different exposure times with regular cell medium. Afterwards, the immunostaining procedure was performed, and their autophagy and exosomes production basal levels were assessed. These samples were used as negative controls of untreated cells. CD9 and LC3 were labelled to monitor exosomes production and autophagy, respectively.

As shown in Figure 11, HeLa untreated cells showed a slight increase of CD9 signal intensity over time, with a peak at t = 8 h. On the other hand, the autophagy marker (LC3) showed a similar tendency, with an increase signal over time with the highest signal being at 8 h.

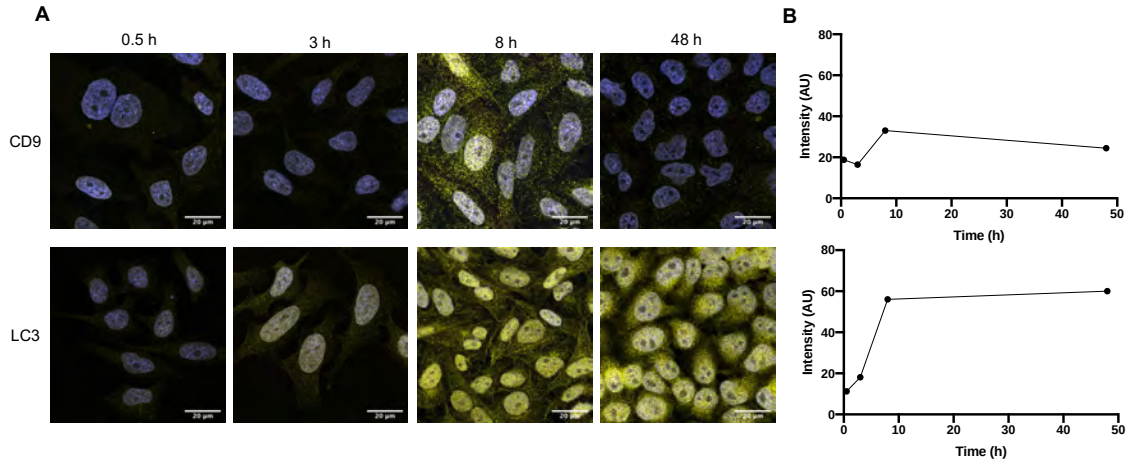

Figure 11. Basal levels of exosomes production and autophagy in HeLa cells at different timepoints. (A) Confocal images are the merge of DAPI staining channel (blue) and CD9 or LC3 channel (yellow). (B) Quantification of the CD9 or LC3 intensity. Scalebars = 20 µm

2.4.3 Assessing exosomes production and autophagy in HeLa cells

After studying the basal levels in untreated HeLa cells of CD9 and LC3 as markers of exosomes and autophagosomes, respectively, cells were incubated with different complexes in order to study variations on the expression of such markers.

HeLa cells were seeded as detailed in the Materials and Methods section and exposed to the samples detailed in Table 4 for different timepoints: 0.5 h was chosen as a short time point because in previous studies, internalization of NPs was already observed after 30 min; 3 h is a common incubation time for *in vitro* uptake studies with nanoparticles[150]; 8 h is an intermediate timepoint; and finally 48 h is the end-point for the expression analysis of genes encoded in a plasmid DNA, such as pGFP.

Table 4. Samples incubated in HeLa cells

Sample name	*Description*	*Polyplex*	*Metallic component*
NP	Standard C6-pBAE NPs (C6CR3 25:1 pGFP)	Yes	No
SP	SPIONs at 5 μg mL-1	No	Yes
NP+SP	pBAE NPs (C6CR3 25:1 pGFP) + SPIONs at 5 μg mL-1 (“S”-NPs)	Yes	Yes
AuNP	Spherical gold NPs at 5 μg mL-1	No	Yes
NP+AuNP	pBAE NPs (C6CR3 25:1 pGFP) + Spherical gold NPs at 5 μg mL-1 (“S”-NPs)	Yes	Yes

Then, after the immunohistochemistry procedure (detailed in Materials and Methods), samples were observed under the confocal fluorescent microscope and the intensity of the CD9 or LC3 markers was quantified (Figure 12 and Figure 13).

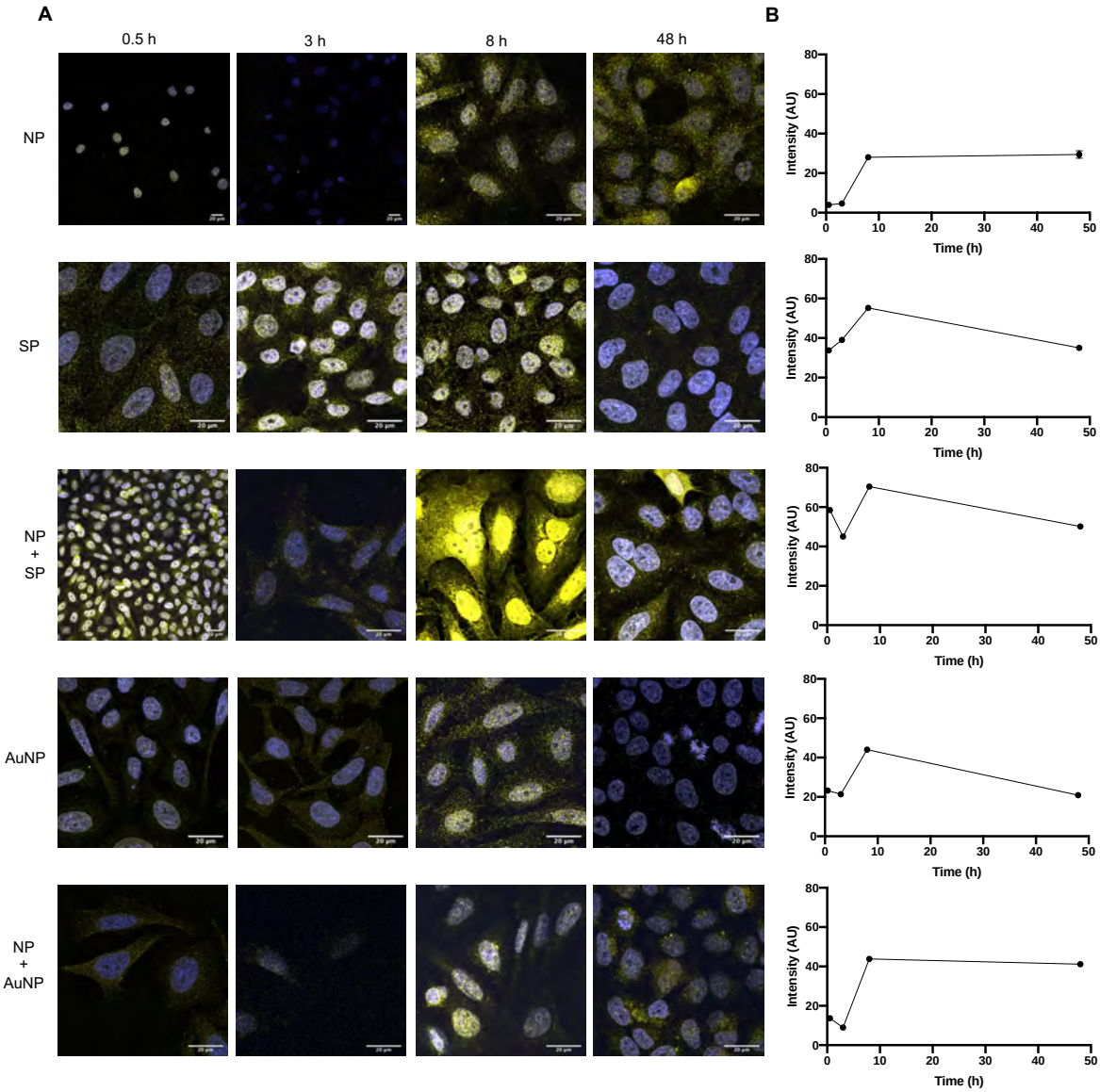

Figure 12. Exosomes production in HeLa cells in response to different nanoparticles at different timepoints. (A) Confocal images are the merge of DAPI staining channel (blue) and CD9 channel (yellow). (B) Quantifications of the CD9 intensity. Scalebars = 20 μm

Figure 12 shows a higher intensity of CD9 when cells were incubated with SPIONs, either in combination with polyplexes or alone, suggesting that SPIONs may trigger exosome biogenesis. However, no significant differences can be appreciated between the negative control of untreated cells (Figure 11) and the cells treated with pBAE-NPs in terms of exosomes production. Only at the longest exposure times (8 and 48 h), the CD9 signal was maintained when cells were exposed to NPs whereas in untreated cells it dropped slightly after 8 h. On the other hand, gold nanoparticles don't seem to have a significant impact on the expression levels of the exosome marker CD9.

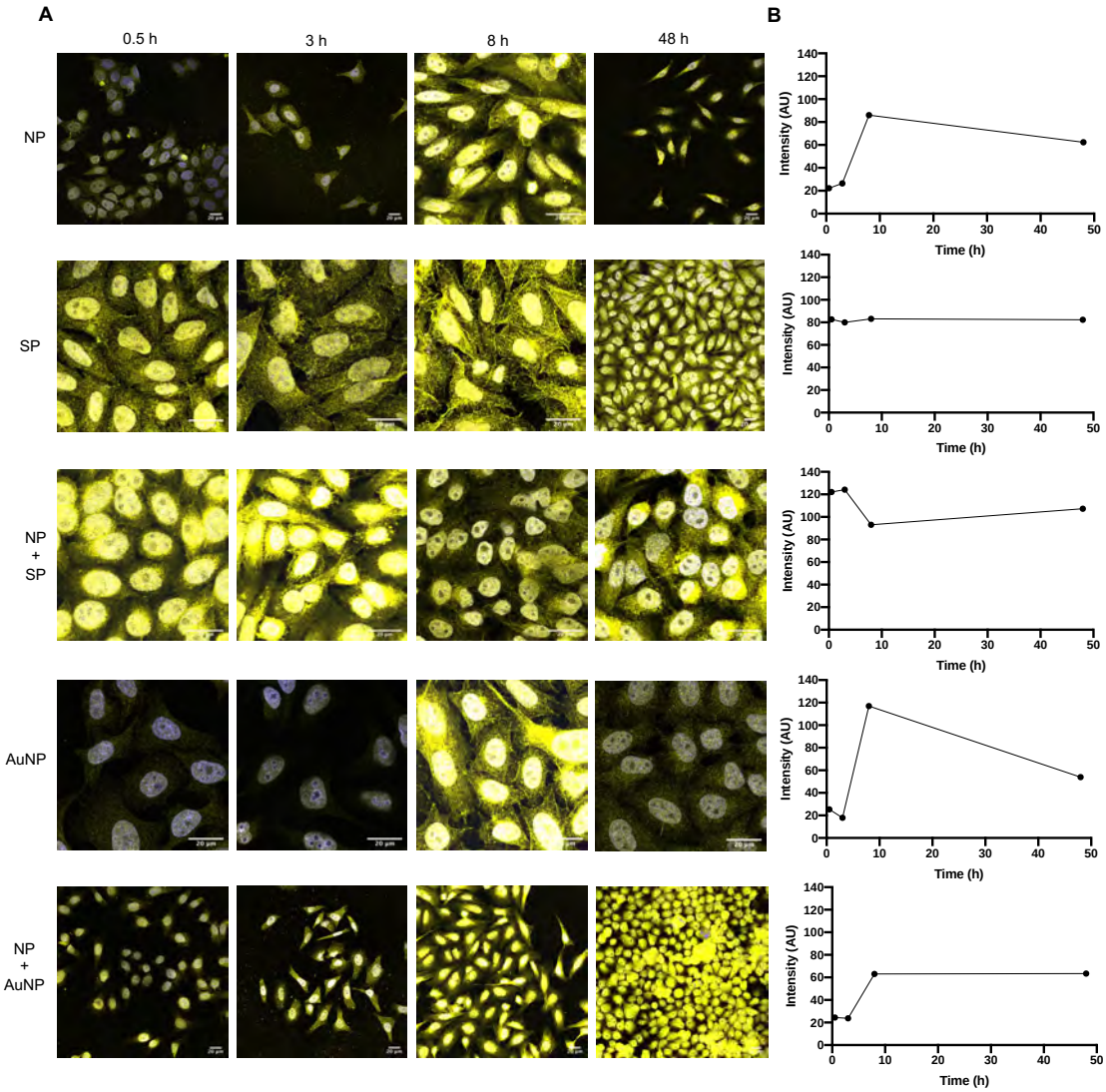

Figure 13. Autophagy in HeLa cells in response to different nanoparticles at different timepoints. (A) Confocal images are the merge of DAPI staining channel (blue) and LC3 channel (yellow). (B) Quantifications of the LC3 intensity. Scalebars = 20 µm

Regarding autophagy, Figure 13 shows that the presence of pBAE-NPs increased the intensity of LC3 marker at t = 8h. The presence of polyplex nanoparticles has been reported to increase autophagy markers[120]. Also, the presence of SPIONs in HeLa cells triggered the autophagy marker levels from time = 0.5 h. The high levels of LC3 were maintained over the different timepoints tested when SPIONs were present. This could be explained by the processes of ferroptosis and ferritinophagy. Ferroptosis is a novel form of programmed cell death characterized by a production of reactive oxygen species from accumulated iron and lipid peroxidation within cell membranes[151,152]. However, the relationship between autophagy and ferroptosis at the genetic level remains

unclear. Nuclear receptor coactivator 4 (NCOA4) mediated ferritinophagy is an autophagic phenomenon that specifically involves ferritin to release intracellular free iron and is a crucial mechanism to maintain iron homeostasis. Notably, ferritinophagy plays a central role in driving some pathological processes, including Parkinson's disease (PD) and urinary tract infections[153]. Therefore, the free-iron in cells induced by the presence of SPIONs may trigger this ferritinophagy in order to eliminate this excess of Fe. The fact that high levels of autophagy markers appeared from very short timepoints (t = 0.5h) is in accordance with the fact that in 30 min SPIONs are able to enter cells[154]. This fast increase in the cytoplasmic iron content might lead to the triggering of ferritinophagy from 30 min after cell incubation with SPIONs.

In the case of bare gold nanoparticles (AuNP) there is a peak of intensity at t = 8h, and the same peak maintained until 48 h time is found in the gold nanoparticles combined with polyplexes (AuNP+NP sample). At short timepoints, AuNPs samples showed much less intensity of signal than the SPIONs' ones. It has previously been reported that gold nanoparticles modulate autophagy in a shape-dependent manner[155]. Also, AuNP treatment can induce autophagosome accumulation and processing of LC3. Autophagosome accumulation may result from two opposite scenarios: autophagy activation (autophagosome formation) versus fusion blockage of autophagosomes and lysosomes (inhibition of autophagosome degradation), which implies a defective autophagy[156]. In the case of AuNPs, consistent previous studies showed that the autophagosome accumulation results from blockade of autophagy flux, rather than induction of autophagy[157].

In the light of these results, the following explanation was proposed: upon cell uptake, autophagy inhibits exosome release. That is, when autophagy level is high, multivesicular bodies (MVB) including exosomes are directed to the autophagic pathway with consequent degradation of their content and exosomes release becomes inhibited[158]. In the same vein, the low production of exosomes can be explained due to the damage caused to endosomes by the endosomal escape process, as already reported[159,160]. Since autophagy mediates the clearance of misfolded proteins and damaged organelles, the damaged endosomes may directly lead to autophagy activation. Therefore, the carrier materials – in this case the pBAEs – could be the cause of autophagy[120]. This activation of autophagy causes damaged endosomes to be self-digested (autophagocytosed) instead of maturing to exosomes. According to these explanations and the obtained results we could simplify this hypothesis using the following formula:

$$\boldsymbol{Cell\ uptake \longrightarrow \uparrow Autophagy \longrightarrow \downarrow Exosomes}$$

The balance between these three elements might be determinant for the fate of gene delivery systems thus dictating the overall result of a cell transfection experiment. That is, the uptake of nanoparticles can increase the endosomal escape, damaging the endosomes and causing the triggering of autophagic mechanisms. However, if the endosomal escape is greater than the autophagy, the system will be efficient in terms of cell transfection although having the autophagy rate increased. In parallel, this triggering of autophagy and endosomal escape will be a handicap for exosomes production. Figure 14 summarizes this hypothesis.

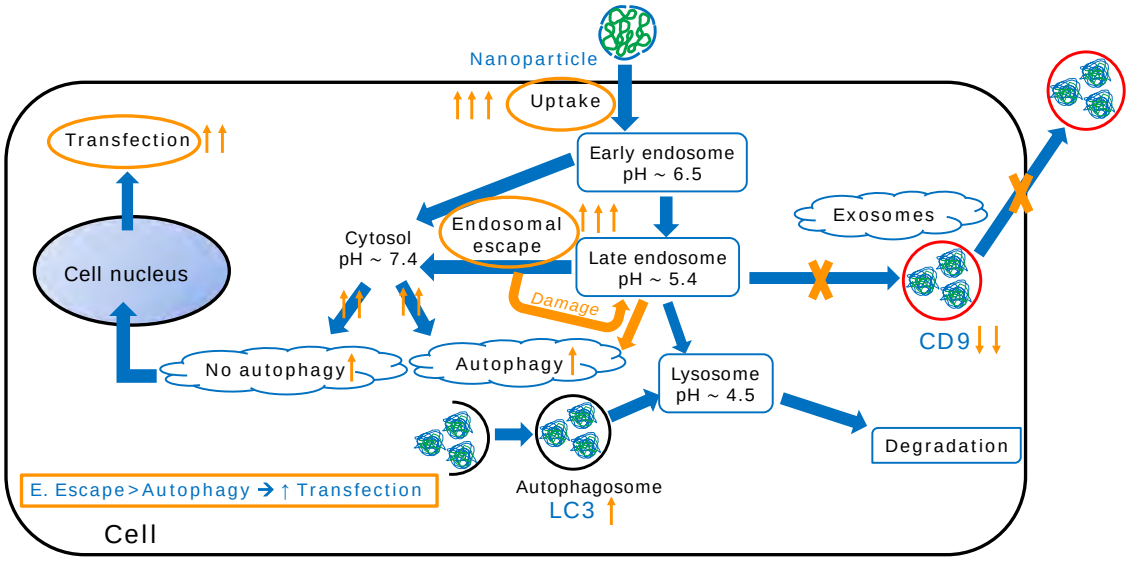

Figure 14. Schematic representation of the variations in the intra and intercellular processes with an impact on cell transfection. The balance between the upregulations and downregulations of these cell processes might rule the fate of gene delivery systems thus dictating the overall result of a cell transfection experiment.

Aimed at demonstrating this hypothesis, it was decided to study cell uptake and transfection using the cellular location of the polymer as an indicative of cell uptake of the polyplexes and the expression of GFP as a successful transfection indicator, respectively. In our group, the labeling of OM-pBAEs in order to track cell uptake has already been reported[94,161] and the use of GFP as reporter gene for pBAE polyplexes transfection efficacy has also been described[86,162]. This way, the whole picture of a cell transfection experiment was obtained.

2.4.4 Overall view of cell transfection

In order to obtain this broader view of the whole experiment, the localization of the four possible different dyes present in a single sample were monitored: DAPI for cell nucleus – expected in all samples; pBAE-Cy5 as an indicator of OM-pBAE-NPs that are internalized by cells – expected in samples with polyplexes and at any timepoint tested (0.5 to 48 h); GFP as a result of a successful transfection and therefore expression of the GFP reporter gene – expected only in samples with polyplexes and at t = 48 h (could be found also at t = 8h in a lesser extent); and CD9 or LC3 for exosomes or autophagosomes – likely in any sample but at unpredicted rates and amounts. As an example, Figure 15 and Figure 16 show confocal images that were taken using the four channels. Samples in these figures correspond to cells incubated with polyplexes at 48 h. In the last column it is displayed the merge of all channels.

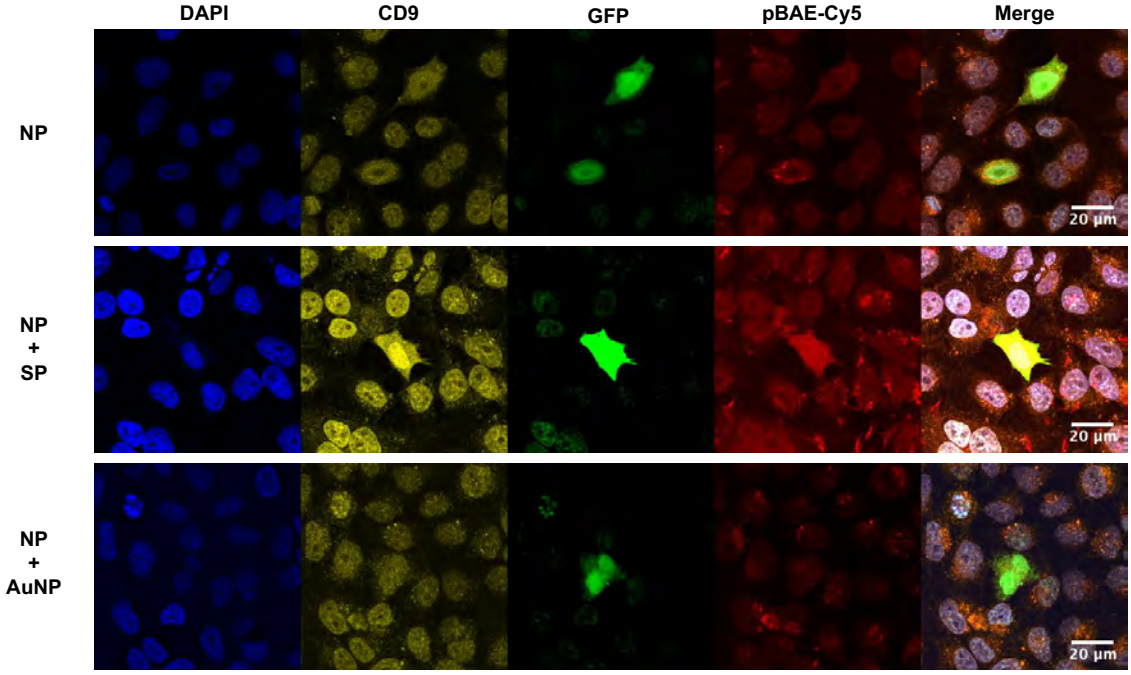

Figure 15. Confocal images of HeLa cells transfected with different polyplexes. Exosomes production was monitored through CD9 marker. Cells were exposed to the different nanoparticles for 48 h before fixation and immunostaining. NP= pBAE NPs (C6CR3 25:1 pGFP); pBAE NPs (C6CR3 25:1 pGFP) + SPIONs at 5 µg mL^{-1} ("S"-NPs); NP+AuNP = pBAE NPs (C6CR3 25:1 pGFP) + AuNPs at 5 µg mL^{-1} ("S"-NPs). Scalebars = 20 µm

As it can be observed in Figure 15, CD9 signal, and therefore exosomes, were detected all over the cells. The CD9 intensity was slightly higher in the case of polyplexes containing SPIONs than in the bare polyplexes (NP) or the polyplexes containing gold NPs (NP+AuNP). The GFP expression varied on its intensity among different samples

and cells, due to the different number of copies from the plasmid that were internalized and effectively transcribed and translated into GFP by each cell. The pBAE signal, despite showing some background signal could be appreciated forming accumulations (red dots). Therefore, after 48 h, the polymer remained at least partially inside cells.

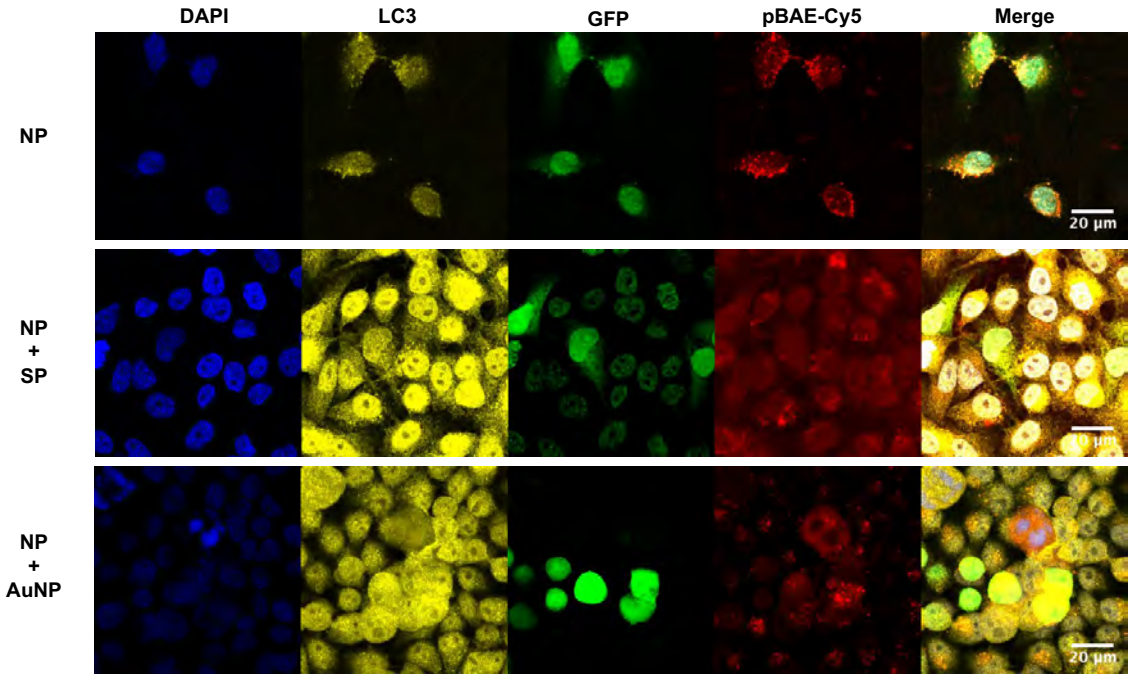

Figure 16. Confocal images of HeLa cells transfected with different polyplexes. Autophagy was monitored through LC3 marker. Cells were exposed to the different nanoparticles for 48 h before fixation and immunostaining. NP= pBAE NPs (C6CR3 25:1 pGFP); pBAE NPs (C6CR3 25:1 pGFP) + SPIONs at 5 µg mL^{-1} ("S"-NPs); NP+AuNP = pBAE NPs (C6CR3 25:1 pGFP) + AuNPs at 5 µg mL^{-1} ("S"-NPs). Scalebars = 20 µm

As it can be observed in Figure 16, the LC3 signal showed higher intensities when a metallic component was present (SP+NP and AuNP+NP samples) than in the case of bare C6R NPs (NP). The LC3 signal was found all over the cells. Again, the GFP intensity varieed among different cells, as expected. The OM-pBAE signal showed a light background noise but it was found forming accumulations close to the cell nuclei.

Given that the intensity of the different channels might difficult the elucidation of cell locations (see the last two columns from Figure 17), images deactivating one channel at a time were taken. For instance, the yellow channel (used to stain exosomes and autophagosomes) was deactivated and the DAPI, GFP and OM-pBAE-Cy5 channels were merged (first column Figure 17). By shutting off the yellow channel, a clearer visualization of the red OM-pBAE dots within the cells was obtained. It can be

appreciated than in effectively transfected (green) cells, OM-pBAE accumulations were close to the cell nucleus or even surrounding it. The vast majority of cells in the images showed red signal, thus indicating that pBAEs enter cells efficiently, as reported for OM-pBAE polyplexes[147].

In order to better study the colocalization of OM-pBAEs (in red) with autophagosomes or exosomes (in yellow), these two channels and the DAPI were merged, deactivating the GFP signal. As a result, it can be seen in the second and third columns of Figure 17 how in the case of polyplexes without metallic components (NP), the localization of the exosomes marker CD9 was mainly perinuclear but there were also yellow dots in different cell locations. Red dots corresponding to the OM-pBAE appeared in different cell regions. The same NP sample showed a clearly perinuclear localization of both the autophagosomes and the OM-pBAEs, which partially colocalized resulting in orange signals. In the case of cells treated with pBAE polyplexes containing SPIONs (NP+SP), the CD9 signal was spread all over the cells and pBAE red dots were mostly orange indicating colocalization with exosomes. Finally, cells incubated with pBAE polyplexes containing gold nanoparticles (NP+AuNP) showed orange dots indicating that pBAE accumulations also colocalize with exosomes (CD9). These dots were in general close to the cell nuclei. Exosomes without pBAEs were also present, in this case distributed all over the cells. Finally, the autophagosome signal (LC3) for this NP+AuNP sample showed higher intensity than that of pBAEs. However, several orange dots indicated perinuclear localization of pBAE and autophagosome accumulations. In conclusion, after 48 h, HeLa cells had either eliminated the polymer or it was trapped in exosomes or autophagosomes and, therefore, in its way to degradation or elimination from the cell.

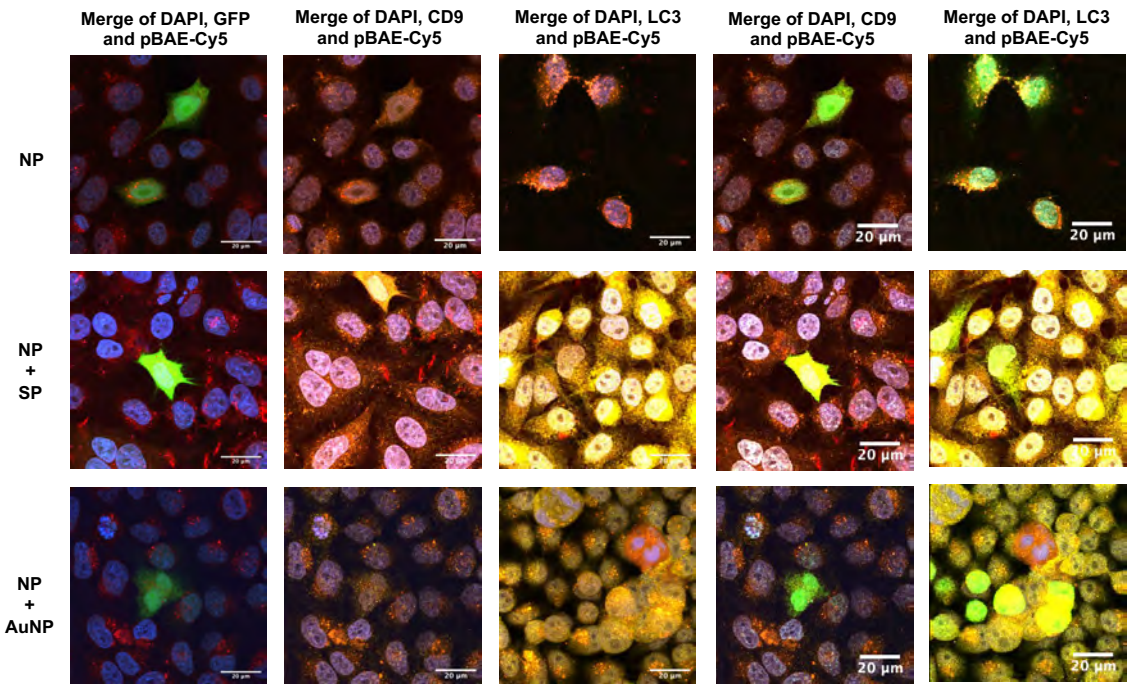

Figure 17. Confocal images of HeLa cells using different channel merges. Cells were exposed to the different nanoparticles for 48 h before fixation and immunostaining. NP= pBAE NPs (C6CR3 25:1 pGFP); pBAE NPs (C6CR3 25:1 pGFP) + SPIONs at 5 µg mL^{-1} ("S"-NPs); NP+AuNP = pBAE NPs (C6CR3 25:1 pGFP) + AuNPs at 5 µg mL^{-1} ("S"-NPs). Scalebars = 20 µm

In conclusion, it have been here studied both the intracellular trafficking of NPs and, in these final experiments, the cell location of Cy5-OM-pBAE as an indicator of the cell uptake of polyplexes and the expression of GFP as a successful transfection indicator. However, these results are insufficient to quantify the amount of internalized particles and to assess differences among different nanoparticles. For this reason, it will be necessary to examine in the following chapter the step preceding cell trafficking: cell endocytosis.

2.5 Concluding remarks

The results of this chapter prove the feasibility of adding SPIONs or gold nanoparticles to C6R polyplexes maintaining desirable physicochemical properties for cell usage. Complexes with hydrodynamic diameters between 277 and 392 nm were obtained. Their net charge remained positive, with values around 13 mV and the polydispersity index of the complexes remained below 0.3.

It has been validated the use of confocal microscopy as a technique to monitor the basal levels of exosomes production and autophagosomes in HeLa cells. Through this technique and the detailed samples preparation, microscope settings and image processing it has been possible to observe and analyze differences in the expression of CD9 and LC3 markers over time. HeLa cells showed low levels of CD9 and LC3 expression, although the LC3 autophagosomes marker signal increased over time.

After assessing the basal levels of expression of these two markers, it was then proposed to incubate HeLa cells with different nanoparticles and study possible changes in the expression of such markers. These nanoparticles included bare OM-pBAE polyplexes, OM-pBAE polyplexes combined with SPIONs or gold nanoparticles and these metallic nanoparticles without the polyplexes. Regarding the exosomes production, no significant changes in CD9 levels were appreciated. Only the presence of SPIONs, either with or without the polyplexes, increased the amount of exosomes in HeLa cells. But neither the presence of bare OM-pBAE polyplexes nor gold nanoparticles caused important changes in CD9 expression.

Regarding autophagy, levels of LC3 expression were definitely altered by the presence of SPIONs. The two samples containing SPIONs (SP and NP+SP) showed significantly higher levels of LC3 expression than the untreated cells. These increased signals were stable over the different timepoints analyzed, indicating that SPIONs do trigger autophagy mechanisms. The concepts of ferritinophagy and ferroptosis have been discussed as a tentative explanation on why these iron-based nanoparticles showed such an increase in autophagosome accumulation from very short exposure times (t = 0.5 h). The free-iron in cells induced by the presence of SPIONs might trigger the mechanism of ferritinophagy in order to eliminate this excess of Fe and maintain cellular iron homeostasis.

The presence of OM-pBAE-NPs slightly increased the intensity of LC3 signal, although no clear differences appeared as compared to the untreated cells. Also, in gold-containing samples (AuNP and NP+AuNP) LC3 levels increased lightly over time. In both

cases there was a peak of intensity at t = 8h, that was maintained until 48 h time in the case of gold nanoparticles combined with polyplexes (AuNP+NP sample).

According to these data, it has been proposed that the activation of autophagy inhibits exosome release through the redirection of exosomes to the autophagic flux with the consequent degradation of their cargo. Also, since gene delivery systems need to escape from endosomes when they are internalized by cells, the damage caused on endosomes by this escaping process causes the autophagy activation as it is a system to eliminate damaged organelles. That is, if endosomes are damaged and autophagocytosed by cells, they cannot mature to exosomes and therefore the exosomes production is decreased. The tentative explanation of what might happen when cells are transfected with polyplexes is that the uptake of such particles triggers autophagy hindering at the same time the exosomes production.

Finally, in order to have a broader view of the cells after a transfection procedure, the polymer was fluorescently labelled– as an indicative of cell uptake of the polyplexes – and the expression of GFP was used as a successful transfection indicator. The images combining different channels allowed the study of the colocalization of different markers and their intracellular localization. It has been observed that C6R colocalizes with both CD9 and LC3 markers at long times of exposure (48 h) in the different types of complexes tested. That might indicate that, after two days, the C6R molecules that remained inside cells were about to be eliminated via exosome release or autophagy and lysosomal degradation.

In conclusion, intra and intercellular mechanisms affecting NP cell trafficking and therefore overall cell transfection have been here studied. Also, the location of different markers within the cells have been employed as indicators of cell uptake of polyplexes and successful transfection. Since these results are indicative but do not provide a quantitative conclusion, in the following chapters quantifications of the cellular uptake and transfection of nanoparticles will be performed. Specifically, the next chapter addresses the step that precedes cell trafficking and that is indispensable for any cell trafficking to occur, named endocytosis. Focus will be shifted to the characteristics of the nanoparticles that affect their cellular internalization. Then, the presence of metallic components in the complexes will be employed to quantify their cell uptake. Finally, a study on the protein corona of such complexes will be performed and will allow for the identification of proteins that might be crucial to explain differences in cell uptake and transfection.

2.6 References

6. Kozielski, K. L., Tzeng, S. Y., Hurtado De Mendoza, B. A. & Green, J. J. Bioreducible cationic polymer-based nanoparticles for efficient and environmentally triggered cytoplasmic siRNA delivery to primary human brain cancer cells. *ACS Nano* **8**, 3232–3241 (2014).

7. Tzeng, S. Y. & Green, J. J. Subtle Changes to Polymer Structure and Degradation Mechanism Enable Highly Effective Nanoparticles for siRNA and DNA Delivery to Human Brain Cancer. *Adv. Healthc. Mater.* **2**, 468–480 (2013).

9. Segovia, N., Dosta, P., Cascante, A., Ramos, V. & Borrós, S. Oligopeptide-terminated poly(ß-amino ester)s for highly efficient gene delivery and intracellular localization. *Acta Biomater.* **10**, 2147–2158 (2014).

83. Zugates, G. T. *et al.* Gene delivery properties of end-modified poly(beta-amino ester)s. *Bioconjug. Chem.* **18**, 1887–1896 (2007).

84. Little, S. R. *et al.* Poly-beta amino ester-containing microparticles enhance the activity of nonviral genetic vaccines. *Proc. Natl. Acad. Sci. U. S. A.* **101**, 9534–9539 (2004).

85. Huang, Y. H. *et al.* Nanoparticle-delivered suicide gene therapy effectively reduces ovarian tumor burden in mice. *Cancer Res.* **69**, 6184–6191 (2009).

86. Sunshine, J. C., Sunshine, S. B., Bhutto, I., Handa, J. T. & Green, J. J. Poly(ß-amino ester)-nanoparticle mediated transfection of retinal pigment epithelial cells in vitro and in vivo. *PLoS One* **7**, (2012).

87. Jere, D. *et al.* Poly(β-amino ester) as a carrier for si/shRNA delivery in lung cancer cells. *Biomaterials* **29**, 2535–2547 (2008).

88. Green, J. J. *et al.* Nanoparticles for gene transfer to human embryonic stem cell colonies. *Nano Lett.* **8**, 3126–3130 (2008).

89. Yang, F. *et al.* Genetic engineering of human stem cells for enhanced angiogenesis using biodegradable polymeric nanoparticles. *Proc Natl Acad Sci U S A* **107**, 3317–3322 (2010).

90. Liu, Y., Li, Y., Keskin, D. & Shi, L. Poly(β-Amino Esters): Synthesis,

Formulations, and Their Biomedical Applications. *Adv. Healthc. Mater.* **8**, 1–24 (2019).

91. Dosta, P., Segovia, N., Cascante, A., Ramos, V. & Borrós, S. Surface charge tunability as a powerful strategy to control electrostatic interaction for high efficiency silencing, using tailored oligopeptide-modified poly(beta-amino ester)s (PBAEs). *Acta Biomater.* **20**, 82–93 (2015).

92. Montserrat, N. *et al.* Simple generation of human induced pluripotent stem cells using poly-β-amino esters as the non-viral gene delivery system. *J. Biol. Chem.* **286**, 12417–12428 (2011).

93. Brugada-Vilà, P. *et al.* Oligopeptide-modified poly(beta-amino ester)s-coated AdNuPARmE1A: Boosting the efficacy of intravenously administered therapeutic adenoviruses. *Theranostics* **10**, 2744–2758 (2020).

94. Fornaguera, C. *et al.* mRNA Delivery System for Targeting Antigen-Presenting Cells In Vivo. *Adv. Healthc. Mater.* **1800335**, 1800335 (2018).

95. Lachowicz, D. *et al.* Biocompatible and fluorescent superparamagnetic iron oxide nanoparticles with superior magnetic properties coated with charged polysaccharide derivatives. *Colloids Surfaces B Biointerfaces* (2016). doi:10.1016/j.colsurfb.2016.11.003

96. Mbeh, D. A. *et al.* Human alveolar epithelial cell responses to core-shell superparamagnetic iron oxide nanoparticles (spions). *Langmuir* **31**, 3829–3839 (2015).

97. Ding, Y. *et al.* Gold nanoparticles for nucleic acid delivery. *Mol. Ther.* **22**, 1075–83 (2014).

98. Wierzbinski, K. R. *et al.* Potential use of superparamagnetic iron oxide nanoparticles for in vitro and in vivo bioimaging of human myoblasts. *Sci. Rep.* **8**, 3682 (2018).

99. Elbakry, A. *et al.* Layer-by-layer assembled gold nanoparticles for siRNA delivery. *Nano Lett.* **9**, 2059–64 (2009).

100. Sarkar, S. Regulation of autophagy by mTOR-dependent and mTOR-independent pathways: Autophagy dysfunction in neurodegenerative diseases

and therapeutic application of autophagy enhancers. *Biochem. Soc. Trans.* **41**, 1103–1130 (2013).

101. Jing, K. & Lim, K. Why is autophagy important in human diseases? *Exp. Mol. Med.* **44**, 69–72 (2012).

102. Xie, Z., Nair, U. & Klionsky, D. J. Atg8 Controls Phagophore Expansion during Autophagosome Formation. *Mol. Biol. Cell* **19**, 3920–3928 (2008).

103. Roberts, R. *et al.* Autophagy and formation of tubulovesicular autophagosomes provide a barrier against nonviral gene delivery. *Autophagy* **9**, 667–682 (2013).

104. Kabeya, Y. *et al.* LC3, a mammalian homolog of yeast Apg8p, is localized in autophagosome membranes after processing. *EMBO J.* **22**, 4577 (2003).

105. Mizushima, N., Yamamoto, A., Matsui, M., Yoshimori, T. & Ohsumi, Y. In Vivo Analysis of Autophagy in Response to Nutrient Starvation Using Transgenic Mice Expressing a Fluorescent Autophagosome Marker. *Mol. Biol. Cell* **15**, 1101–1111 (2004).

106. Cecconi, F. & Levine, B. The Role of Autophagy in Mammalian Development: Cell Makeover Rather than Cell Death. *Dev. Cell* **15**, 344–357 (2008).

107. Deretic, V. & Levine, B. Autophagy, Immunity, and Microbial Adaptations. *Cell Host Microbe* **5**, 527–549 (2009).

108. Levine, B. & Kroemer, G. Autophagy in the Pathogenesis of Disease. *Cell* **132**, 27–42 (2008).

109. Mizushima, N., Levine, B., Cuervo, A. M. & Klionsky, D. J. Autophagy fights disease through cellular self-digestion. *Nature* **451**, 1069–1075 (2008).

110. Rubinsztein, D. C. The roles of intracellular protein-degradation pathways in neurodegeneration. *Nature* **443**, 780–786 (2006).

111. Amaravadi, R. K. *et al.* Autophagy inhibition enhances therapy-induced apoptosis in a. *J. Clin. Invest.* **117**, 326–336 (2007).

112. Song, K. S. *et al.* Rottlerin induces autophagy and apoptotic cell death through a PKC-δ-independent pathway in HT1080 human fibrosarcoma cells: The protective role of autophagy in apoptosis. *Autophagy* **4**, 650–658 (2008).

113. Berry, D. L. & Baehrecke, E. H. Growth Arrest and Autophagy Are Required for Salivary Gland Cell Degradation in Drosophila. *Cell* **131**, 1137–1148 (2007).

114. Yuk, J. M. *et al.* Bacillus calmette-guerin cell wall cytoskeleton enhances colon cancer radiosensitivity through autophagy. *Autophagy* **6**, 46–60 (2010).

115. Jing, K. *et al.* Docosahexaenoic acid induces autophagy through p53/AMPK/mTOR signaling and promotes apoptosis in human cancer cells harboring wild-type p53. *Autophagy* **7**, 1348–1358 (2011).

116. Shao, Y., Gao, Z., Marks, P. A. & Jiang, X. Apoptotic and autophagic cell death induced by histone deacetylase inhibitors. *Proc. Natl. Acad. Sci. U. S. A.* **101**, 18030–18035 (2004).

117. Yousefi, S. *et al.* Calpain-mediated cleavage of Atg5 switches autophagy to apoptosis. *Nat. Cell Biol.* **8**, 1124–1132 (2006).

118. Man, N., Chen, Y., Zheng, F., Zhou, W. & Wen, L. P. Induction of genuine autophagy by cationic lipids in mammalian cells. *Autophagy* **6**, 449–454 (2010).

119. Remaut, K., Oorschot, V., Braeckmans, K., Klumperman, J. & De Smedt, S. C. Lysosomal capturing of cytoplasmic injected nanoparticles by autophagy: An additional barrier to non viral gene delivery. *J. Control. Release* **195**, 29–36 (2014).

120. Song, W., Ma, Z., Zhang, Y. & Yang, C. Autophagy plays a dual role during intracellular siRNA delivery by lipoplex and polyplex nanoparticles. *Acta Biomater.* **58**, 196–204 (2017).

121. Vercauteren, D. *et al.* Dynamic colocalization microscopy to characterize intracellular trafficking of nanomedicines. *ACS Nano* **5**, 7874–7884 (2011).

122. Gao, W. *et al.* Biochemical isolation and characterization of the tubulovesicular LC3-positive autophagosomal compartment. *J. Biol. Chem.* **285**, 1371–1383 (2010).

123. Sarkar, S., Korolchuk, V., Renna, M., Winslow, A. & Rubinsztein, D. C. Methodological considerations for assessing autophagy modulators. *Autophagy* **5**, 307–313 (2009).

124. Théry, C., Zitvogel, L. & Amigorena, S. Exosomes: Composition, biogenesis and

function. *Nat. Rev. Immunol.* **2**, 569–579 (2002).

125. Hessvik, N. P. & Llorente, A. Current knowledge on exosome biogenesis and release. *Cell. Mol. Life Sci.* **75**, 193–208 (2018).

126. Gould, S. J., Booth, A. M. & Hildreth, J. E. K. The Trojan exosome hypothesis. *Proc. Natl. Acad. Sci. U. S. A.* **100**, 10592–10597 (2003).

127. Kooijmans, S. A. A., Schiffelers, R. M., Zarovni, N. & Vago, R. Modulation of tissue tropism and biological activity of exosomes and other extracellular vesicles: New nanotools for cancer treatment. *Pharmacol. Res.* **111**, 487–500 (2016).

128. Schiller, M. *et al.* Autoantigens are translocated into small apoptotic bodies during early stages of apoptosis. *Cell Death Differ.* **15**, 183–191 (2008).

129. Gregory, C. D. & Pound, J. D. Microenvironmental influences of apoptosis in vivo and in vitro. *Apoptosis* **15**, 1029–1049 (2010).

130. Johnstone, R. M. Revisiting the road to the discovery of exosomes. *Blood Cells, Mol. Dis.* **34**, 214–219 (2005).

131. Simons, M. & Raposo, G. Exosomes - vesicular carriers for intercellular communication. *Curr. Opin. Cell Biol.* **21**, 575–581 (2009).

132. Qin, J. & Xu, Q. Functions and applications of exosomes. *Acta Pol. Pharm.* **71**, 537–543 (2014).

133. Urbanelli, L. *et al.* Signaling pathways in exosomes biogenesis, secretion and fate. *Genes (Basel).* **4**, 152–170 (2013).

134. Katzmann, D. J., Odorizzi, G. & Emr, S. D. Receptor downregulation and multivesicular-body sorting. *Nat. Rev. Mol. Cell Biol.* **3**, 893–905 (2002).

135. Alvarez-Erviti, L. *et al.* Delivery of siRNA to the mouse brain by systemic injection of targeted exosomes. *Nat. Biotechnol.* **29**, 341–345 (2011).

136. Taylor, D. D. & Gercel-Taylor, C. MicroRNA signatures of tumor-derived exosomes as diagnostic biomarkers of ovarian cancer. *Gynecol. Oncol.* **110**, 13–21 (2008).

137. Kowal, J. *et al.* Proteomic comparison defines novel markers to characterize

heterogeneous populations of extracellular vesicle subtypes. *Proc. Natl. Acad. Sci. U. S. A.* **113**, E968–E977 (2016).

138. Nakamura, Y. *et al.* Mesenchymal-stem-cell-derived exosomes accelerate skeletal muscle regeneration. *FEBS Lett.* **589**, 1257–1265 (2015).

139. Joo, H. S., Suh, J. H., Lee, H. J., Bang, E. S. & Lee, J. M. Current knowledge and future perspectives on mesenchymal stem cell-derived exosomes as a new therapeutic agent. *Int. J. Mol. Sci.* **21**, (2020).

140. Lou, G., Chen, Z., Zheng, M. & Liu, Y. Mesenchymal stem cell-derived exosomes as a new therapeutic strategy for liver diseases. *Exp. Mol. Med.* **49**, (2017).

141. Villarroya-Beltri, C. *et al.* ISGylation controls exosome secretion by promoting lysosomal degradation of MVB proteins. *Nat. Commun.* **7**, (2016).

142. Kumar, D., Gupta, D., Shankar, S. & Srivastava, R. K. Biomolecular characterization of exosomes released from cancer stem cells: Possible implications for biomarker and treatment of cancer. *Oncotarget* **6**, 3280–3291 (2014).

143. Grilc, J. G. V. & Zadnlk, B. Extraction of Acetic Acid from Dilute Aqueous Solutions with Trioctylphosphine Oxide. *Ind. Eng. Chem. Process Des. Dev.* **20**, 433–435 (1981).

144. Roca, A. G. *et al.* Surface functionalization for tailoring the aggregation and magnetic behaviour of silica-coated iron oxide nanostructures. *Nanotechnology* **23**, (2012).

145. Turkevich, J., Stevenson, P. C. & Hillier, J. A study of the nucleation and growth processes in the synthesis of colloidal gold. *Discuss. Faraday Soc.* **11**, 55–75 (1951).

147. Dosta, P., Ramos, V. & Borrós, S. Stable and efficient generation of poly(β-amino ester)s for RNAi delivery. *Mol. Syst. Des. Eng.* **3**, 677–689 (2018).

148. Near, R. D., Hayden, S. C., Hunter, R. E., Thackston, D. & El-Sayed, M. A. Rapid and efficient prediction of optical extinction coefficients for gold nanospheres and gold nanorods. *J. Phys. Chem. C* **117**, 23950–23955 (2013).

149. Balcells, L. *et al.* SPIONs' Enhancer Effect on Cell Transfection: An Unexpected Advantage for an Improved Gene Delivery System. *ACS Omega* **4**, 2728–2740 (2019).

150. Betzer, O. *et al.* In-vitro Optimization of Nanoparticle-Cell Labeling Protocols for In-vivo Cell Tracking Applications. *Sci. Rep.* **5**, 1–11 (2015).

151. Ng, S. W., Norwitz, S. G. & Norwitz, E. R. The impact of iron overload and ferroptosis on reproductive disorders in humans: Implications for preeclampsia. *Int. J. Mol. Sci.* **20**, (2019).

152. Hou, W. *et al.* Autophagy promotes ferroptosis by degradation of ferritin. *Autophagy* **12**, 1425–1428 (2016).

153. Tang, M., Chen, Z., Wu, D. & Chen, L. Ferritinophagy/ferroptosis: Iron-related newcomers in human diseases. *J. Cell. Physiol.* **233**, 9179–9190 (2018).

154. Schweiger, C. *et al.* Quantification of the internalization patterns of superparamagnetic iron oxide nanoparticles with opposite charge. *J. Nanobiotechnology* **10**, 1 (2012).

155. Zhou, H. *et al.* Gold nanoparticles impair autophagy flux through shape-dependent endocytosis and lysosomal dysfunction. *J. Mater. Chem. B* **6**, 8127–8136 (2018).

156. Wang, J. *et al.* Silica nanoparticles induce autophagy dysfunction via lysosomal impairment and inhibition of autophagosome degradation in hepatocytes. *Int. J. Nanomedicine* **12**, 809–825 (2017).

157. Ma, X. *et al.* Gold nanoparticles induce autophagosome accumulation through size-dependent nanoparticle uptake and lysosome impairment. *ACS Nano* **5**, 8629–8639 (2011).

158. Fader, C. M., Sánchez, D., Furlán, M. & Colombo, M. I. Induction of autophagy promotes fusion of multivesicular bodies with autophagic vacuoles in K562 cells. *Traffic* **9**, 230–250 (2008).

159. Thurston, T. L. M., Wandel, M. P., Von Muhlinen, N., Foeglein, Á. & Randow, F. Galectin 8 targets damaged vesicles for autophagy to defend cells against bacterial invasion. *Nature* **482**, 414–418 (2012).

160. Chen, X. *et al.* Autophagy induced by calcium phosphate precipitates targets damaged endosomes. *J. Biol. Chem.* **289**, 11162–11174 (2014).

161. Fornaguera, C. *et al.* In Vivo Retargeting of Poly(beta aminoester) (OM-PBAE) Nanoparticles is Influenced by Protein Corona. *Adv. Healthc. Mater.* **8**, 1–11 (2019).

162. Kim, J., Sunshine, J. C. & Green, J. J. Differential polymer structure tunes mechanism of cellular uptake and transfection routes of poly(β-amino ester) polyplexes in human breast cancer cells. *Bioconjug. Chem.* **25**, 43–51 (2014).

Chapter III. The nanoparticle journey: from synthesis to inside the cell

This chapter is submitted to ACS Applied Biomaterials as: *The protein corona of DNA-loaded PBAE coated gold and superparamagnetic iron oxide nanoparticles impacts cell transfection*

Authors: L.Balcells, C. Rodriguez-Quijada, A. Cascante, S. Borrós, K. Hamad-Schifferli

This page left blank intentionally

3.1 Introduction

In the previous chapter, a study on the cellular trafficking of NPs has been detailed. However, for any cellular trafficking to occur it is required that gene delivery systems are internalized by cells. In other words, it is useless to look at the cellular mechanisms once nanoparticles are inside cells if they are unable to enter cells. This fundamental process through which NPs enter cells is named endocytosis and will be detailed hereinafter. Although being a widely studied process, it is important to understand the factors that modulate it in order to achieve our global goal of understanding the cellular fate of our gene delivery systems.

Gene delivery systems need to reach the cell cytosol and deliver their genetic cargo in order to cause their intended effect. However, until nanoparticles reach the cytoplasm, they suffer different modifications and must overcome several barriers. The journey of nanoparticles towards the inside of the cell begins with their synthesis.

When nanoparticles are manufactured, the parameters employed in their synthesis (temperature, time, stirring, reagents concentration and others) lead to NPs with defined properties. The set of these properties is known as synthetic identity (SI). This SI is defined by the physicochemical properties of the NPs, including surface chemistry[163–166] and physical properties (size, shape and surface area)[165,167]. All these properties play an important role in determining interactions at the nano-bio interface[168,169] and affect not only the mechanism of cell uptake but also intracellular trafficking and biological function (biodistribution, toxicity and targeting ability) of the nanoparticles[170–173].

Then, once NPs are either incubated for any *in vitro* or administered for any *in vivo* purpose, they are exposed to a biological medium (cell culture medium in the case of *in vitro* experiments and blood in the case of *in vivo* administration). All these media contain several thousands of biomolecules, mainly proteins, and it has been widely demonstrated that nanoparticles can adsorb immediately proteins on their surface[174,175]. Thus, when a NP enters a biological medium a competition between different biological molecules to adsorb on the surface of the nanoparticles starts immediately. This coating that is formed on the NP's surface is known as the protein corona (PC). The PC confers to the nanoparticle a new identity known as biological identity (BI) that is the one that the cell will "see". This protein corona will determine a new group of physicochemical properties such as the surface modifications after the PC formation[165,176,177], the dispersion, aggregation and agglomeration of nanoparticles[178,179] and the stability in

physiological conditions[180–182]. Thus, the PC highly influences the physiological response; that is, bioavailability, cell uptake, circulating time and toxicity of NPs[183,184]. Therefore, the understanding of the PC becomes crucial to control the cellular response and the fate of the designed nanoparticles.

The first cell response towards the nanoparticles is their internalization or cell uptake. This process takes place through a cellular mechanism named endocytosis. Endocytosis is the energy-consuming process by which a cell takes up extracellular molecules by engulfing them with the cell membrane. The membrane folds over the substance and it becomes completely enclosed forming what is known as vesicle. Endocytosis is, thus, the major transport route for nanomedicines across the cell membrane. It is generally classified into phagocytosis and pinocytosis. Phagocytosis was originally discovered in macrophages. Pinocytosis is present in all types of cells in four forms, such as clathrin-dependent endocytosis, caveolae-dependent endocytosis, macropinocytosis, and clathrin- and caveolae-independent endocytosis[185,186]. Many types of cells use the clathrin- and caveolae-mediated endocytosis pathways to internalize nanoscale materials, including viruses and nanoparticles[187–189].

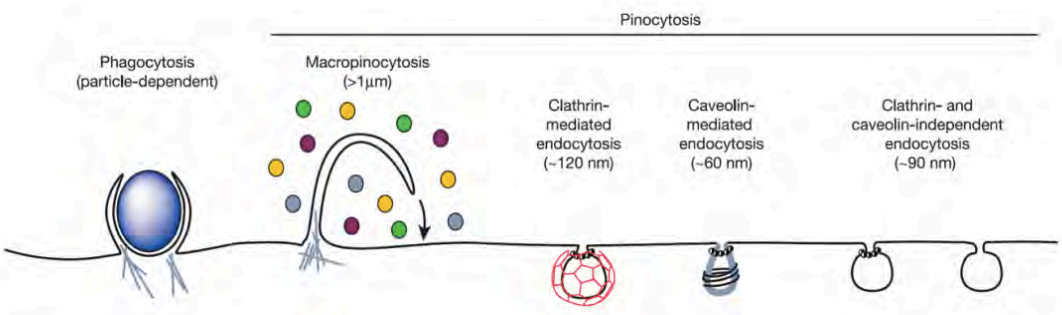

Figure 18. Entry pathways for mammalian cells. The endocytic pathways depend on the size of the endocytic vesicle, the nature of the cargo (ligands, receptors, and lipids) and the mechanism of vesicle formation[190].

Once endocytic vesicles are internalized into the cytosol, they are rapidly targeted to the early endosome (EE) that is the primary sorting station from which endocytosed materials can be recycled back to the plasma membrane[191], or brought to late endosomes (LEs) on the way to the lysosome/vacuole for degradation[192]. Thus, once inside the endosomes, gene delivery systems must escape from them in order to avoid lysosomal degradation and reach the cytosol. In other words, bypassing the regular endocytic pathway that leads to cargo degradation is crucial to produce any cellular effect.

One of the most explored mechanisms to bypass the regular endocytic pathway is inherent to many cationic polymers. These molecules count on an important feature which is the presence of amine groups with pK_a values in the physiological pH range, resulting in their ability to buffer acidic endosomal vesicles. This buffering capacity is thought to promote the so-called sponge effect, which consist on the osmotic swelling and physical rupture of endosomes, assisting the release of DNA into cytoplasm prior to fusion with lysosomes[193]. Sonawane et al.[194] recently showed that endosomes containing vectors with physiologically titratable amine groups buffered H^+ ions, increased the counterion Cl^- concentration within the endosome, swelled the endosome in size, and led to lysis of the endosome (Figure 19).

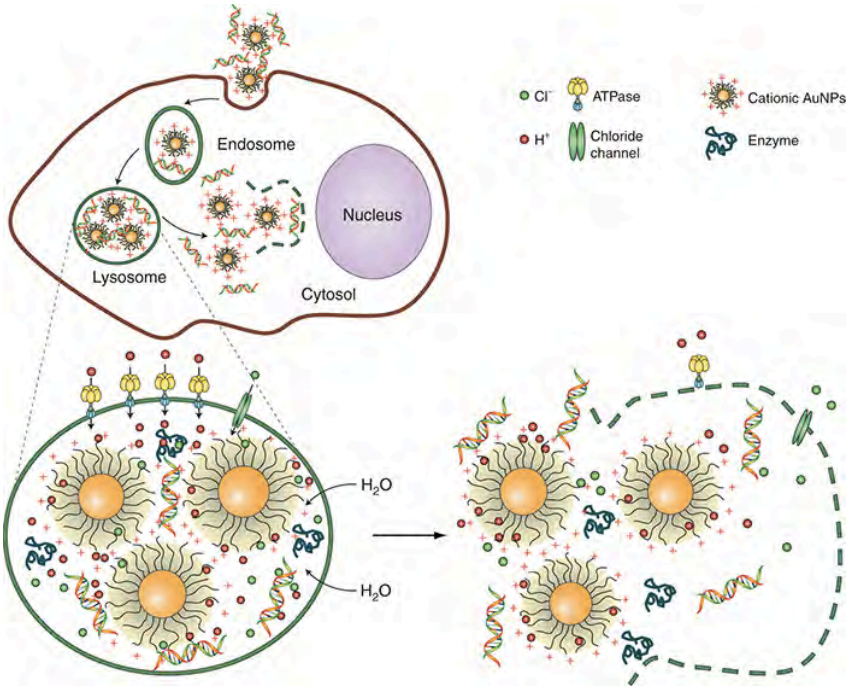

Figure 19. Schematic illustration of the proton sponge effect leading to endosomal escape for cationic nanoparticles. ATPase stands for adenosine triphosphatase[97].

Given their cationic nature, after binding to the cell surface OM-pBAEs conjugates are internalized, and a fraction of them escapes the endocytic network – as a result of the proton sponge effect – and translocate to the nucleus, where genes encoded by the foreign DNA are expressed. Normal cellular trafficking usually directs the endocytosed particles to lysosomes, where the accumulated polyplexes would eventually be degraded by the lysosomal hydrolytic enzymes, strongly limiting gene expression[195]. In consequence, the escape of vectors from the lysosomal tracking pathway is an important step for efficient gene delivery. In this sense, it has been described that OM-pBAEs can

actually scape from the endosomes through the previously described “proton sponge” effect. In particular, the tertiary amines that are a major component of the OM-pBAEs are important to the endosomal buffering capacity of these polymers. These titratable amines provide OM-pBAE-containing particles with a mechanism to escape from endosomes and accomplish their objective of reaching the cell cytosol and deliver their genetic cargo to the cell. In other words, the OM-pBAE polyplexes have proved to be effective gene delivery systems in terms of cell uptake and endosomal escape ability. For these reasons, they will be used in the present chapter as a tool to study cell uptake of different OM-pBAE-based complexes.

Considering the importance of endocytosis in the cellular fate of gene delivery systems and the need to understand the interactions of nanoparticles with the environment, in the present chapter a study of the cell uptake of different NPs is detailed. The effect of every component of our gene delivery systems will be discussed and the isolation of the protein corona formed around these systems will give clues on the reasons why differences in cell uptake appear. The aim of this chapter is to help understand the disparities in cell internalization profiles among different nanoparticles and to identify proteins that might be key for cell uptake and transfection.

3.2 Aims

In order to achieve the main objective, described in the previous subsection, the following tasks were proposed:

- Quantify the cell biocompatibility of our gene delivery systems.
- Perform a broad study on cell uptake of the different nanoparticles and complexes in different cell lines.
- Study disparities in cell uptake of nanoparticles according to their morphology.
- Analyze the transfection efficiency of the complexes at different concentrations of metallic components.
- Study the protein corona of the different samples as an explanation to their different cell uptake profiles.

3.3 Materials and Methods

3.3.1 Materials

Reagents and solvents used in the present chapter were purchased from Sigma-Aldrich. DMSA-coated SPIONs (hydrodynamic size = 45 nm; surface charge = -12 mV; stock SPIONs dispersion, dispersed in water as the dispersant) were performed by Unit 9 of the Platform of Production of Biomaterials and Nanoparticles of the NANBIOSIS ICTS, by the *Superfícies y Partículas Nanoestructuradas del Instituto de Nanociencia de Aragón* (PI J. Santamaría) group[143,144]. C6-pBAE NPs, gold NPs and SPIONs or AuNP-containing NPs were synthetized as described in chapter II. Dithiothreitol and iodoacetamide were obtained from Thermofisher. NuPAGE 4X LDS was obtained from Invitrogen. Ammonium bicarbonate and acetonitrile were obtained from Fisher scientific. Acetone MS grade was obtained from Fisher Chemical. Trypsin/lysine mixture was obtained from Promega. HeLa and PANC-1 cells were obtained from American Type Culture Collection (ATCC, Manassas, VA). Products for cell culture (media, PBS, glutamine, penicillin-streptomycin solution) were obtained from Gibco and Hyclone.

3.3.2 Synthesis of Gold nanorods (AuNR)

Gold nanorods were synthesized using a seed mediated approach[196]. The seed solution was first prepared by dissolving cethyl-trimentylammonium bromide (CTAB, 0.273 g) in water (deionized, 7.5 mL) with mild stirring and slight heating. Hydrogen tetracholoroaurate ($HAuCl_4$, 250 µL, 10 mM) was added, and the gold was reduced with sodium borohydride ($NaBH_4$, 600 µL, 0.1 M). The solution was stirred for 5 min before use. The growth solution was prepared by dissolving CTAB (15.49 g) in water (deionized, 425 mL) with mild stirring and slight heating. $HAuCl_4$ (20 mL, 10 mM) was then added, yielding a clear, bronze-colored solution. Silver nitrate ($AgNO_3$, 8.5 mL, 4 mM) was added, and then the gold was reduced with ascorbic acid (11.6 mL, 79 mM), yielding a clear, colorless solution. Seed solution (960 µL) was injected, and the solution was left undisturbed overnight. The nanoparticles were cleaned via 2x successive centrifugation at 10000 rpm for 8 min and re-diluted to their original volume in deionized water.

3.3.3 Gold NR characterization

The morphology of the AuNPs and SPIONs was determined by TEM (FEI Tecnai G2 at 100 kV). ImageJ was used to determine their size.

The optical properties of the gold NR were characterized by UV-vis spectroscopy (Agilent Cary 5000 UV-Vis NIR).

3.3.4 Cell culture

PANC1 cells (ATCC CRL-1469) are a tumor cell-line derived from a human carcinoma of the exocrine pancreas. HeLa cells (ATCC CCL-2) are derived from a cervical cancer taken from a 31-years-old patient. HeLa and PANC-1 cells were grown according to ATCC guidelines. Cells were seeded in 96 well plates at a concentration of $1.2x10^4$ cells/well in DMEM complemented with 10% fetal bovine serum, 100 IU mL^{-1} penicillin and 1% streptomycin at 37°C in a humidified 5% CO_2 incubator for 24 h. The cell media was then replaced with the NP solution for 48 h before performing MTT, MTS or transfection assays. For ICP-MS, cells were seeded at a concentration of $7.2x10^4$ cells/well in 24 well plates maintaining the OM-pBAE NP/cell ratio.

3.3.5 MTT and MTS cytotoxicity assays

The MTT is a colorimetric assay used to assess cell metabolic activity and thereby reliably estimate percentages of cell viability[197]. Yellow MTT (3-(4,5-dimethylthiazol-2-yl)-2,5-diphenyltetrazolium bromide, a tetrazole) is reduced to purple and insoluble formazan in the mitochondria of living cells. This reduction takes place only when the NAD(P)H-dependent mitochondrial oxidoreductase enzymes are active and therefore conversion can be directly related to the number of living cells. Cells cultivated in 96-well plates were treated with different concentrations of SPIONs and incubated for 48 h at 37 ºC and 5% CO_2. Then, they were washed with PBS and incubated in complete medium supplemented with MTT solution (5 mg mL^{-1}), added at 10% v/v for 3 h at 37 ºC and 5% CO_2. DMSO was then added to solubilize the insoluble formazan crystals formed. Absorbance was measured (Elx808 Biotek Instruments Ltd, USA) at a wavelength of 550 nm and values were converted to percentages of cell viability relative to untreated cells, by normalizing with the absorbance of non-treated cells.

MTS assays work with the same principle as MTT with the convenience of adding the reagent straight to the cell culture without the intermittent steps required in the MTT assay. The reduction of MTS tetrazolium compound generates a colored formazan product that is soluble in cell culture media. MTS cell viability experiments were conducted after a 48 h incubation with PBAE NPs (NP) or metallic complexes (NP-SP or

NP-SPH) at different concentrations. Complemented media was used as a negative control (Neg). Wells were then washed with PBS 1X three times and incubated with the CellTiter 96 Aqueous One Solution at the concentration indicated by the supplier for 3 h at 37°C. Absorbance was measured at 490 nm.

3.3.6 NPs cell uptake

The iron content of the cells treated with bare SPIONs, bare gold NPs, SPION-containing nanoparticles or AuNP-containing nanoparticles was determined through an Inductively Coupled Plasma Optical Emission Spectrometry (ICP- OES) or inductively coupled plasma mass spectrometry (ICP-MS). The differences in the uptake of gold nanoparticles of different morphologies were studied using Single Cell ICP-MS.

3.3.6.1 ICP-OES

In the case of ICP-OES, HeLa cells were seeded on a 24-well plate and incubated with the different NPs for 48 h. Subsequently, cells were gently washed with PBS in order to eliminate the SPIONs that were not internalized. Then, cells were trypsinized, counted and digested with an oxidative mixture of hydrogen peroxide (30% v/v) and nitric acid (50% v/v) while heating until nitrous vapors were observed. The obtained sample was diluted to a final volume of 10 mL and a nitric acid concentration lower than 5%. The iron content, in terms of mg of iron per mL, was calculated by an Optima 2100 DV ICP analyzer (PerkinElmer, Waltham, Massachusetts, USA). Finally, the pg of iron/cell were determined according to the number of cells counted and normalizing the untreated cells (control) as zero pg of iron/cell.

3.3.6.2 ICP-MS

In the case of ICP-MS, HeLa and PANC1 cells exposed to the PBAE-metallic particle complexes were gently washed with PBS three times, trypsinized and counted. The pellets were then pulled down and digested with 1 mL of aqua regia for 24 h. Gold and Iron content was determined by inductively coupled plasma mass spectrometry (ICP-MS, ELAN DRC II PerkinElmer, Waltham, Massachusetts, USA).

3.3.6.3 Single cell ICP-MS

For single cell ICP-MS analysis, HeLa cells were seeded in 24-well plates for 24 h and then, incubated for 3 h with either bare gold nanospheres, gold nanorods or with one of these two gold NPs complexed with pBAE-NPs. After the incubation, cells were gently washed with PBS 1X three times, trypsinized, fixed using formalin 10 %, filtered through

a nylon syringe filter of 0.45 µm diameter and analyzed through Single cell ICP-MS using NexION® 2000 equipment (PerkinElmer, Waltham, Massachusetts, USA). The sample introduction was controlled using an automated syringe system with the flux fixed at 20 µl min^{-1}. The single cell operating mode requires from two calibrations: one to determine the ionic or dissolved part and another for the determination of the number and size of the NPs. These calibrations were performed by expert technicians from PerkinElmer. Also, the transport efficiency (TE) factor was calculated. This factor defines the percentage of NPs of a solution that arrive to the detector and is used by the equipment for analytical calculations. Then, the different samples were analyzed.

3.3.7 Transfection Efficacy

Transfection of HeLa and PANC1 cells was first checked under the microscope and then quantified by flow cytometry (FACS) (BD Fortessa cell analyzer). After incubation with nanoparticles, cells were trypsinized and fixed with a solution of paraformaldehyde 2% in PBS 1X. GFP expression was quantified and compared to the positive control of PBAE-NP and a negative control of untreated cells.

3.3.8 nanoDSC for protein corona characterization

The protein corona was formed around gold nanoparticles incubating them in a solution of 10 mg mL^{-1} of albumin (BSA) in water overnight. No washes were performed. Then, the nanoDSC cell was filled with the solution formed with 1 mg of AuNPs or AuNR and 10 mg of HSA. Three temperature cycles between 37 to 98 ºC were performed. The baseline was obtained, subtracting each third cycle from the respective first one using Origin® software.

3.3.9 Protein Isolation for MS

PC isolation was performed as described elsewhere with minor alterations[198]. Briefly, AuNPs, SPIONs and PBAE NP alone or combined with metallic particles resuspended in DMEM were centrifuged at 16000g for 1 h at 4°C to separate the excess of proteins from the cell media. The supernatant was discarded and the pellets were resuspended in a PBS-Tween20 0.05% (w/v) solution. The pellet was washed twice with the PBS-Tween20 solution and a fourth time with PBS alone by centrifuging at 15000g for 1h at

4°C. A solution of 8 µL of NuPAGE 4X LDS and 4 µL of 500 mM dithiotheitol (DTT) is added mixed gently to resuspend each pellet. The solution is incubated at 70°C for 1h and centrifuged for 15 min at 16000g and the 12µL-supernatant is used for the next steps. The Protein precipitation and Cleanup protocol from Walkey et al. was followed with no modifications[198]. The MS sample preparation was conducted with minor modifications. In short, 95 µL of an aqueous solution of ammonium bicarbonate at 100 mM, 5 µL of acetonitrile and 5 µL of DTT 100 mM were added to the protein pellets and left at 80°C for 45 minutes. The solution was left to cool down until room temperature reached and 11.5 µL of 500 mM iodoacetamide in ammonium bicarbonate 50 mM (pH 7-8) was added and incubated in dark conditions and room temperature for 1h. 460 µL of pure acetone prechilled at -20C was added and the solution was left at -20°C for protein precipitation. Proteins were centrifuged at 16000g for 10 min at 4°C, the supernatant was discarded and pellets were air dried before resuspending them in 100 µL of ammonium bicarbonate at 50 mM (pH 7-8). 4 µL of a protease mixture of trypsine and lysine was added at the concentration indicated by the supplier and incubated overnight at 37°C. Finally, the protein digestion was stopped by a 10 min incubation at -80°C and samples were kept at -20°C until MS analysis.

3.3.10 Proteomic studies: Inductively Coupled Plasma – Mass Spectrometry (ICP-MS)

All mass spectrometric experiments were performed using an Orbitrap Fusion Lumos mass spectrometer (Thermo Scientific). The MS was coupled to an EASY-nLC 1200 system (Thermo Scientific). The HPLC mobile phases were 96.1:3.9 water/acetonitrile with 0.1% formic acid (A) and 20.0:80.0 water/acetonitrile with 0.1% formic acid (B). The flow rate was 300 nL min^{-1} and the following gradient was used for each run; 0% B for 5 min, 0-5% B in 10 min, 5-30% B in 150 min, 30-90% B in 30 min, 90% B for 10 min. The tryptic peptide digests were diluted by a factor of ten with 0.1 % formic acid and aliquots of 1 µL of the diluted digests were injected onto and separated by a PepMap RSLC, C18, 3 µm, 100 Å, 75 µm × 150 mm EASY-Spray column (Thermo Scientific). Electrospray ionization was performed at a voltage of 1.9 kV.

The mass spectrometer was operated in data-dependent mode. Survey scans were collected in a range of 400-1600 *m/z* in the orbitrap at a resolution of 120,000 and an AGC target of 2×10^5 (or maximum injection time of 100 ms). Precursor ions were filtered by charge state (2-6 *z)*, dynamic exclusion for 30 s at a 20 ppm mass width and monoisotopic precursor selection. For charge states 2 and 3, the precursors were

isolated in the ion trap with a 1.2 *m/z* isolation window and an AGC target of 2×10^4 with a maximum injection time of 50 ms. CID was performed on the isolated parent ions using a 35 % collision energy and 10 ms activation time. EThCD was used to dissociate precursors having charge states of 3-6 using a 1.2 *m/z* isolation window and an AGC target of 2×10^4 (or maximum injection time of 50 ms).

The Proteome Discoverer (PD) Software Version 2.1 (Thermo Scientific) was used for peptide sequencing and protein identification. The SEQUEST search algorithm was used to analyze the data against fasta files from a human protein database downloaded from Uniprot. The cleavage enzyme was set to trypsin (full) and the maximum missed cleavages was set to 2. Precursor mass tolerance was set to 10 ppm and fragment mass tolerance to 0.6 Da. The following peptide modifications were also set for the SEQUEST search; oxidation (methionine, dynamic), acetyl (N-terminus, dynamic), and carbamidomethyl (cysteine, static). For protein validation the Percolator algorithm in PD was utilized. It was set to a false discovery rate (FDR) of 1 %. All proteomic data presented in this paper is based on identifications that met this 1% FDR threshold. The protein identification output from the PD search was downloaded into an Excel spreadsheet for further analysis.

Further analysis. Two biological replicates were conducted per sample and two technical repetitions were used for analysis. Samples were filtered for those who had a score sequest HT and peptide sequest HT ≥ 2 to ensure high quality of the measurement. EmPAI values were used to determine the top 50 proteins with the highest abundance per each of the samples, leading to a list of 61 proteins in total. Exponentially Modified Protein Abundance Index (emPAI) is an established method of estimating protein abundances from peptide counts in a single LC-MS/MS experiment. EmPAI is defined as 10^{PAI} minus one, where PAI (Protein Abundance Index) denotes the ratio of observed to observable peptides. EmPAI was first proposed by Ishihama et al[199], who found that PAI is approximately proportional to the logarithm of absolute protein concentration[200]. Heatmap was generated with R function heatmap.2 from RStudio Version 1.0.153.

3.4 Results and discussion

In the previous chapter, the physicochemical characterization of the complexes used hereinafter was performed. Complexes with appropriated nanometric sizes and positive surface charge values were obtained. These complexes were used to study intracellular mechanisms and their locations within the cells. Here, they will be employed to shed light to their cell internalization profiles and to help understand the overall cell response to nanoparticles.

3.4.1 SPION or AuNP–containing polyplexes do not impair cell viability

Considering the physicochemical properties of gold nanospheres and SPIONs for cell usage (chapter II) and in order to study their cellular uptake, it was first evaluated if the NP candidates induced any sign of cytotoxicity. In order to do so, cell viability was determined by MTT and MTS assays on two types of cell cultures (HeLa and PANC-1) exposed to both NPs and NP+SP or NP+AuNP at different concentrations. The untreated cells (C-) were used as a reference for 100% viability.

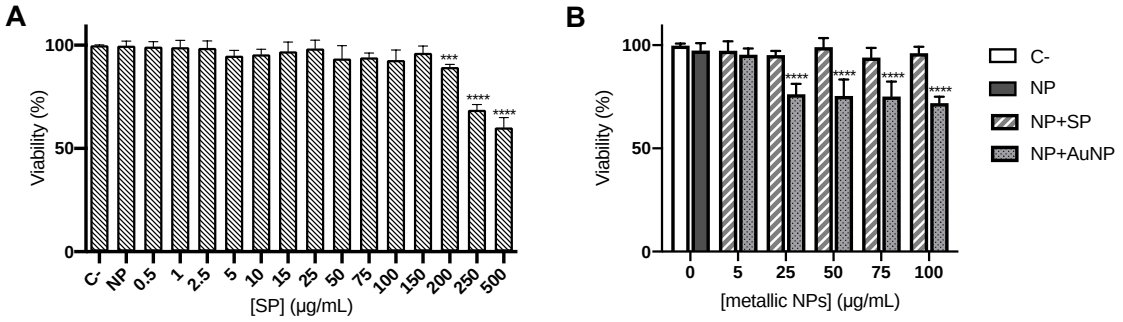

Figure 20. HeLa and PANC-1 cell viability when incubated with OM-pBAE-NPs. (A) MTT assay of HeLa cells treated for 48 h with OM-pBAE NPs without SPIONs (NP) and with increasing ratios of SPIONs; (B) MTS of PANC-1 cells treated with OM-pBAE NPs without SPIONs (NP) and with increasing ratios of SPIONs (NP+SP) or AuNPs (NP+AuNPs). The variability values are the mean ± SD of triplicates. The significance of the difference in the data is ***p<0.001 and ****p<0.0001 regarding the controls of untreated cells (C-).

As expected, pBAE NPs alone did not impair the viability of neither HeLa nor PANC-1 cells. Metallic NPs were complexed to a fixed OM-pBAE NP concentration at increasing ratios. In the case of HeLa, the study was performed only with SPIONs. Up to 250 µg mL^{-1} these metallic particles did not compromise HeLa viability. In the case of PANC-1 cells, SPIONs showed a similar result, not impairing cell viability in the range of

concentrations tested (0 to 100 μg mL^{-1}). On the other hand, gold-based NPs led to higher cytotoxicity levels compared to SPIONs starting from 25 μg mL^{-1}. This increased cytotoxicity was even more intensified when bare metallic nanoparticles were incubated (Figure 21).

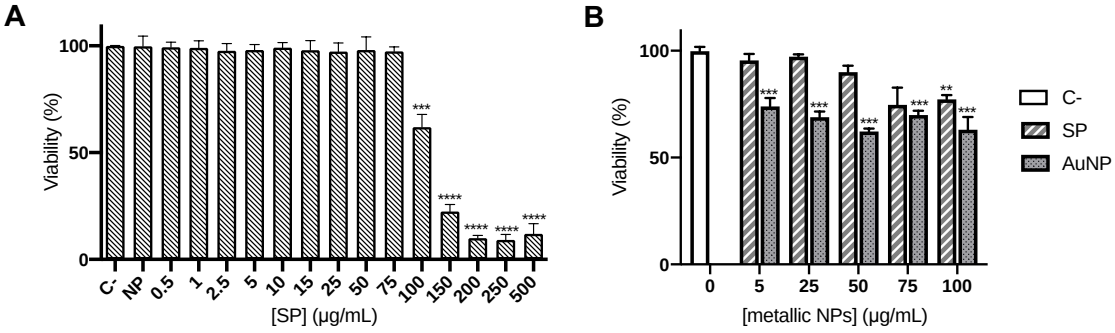

Figure 21. HeLa and PANC-1 cell viability when incubated with metallic NPs. (A) MTT assay of HeLa cells treated for 48 h with bare SPIONs; (B) MTS of PANC-1 cells treated with bare SPIONs (SP) or AuNPs (AuNPs). The variability values are the mean ± SD of triplicates. The significance of the difference in the data is ***p<0.001 and ****p<0.0001 regarding the controls of untreated cells (C-).

These results are in accordance with previously published data, where bare gold NPs have impaired cell viability in different cell lines while SPIONs have shown high levels of biocompatibility201. However, the incubation of the two tested cell lines with both metallic complexes at the lowest concentrations did not cause significant drops in cell viability (Figure 21). Therefore, further transfection studies were performed with metallic NPs at concentrations below 25 μg mL^{-1}.

3.4.2 Cells internalize more metallic nanoparticles when they are complexed with OM-pBAE-NPs

In order to understand the differences in cell mechanisms observed in chapter I, it was next evaluated if the differences in composition of these gene delivery systems caused differences in cell uptake.

3.4.2.1 Uptake of SPIONs in HeLa cells

First, since SPIONs have been broadly employed as gene delivery systems complexing biological molecules such as antibodies, peptides, hormones or drugs to

their surface[202,203], our aim was to demonstrate that a multicomponent nanoparticle comprising, apart from the SPIONs, OM-pBAE and DNA would be more efficient in terms of cellular uptake than the bare SPIONs. Therefore, the iron content of HeLa cells treated with bare SPIONs and with SPION-containing S-type NPs was studied. 48 h after transfection the cellular iron content was quantified through ICP-OES.

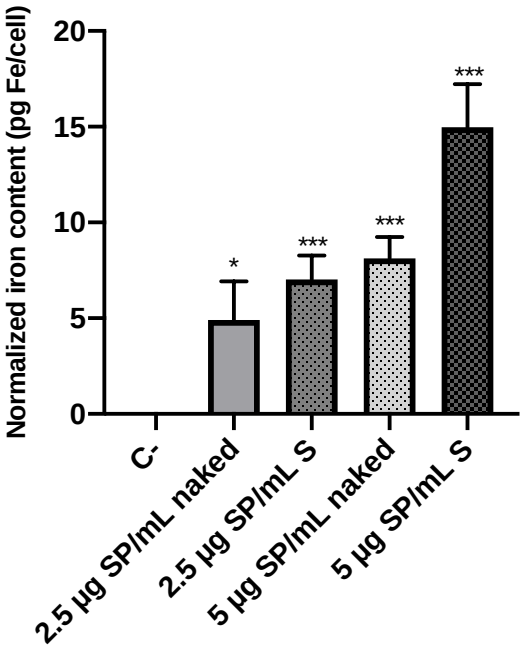

Figure 22. HeLa iron content after incubation with nanoparticles. Inductively coupled plasma-optical emission spectrometry (ICP-OES) analysis to determine cellular iron content of HeLa cells treated with SPIONs at two different concentrations and with or without OM-pBAE polyplexes. Untreated cells' iron content was normalized to 0 pg of Fe/cell. Results are the mean ± SD of triplicates. *p<0.05 and ***<0.001.

Given that cells have a basal level of intracellular iron content, the obtained results were normalized so that only the excess of iron due to the presence of internalized magnetic nanoparticles is plotted. As it can be observed in Figure 22, cells treated with bare SPIONs (naked) at 2.5 µg of SPIONs mL^{-1} internalized 4.91 ± 2.02 pg of Fe/cell more than untreated cells, whereas those treated with bare SPIONs at 5 µg mL^{-1} had a difference of 8.12 ± 1.12 pg of Fe/cell. On the other hand, C6-CR3/pGFP (25:1) S nanoparticles prepared at 2.5 µg of SPIONs mL^{-1} showed 7.03 ± 1.25 pg of Fe/cell more than control cells, whereas those treated with the same nanoparticles prepared at 5 µg of SPIONs mL^{-1} internalized 14.98 ± 2.25 pg of Fe/cell more. These results were in accordance with what was expected since the more the SPIONs were provided to the cells, the more the iron was internalized. In addition, several other studies have reported

a range of 10−25 pg of Fe/cell in HeLa cells (the same employed here) when SPIONs were used with a transfection agent[204–206].

The fact that the cells treated with complexed SPIONs showed more iron content compared to those treated with bare SPIONs at both SPION concentrations tested was, at first, surprising. However, we could hypothesize the following: since the coating of 2,3-dimercaptosuccinic acid (DMSA) causes SPIONs to be negatively charged, they may experiment repulsion with cell membranes. This effect might be reversed by the presence of positively charged OM-pBAEs, thus explaining the higher uptake values of complexed SPIONs compared to the bare ones. Although it is not yet clear, it has been reported that the mechanism of cellular uptake of DMSA-SPIONs may be related to endocytosis[207]. Moreover, such cell uptake pathways are susceptible to saturation. Therefore, it is most probable that a high concentration of free SPIONs (in the naked sample) will saturate the route of entry, and this may lead to a high number of SPIONs to remain in the extracellular media. In other words, when one single SPION-containing NP enters a cell, several SPIONs attached to the pBAE will enter at once. By contrast, the bare SPIONs must be internalized one at a time by each cell receptor.

To sum up, these results indicated that more intracellular iron is obtained for a fixed concentration of SPIONs when these magnetic nanoparticles were complexed with pBAE and pDNA as compared to when SPIONs were internalized alone. Thus, in terms of cell uptake, the gene delivery system consisting of a multicomponent nanoparticle was more efficient than naked SPIONs.

3.4.2.2 Uptake of complexed SPIONs and spherical AuNPs in PANC-1 cells

Next, an uptake study regarding both SPIONs and spherical gold nanoparticles was proposed. In this case, the cell line was PANC-1 and all samples contained polyplexes at a fixed concentration. Complexes of OM-pBAE polyplexes and SPIONs or AuNPs were incubated at different metallic NP concentrations for 48 h. After this incubation, the washing and digestion procedure of cells, detailed in Materials and Methods section, was carried out before determining their intracellular content of iron or gold through ICP-MS.

In both the cases of iron and gold OM-pBAE-metallic complexes, higher uptake values with increasing concentrations of the metallic NPs at a fixed OM-pBAE-NP concentration

were obtained (Figure 23). For all the metallic NP concentrations tested (2.5 to 10 μg mL^{-1}), OM-pBAE-gold NP complexes showed higher cell uptake as compared to the OM-pBAE-SPIONs at the same concentrations. This difference was accentuated at 10 μg mL^{-1} of metallic NPs. These results are in accordance with the higher impairment of cell viability previously discussed for OM-pBAE-AuNP complexes.

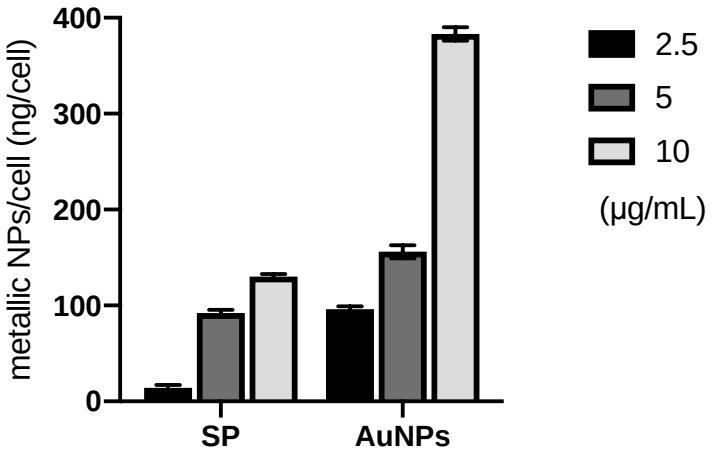

Figure 23. PANC-1 iron and gold content after incubation with nanoparticles. Inductively coupled plasma-mass spectrometry (ICP-MS) analysis to determine cellular iron content of PANC-1 cells treated with SPIONs and gold NPs at three different concentrations and with OM-pBAE polyplexes.

3.4.3 Gold NPs are internalized in a shape-dependent manner

Then it was studied if for a same metallic element, the shape of nanoparticles would imply differences in cell uptake. To do so, non-spherical gold nanoparticles were synthetized. In other words, aimed at analyzing differences in the uptake of metallic NPs regarding their morphology, the uptake of gold nanospheres and gold nanorods (AuNR) was compared. First, the physicochemical characterization of this type of gold NP was carried out.

3.4.3.1 Gold nanorods synthesis and characterization

The synthesis of gold nanorods (AuNR) was performed as detailed in Materials and Methods section. The TEM images in Figure 24A showed that rod-shaped gold nanoparticles (AuNR) were effectively obtained. The sizes of these particles were determined using ImageJ software, resulting in a mean length of 26.9 ± 1.7 nm and mean width of 10.3 ± 1.3 nm. Thus, the aspect ratio (length divided by width) of our AuNR was

2.6. The UV-vis spectrum of AuNR (Figure 24B) showed two peaks, with their maximums at 530 and 650 nm, corresponding to their two distinct surface plasmon resonances (SPRs). There is one resonance that is due to the width of the nanorod (the one at 530 nm in this case), called the transverse SPR, and one caused by the length of the nanorod (at 650 nm in our synthesis), called the longitudinal surface plasmon resonance (LSPR)[208]. These SPRs are easily tuneable with slight variations in synthesis. A red shift of the LSPR occurs when the aspect ratio of the gold nanorods is increased while the transverse SPR remains at the same wavelength[209]. Size, aggregation, and changes in the media surrounding the gold nanorods can also be observed using UV-Visible spectrophotometry. To sum up, gold nanorods with the typical morphology and UV-vis spectrum were obtained.

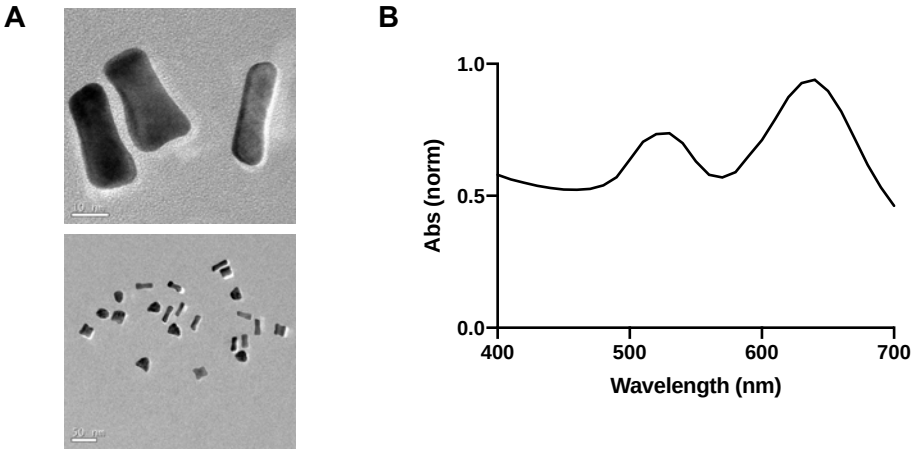

Figure 24. Characterization of gold nanorods. (A) TEM images of gold nanorods. Scalebars = 10 nm in the upper image and 50 nm in the lower one; (B) UV-vis spectrum of gold nanorods.

3.4.3.2 Single cell ICP-MS

Once the properties of these NPs were proven to be the desired ones, HeLa cells were incubated with them and with gold nanospheres in order to study differences on cellular uptake according to the shape of nanoparticles.

The gold content of HeLa cells treated with different-shaped gold nanoparticles was quantified. Cells were treated with either bare gold nanospheres (AuNPs), bare gold nanorods (AuNR) or complexes made of C6R OM-pBAE and one of these gold NPs (S-type NPs). 3 h after incubation, the cellular gold content was quantified through single cell ICP-MS.

The introduction and development of Single Particle ICP-MS (SP-ICP-MS) has opened a new area of research which allows the rapid detection and analysis of metal-based particles in a variety of matrices and applications[210–213]. The key feature of SP-ICP-MS is that it allows discrete pulses of positively charged ions to be detected and measured in a time-resolved manner using microsecond (μs) data acquisition rates. Briefly, when a nanoparticle enters the plasma, it is completely ionized, producing a burst of ions which can be detected with ICP-MS. While conventional ICP-MS looks at a continuous signal, the output from SP-ICP-MS looks at discrete signals: one nanoparticle yields one ion burst, with the intensity of the resulting signal being related to the size of a particle (nm) and the number of pulses being related to the particle concentration (part/mL). The key to SP-ICP-MS is rapid, continuous measurement, which minimizes the chance of more than one particle being detected at the same time and ensures that particles are all counted. SC-ICP-MS allows users to monitor metal content within single cells for intrinsic metal content, uptake of ionic and/or nanoparticulate contaminants, handle lower cell numbers compared to conventional methods, and use minimal sample preparation[214].

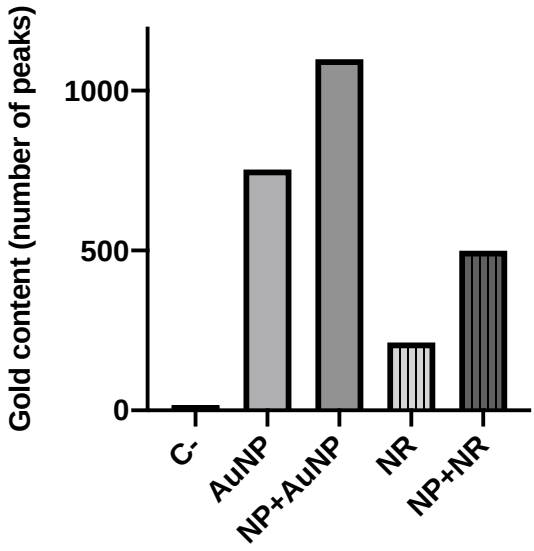

Figure 25. Single cell ICP-MS analysis of HeLa cells.

The single cell ICP-MS analysis (Figure 25) verified, first, that untreated cells did not contain a significant number of peaks corresponding to gold particles. By contrast, all the other tested samples did. Interestingly, the cell content of gold for both spherical and rod-shaped gold nanoparticles – and therefore the uptake of such particles – was increased when combined with OM-pBAE polyplexes. The presence of OM-pBAE has shown a similar effect on both spherical and rod-shaped gold nanoparticles. That is, OM-

pBAE enhanced the internalization of gold nanoparticles. This result shows a shared tendency with the ICP-OES performed in HeLa cells with SPIONs (Figure 22), where iron particles were more internalized when complexed to our polyplexes. It is also consistent with the prior ICP-MS performed in PANC-1 cells (Figure 23).

Between the two different shapes of gold nanoparticles tested, the spherical gold NPs (AuNPs) showed higher cell uptake than the nanorods (NR). In fact, OM-pBAE-complexed NR showed lower uptake than bare gold nanospheres. This result is in accordance with previous studies that have reported that with increasing aspect ratios, the cell uptake of nanoparticles is decreased and that, therefore, the spherical morphology of nanoparticles favors their cell uptake[171,215]. In addition, the traces of the CTAB surfactant that is employed in the synthesis of gold nanorods lead to positive net charges of these NPs[216], which may impair their interaction with proteins in the medium and cellular receptors involved in cell uptake. The difference in the net charge of AuNP versus NR might also be determinant in both their interaction with OM-pBAE molecules and their cellular uptake profile.

According to the calibrations performed, the mass of a gold nanoparticle was calculated to 275 ag ($2.8*10^{-19}$ kg). Using this value and the data from the equipment, it was possible to build Table 5.

Table 5. Single cell ICP-MS results

Sample	*Most frequent mass detected*	*Most frequent number of NP/cell*	*Average mass detected*	*Average number of NP/cell*
AuNP	56	1.5	148	1.5
NP+AuNP	246	6.6	426	4.3
NR	46	1.2	136	1.4
NP+NR	141	3.8	289	2.9

This table shows the average and most frequent mass detected in each sample (second and fourth columns) and the calculation of the equivalent numbers of gold nanoparticles per cell (columns 3 and 5). This is one of the most interesting properties of single cell ICP-MS, which allows to estimate the number of NPs internalized by each cell. It is worth noting that since for gold nanorods no standard samples were available for calibration, the analysis was performed as if they were gold nanospheres. Therefore, although the mass of gold detected was correct, the calculated numbers of NP/cell were an approximation.

3.4.4 Transfection efficiency does not correlate with NP uptake

Once the different studies on cell uptake of the different complexes and metallic NPs were carried out, it was next evaluated which factors were behind these results. To do so, SPIONs and spherical gold nanoparticles were employed together with the C6R polyplexes, but the gold nanorods were not used for this study, since they showed lower cell uptake.

Considering that one of the major challenges for non-viral vectors is the effective dissociation of nucleic acid from their carriers and subsequent endosomal escape when internalized inside the cells[217], an efficient cell uptake does not necessarily imply a successful transfection. For this reason, the transfection efficacy of our complexes was explored.

To determine transfection efficacy, flow cytometry was employed. The percentage of cells expressing the reporter gene GFP was the parameter used for quantification and untreated cells were used as negative control (C-). Figure 26 shows that cells treated with OM-pBAE-based NPs alone or with metallic complexes exhibited transfection efficacies of at least 15%. This indicated that all vectors were not only uptaken by cells, but also reached the cytosol and delivered their cargo to the nucleus for GFP to be expressed. These results illustrated that metallic NPs did not impair the translocation to the cells nuclei nor the GFP expression. In fact, PANC1 cells treated with complexes at any metallic NP concentration led to significantly higher transfection efficacies as compared to those incubated only with OM-pBAE NPs (Figure 26).

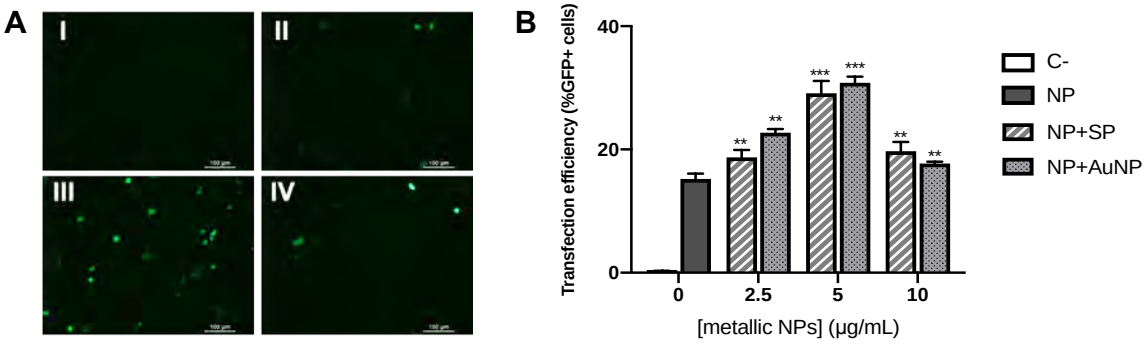

Figure 26. Transfection efficacy of the complexes on PANC1 cells. (A) Representative fluorescent images of PANC1 cells treated with different complexes: I= C-; II=NP; III=NP+SP at 5 μg mL^{-1}; IV= NP+AuNP at 10 μg mL^{-1}. Scalebars = 100 μm; (B) Transfection efficacy as measured by FACS. Error bars correspond to six independent replicates. P values were calculated as compared to the cells exposed to pBAE NPs alone (NP), where ***p<0.001 and **p<0.01.

GFP fluorescence increased for SPIONs concentration up to 5 μg mL^{-1} and decreased at 10 μg mL^{-1}. The same sweet spot was observed for the second metallic NP complexes tested in this study, AuNP (Figure 26). In both cases, NP internalization did not correlate with the transfection efficacy. While metallic NP concentration showed a positive correlation with cell uptake (Figure 23), transfection efficacy exhibited a drop when cells were incubated with NP-metallic complexes above 5 μg mL^{-1}. This is especially remarkable for NP+AuNP complexes at this concentration, which showed three times more cell uptake than the NP+SP counterpart but no disparities in transfection efficacy. Two explanations could be behind these findings: 1) despite multiple cleaning steps, OM-pBAE-metallic particles measured with ICP-MS could be physically adsorbed to cell surface rather than internalized. 2) In addition, as it has been previously stressed, not only cell uptake defines a good transfection vector. The endosomal escape, DNA integrity and dissociation from their carriers are equally important to ensure a good transfection efficacy[217]. Although NP design helps ensure DNA integrity[218,219] and dissociation[220], some studies point out that proteins found at the surface of the vector may also play a key role not only in cell internalization, but also within the cell[221,222]. Thus, studying the PC formation of these OM-pBAE and OM-pBAE-metallic complexes is crucial to understand the enhanced transfection efficacy to better engineer efficient gene transfection vectors.

3.4.5 Protein corona modulates uptake and transfection

As discussed in the introduction of this chapter, NP cell uptake and subsequent release of their cargo to the cytoplasm determine the efficacy of gene delivery vectors. Cell uptake is altered by the components found in biological media that are adsorbed on their surface and trigger distinct internalization pathways[223]. A drastic surface modification is suffered by NPs when placed in complemented cell medium, due to the presence of biomolecules that immediately bind to their surface. This leads to the formation of a dynamic multilayer protein deposition known as protein corona. This PC will vary depending on the physical properties of the nanoparticle[223]. The PC confers a new identity to the NP that will dictate the biological behavior of the vectors as some proteins forming the PC may enhance or impair the NP internalization. For this reason, the physical properties of the complexes have been characterized after incubation in complemented cell medium. Since the most abundant proteins in FBS are mostly negatively charged, the protein corona formed around the different complexes has led to negatively charged vectors: -36.2 ± 1.9 mV for pBAE-NPs, -36.5 ± 1.2 mV for NP+SP

and -38.1 ± 1.4 mV for NP+AuNPs. These very similar values of net charge obtained among the different vectors indicated that the protein-driven interactions might be behind the differences in cell uptake of these complexes.

3.4.5.1 Preliminary protein corona characterization

In order to demonstrate the role of proteins in modulating cell uptake, different techniques were employed. First, the widely used Bicinchoninic acid assay (BCA) and sodium dodecyl sulphate polyacrylamide gel electrophoresis (SDS-PAGE) techniques were proven inefficient for the characterization of the protein corona of OM-pBAE complexes (data not shown). The reason, probably, was that polymeric nanoparticles were destabilized by the washing steps and reagents used in these techniques, and results were senseless.

Then, since in our group there is recent expertise in the use of nanoDSC for the characterization of biocoronas, this equipment was employed for a preliminary characterization of PC[25,224]. This technique enables the study of the denaturation of the hard corona and provides a static information[225]. Although nanoDSC is a technique commonly used for thermal studies of biomolecules (conformational transition of biological macromolecules)[226], biochemical reactions[227] or characterization of nanoparticles[228–230], only recently, nanoDSC has emerged as a standard technique for the characterization of the protein corona. It should be noted that this technique studies both hard PC and soft PC, due to the absence of previous washes during sample preparation to remove weakly bound proteins. In nanoDSC while heating or cooling a sample, thermal changes in the same sample are accompanied by an exchange of heat; hence the temperature of these transformations and heat flow can be determined.

During the incubation, some of the proteins in the media begin to form the protein corona. Consequently, after the protein corona formation, the amount of free proteins decreases. During adsorption on the nanoparticles, proteins may undergo structural rearrangements called “conformational changes”. The nature of a protein is different if the protein is part of the protein corona or if it is a free (unbound) protein. It is possible to differentiate the proteins’ stability according to the binding state of the protein. The major part of proteins that form protein corona are less stable than the free proteins (soft PC). It has been reported that the binding of proteins to planar surfaces often induces significant changes in secondary structure. Study of a variety of NP surfaces and proteins will allow the demonstration that the perturbation of protein structure appear. For

instance, serum albumin adsorbed on NPs surfaces shows a rapid conformation change at both secondary and tertiary structure levels[231].

More in detail, in the present work, the T_m of the protein coronas of two different nanoparticles was compared to the T_m of the serum bovine albumin (BSA). This temperature (T_m) is known as transition midpoint and it is considered as the temperature at which 50% of the protein is in its native conformation, while the rest is denatured. The proteins denatured undergo the destruction of both the secondary and tertiary structures, only the primary structure (sequence of amino acids) remaining the same. Higher T_m values would be representative of more stable molecules[226,227].

Firstly, the BSA protein corona was formed on the AuNPs surface following the methodology described in materials and methods. No washes were performed. After the formation of PC, the cell of the nanoDSC was filled with this suspension. Three temperature cycles were performed, between 37 and 98 ºC (melting point of albumin depending on literature and conditions is between 59.7 and 79.5 ºC)[232,233]. During the first cycle the denaturation of the protein that form the protein corona occurred and therefore the melting point (T_m) can be calculated in this cycle. The second one was to cool down the cell. Finally, the third cycle, where all protein was denatured, was to obtain the baseline.

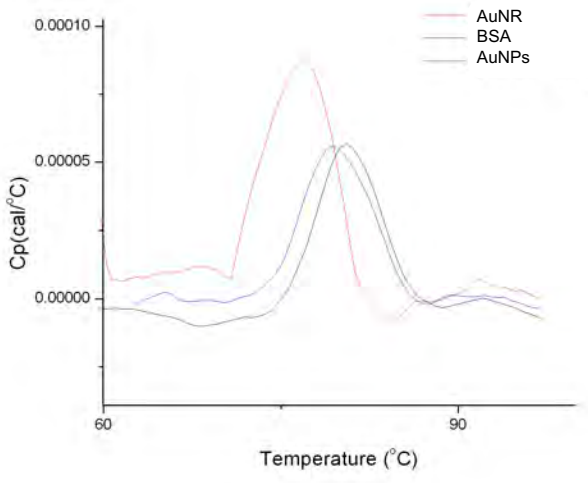

Figure 27. Thermograms of gold nanoparticles and nanorods incubated with BSA.

Figure 27 shows the T_m of BSA at 79.1 ºC. Then, the two T_m of the PC of gold nanospheres (AuNPs) and gold nanorods (AuNR) are dependent on the characteristics of each of the nanoparticles. Therefore, the thermodynamic profiles are different. Gold nanospheres present their peak (T_m) at 80.5 ºC, while nanorods T_m is found at 76.9 ºC. This result indicates that the protein corona formed on nanorods is less stable (lower temperature of melting) than the bare BSA. By contrast, the deposition of albumin over spherical gold nanoparticles increases slightly the T_m of the system (from 79.1 to 80.5 ºC). This is in accordance with the morphology of these two gold nanoparticles: as earlier detailed, rod-shaped particles show a higher aspect ratio and therefore, their curvature is lower (only present in the edges). Thus, the proteins deposited along the planes of the nanorods have lower space available and might show steric impediments and repulsion among them (Figure 28). For this reason, BSA molecules may deposit on the surface of spherical gold nanoparticles (that possess high curvature) with higher stability.

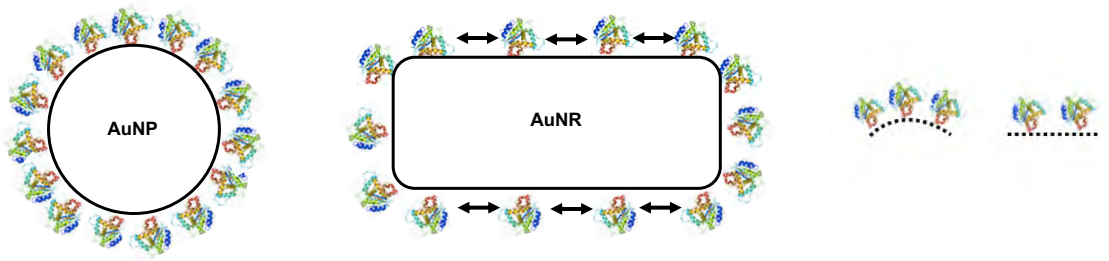

Figure 28. Schematic representation of the BSA deposition on gold nanospheres and nanorods.

In conclusion, the less stable PC formation of NR as compared to nanospheres could explain the differences in cell uptake observed in Figure 25. It has been here proved that the morphology of NPs influences the protein corona formation and stability.

3.4.5.2 Proteomics studies of PC

It was next studied the PC formation in a mixture of proteins, rather than a dispersion with one single protein, as for nanoDSC experiments. The aim was to correlate uptake and transfection studies performed so far with specific proteins present in the cell medium that may adsorb on nanoparticles' surface.

When designing gene delivery vectors, it is desired to obtain vectors with a net positive charge so that they can interact with anionic cell membranes. However, the study of how the protein corona around NPs modifies their charge has been gaining relevance as it impacts gene transfection. The PC formation was initially categorized as an unavoidable

but undesired phenomenon that impairs transfection efficacy[234,235]. Nonetheless, different studies have proposed that some components of the biocorona might have a positive impact in cell uptake and, similarly, the presence of certain proteins can also enhance transfection[236,237]. Thus, the goal of the proteomic studies presented here was to characterize the PC of the carriers studied in this work in order to better understand the enhanced transfection efficacy with OM-pBAE-metallic complexes obtained so far (Figure 26).

To this end, the protein corona formed when NPs were added to the cell media complemented with FBS was characterized with MS. Since proteins from the soft corona exchange with high dissociation rates, the hard PC is more likely to interact with cell receptors to allow internalization and cause some effect on transfection. Therefore, the hard corona was isolated using a protocol described elsewhere[198]. OM-pBAE polyplexes, metallic NPs and complexes of both were incubated with DMEM complemented with FBS. After PC isolation, LC-MS was used to determine the Exponentially Modified Protein Abundance Index (emPAI) value for each sample, which is proportional to the absolute protein concentration. Then, the 50 most abundant proteins were selected and a heatmap was built (Figure 29). This figure shows different protein corona profiles for each of the samples characterized in this work. Bare gold nanoparticles (AuNP) resulted in a less diverse protein corona spectrum as compare to bare SPIONs (SP). This is in agreement with a previous work that showed that the NP material, among other parameters, plays a key role in the biocorona formation and composition[238].

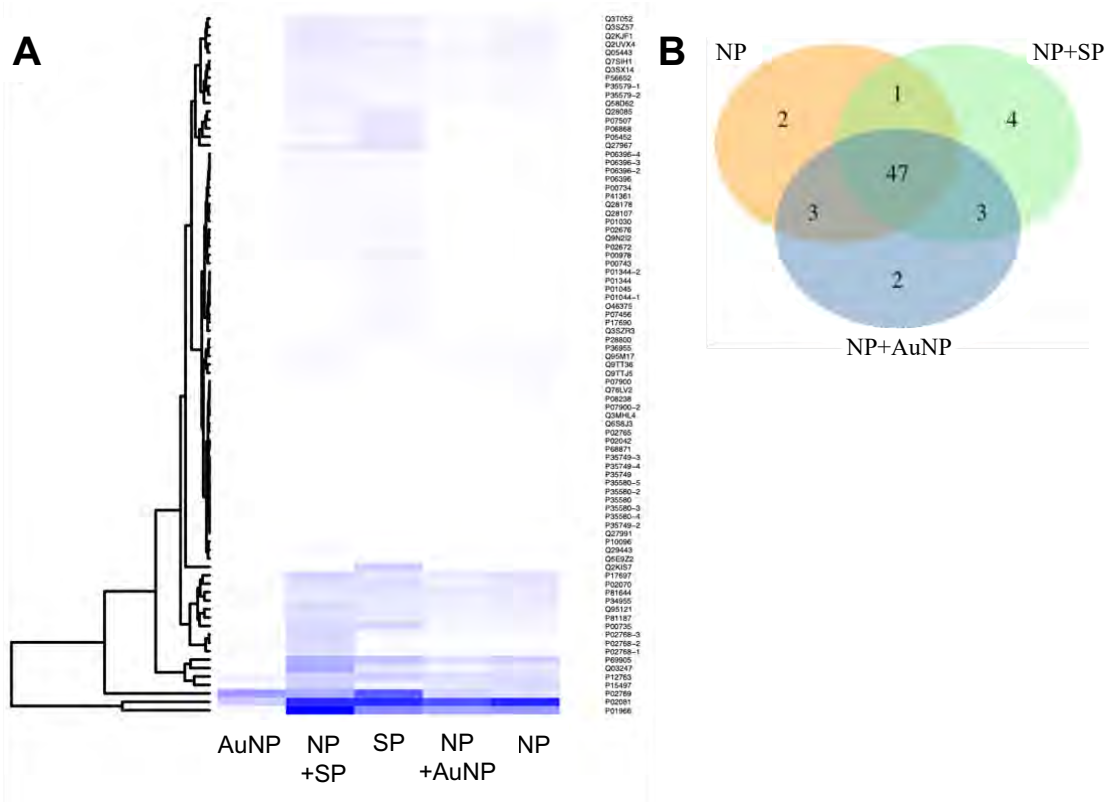

Figure 29. Mass spectrometry data for the different NPs used. . (A) Heatmap of the bare metallic particles (AuNP and SP), the OM-pBAE alone (NP) and the OM-pBAE combined (NP+SP and NP+AuNP) where blue indicates high emPAI value and white indicates absence of protein; (B) Venn Diagram of the proteins found in each transfection complex studied.

Similarly, complexation of pBAE NPs with metallic NPs also led to distinct protein profiles. Differences in the protein coronas of these three systems (NP, NP+SP and NP+AuNP) were less noticeable as compared to the clear differences in PC profiles between the two bare metallic NPs, probably because the addition of metallic particles did not modify entirely the surface area of original polyplexes as reported in chapter II. However, the data here presented indicated that the addition of metallic NPs greatly modifies individual protein abundances, which may trigger the observed differences in cell transfection. Due to the high sensitivity of this technique, 68% of the proteins from this top 50 list were shared, at least at low abundances, between the tree vectors (Figure 29B).

Previous studies have linked albumin – the most abundant protein in serum – adsorption with higher transfection rates by triggering unspecific cell uptake and endosomal escape under acidic conditions239,240. Although both OM-pBAE-metallic complexes exhibited higher emPAI values for albumin presence compared to bare OM-pBAE NP, the

differences of NP+AuNP with the bare OM-pBAE counterpart resulted non statistically significant. Only three proteins found in both pBAE-metallic particle complexes were absent in the bare OM-pBAE polyplexes (Figure 29B): secreted phosphoprotein 24, hyaluronan-binding protein 2 and serotransferrin. Phosphoprotein 24 (Spp-24) is a secreted bone matrix protein that is involved in bone remodelling. It binds to bone morphogenetic proteins (BMPs), which orchestrate cell survival and have been linked to cancer initiation and progression. Spp-24 has been shown to affect the activity of BMP by triggering cell apoptosis of PANC-1 cells241. Hyaluronan-binding protein 2 (HABP2) is a serine protease that undergoes an autocatalytic cleavage that converts the expressed single chain into a functional heterodimer. It may play a role in the coagulation cascades as it is known to activate the coagulation factor VII242. Similarly, to the Spp-24, it may act as a tumor suppressor by inhibiting cell proliferation and migration243. In the present work, no differences in cell viability have been observed between complexes that lack these proteins on the biocorona (bare OM-pBAE NP) and those that contain them (Figure 20

Figure 20. HeLa and PANC-1 cell viability when incubated with OM-pBAE-NPsB, 5 μg mL-1). These proteins found in the OM-pBAE-metallic complexes may have been found at too low concentrations to impair the cell viability in PANC-1 cells. Serotransferrin is known to bind to iron and was also found in the top 50 most abundant proteins for both, bare SPIONS and NP+SP. This was the only transferrin found in the top 50 list from all the NP studied and was not found in OM-pBAE NP alone but on the NP-metallic complexes. This protein has been linked to higher cell uptake through two internalization pathways depending on their size as proposed by Simões et al. Larger carriers are unspecifically uptaken by cells through non-coated pi-mediated endocytosis, similarly to albumin. On the other hand, smaller complexes found in the range of the particles used in this work undergo a transferrin receptor (TfR) driven endocytosis[221]. The latter internalization pathway has been previously described in different cell types, especially in tumor cells which overexpress this TfR[244,245]. Thus, the presence of transferrin upon the addition of metallic NPs might trigger a higher cell uptake as compared to the bare OM-pBAE NPs. More importantly, this protein has been described as a transfection enhancer as it facilitates the endosomal escape into the cytoplasm[222,244,246,247]. These internalization pathways triggered by albumin and transferrin explain, at least partially, the enhanced transfection of both metallic complexes. Thus, the different protein corona profiles observed might drive the enhanced gene transfection efficacy of the carriers studied in the present work.

It is important pointing out that because of the complex and dynamic behaviour of this biocorona, multiple events can be triggered simultaneously. That is, other proteins composing the PC may also contribute to the enhancement of the transfection efficacies observed so far in this work. Although this proteomic data may not completely explain the uncorrelated effects between transfection and cell uptake, it has shown an effect in transfection efficacy, probably due to the role of distinct protein adsorption. Therefore, studying the PC of gene delivery systems is crucial to understand the proteins that are implied in NPs' cell uptake and endosomal destabilization. That is, knowledge on PC of gene delivery systems is key to understand the overall cell response to their presence. These findings could be further exploited to pre-form the biocoronas to engineer high performance gene delivery vectors.

3.5 Concluding remarks

In this chapter, the quantification of the cell biocompatibility of our gene delivery systems has been performed in order to establish the working concentrations range with no adverse effects. Cell viability of both HeLa and PANC-1 cells was not impaired by either bare SPIONs, bare gold nanoparticles or complexes of these metallic particles with OM-pBAEs in a broad range of concentrations. SPIONs showed cell compatibility up to 100 μg ml^{-1} in HeLa cells. AuNPs showed higher levels of toxicity as compared to SPIONs, since PANC-1 viability was reduced from 25 μg of AuNP ml^{-1} on. For these reasons, the working concentration for any further cell experiment comprising SPIONs or gold NPs was fixed below 25 μg mL^{-1} of metallic particles.

Different versions of Inductively Coupled Plasma (ICP) have been employed for the study of cellular uptake. A broad study comprising different cell lines (HeLa and PANC-1), nanoparticles and complexes has been carried out. Cell uptake of the complexes increased at higher metallic NP concentrations, with AuNP exhibiting greater internalization compared to SPIONs. Moreover, rod-shaped gold nanoparticles have been also effectively synthetized. However, as expected, they showed a less efficient cell uptake than spherical gold nanoparticles. This might be explained by both the morphology and net charge differences between the two types of gold nanosystems. Interestingly, cell uptake of both gold nanospheres and nanorods as well as of SPIONs was increased when the metallic particles were complexed to OM-pBAEs. In the specific case of SPIONs, the internalization of such particles was nearly doubled in the presence of OM-pBAEs.

On the other hand, the addition of metallic particles to the OM-pBAE NPs enhanced the transfection efficacy on PANC-1 cells at any of the ratios tested (2.5 to 10 μg mL^{-1} of metallic particles). However, differently to cell uptake, transfection profiles showed a sweet spot at 5 μg mL^{-1} of SPIONs and AuNPs. Therefore, higher uptakes did not correlate completely with higher cell transfection rates.

In order to understand the obtained differences in the uptake and transfection profiles among NPs, the protein corona of the different complexes was isolated and analyzed. Proteomic data identified protein candidates that correlate with this enhanced transfection. Albumin and transferrin have been previously linked with higher transfection efficacies due to an enhanced unspecific and receptor-driven cell internalization, respectively. More importantly, they have shown to trigger endosomal escape allowing the cargo molecules to reach the cytosol of the cell. These findings highlight the

importance of understanding the biocorona composition and its correlation with transfection, which can be used to engineer pre-formed PC to enhance gene delivery efficacies.

Once the cell uptake and the transfection of our gene delivery system and the factors that might affect them have been assessed, in the next chapter the properties of SPIONs and gold nanoparticles will be exploited in order to obtain improved gene delivery systems and to modulate cellular mechanisms in cell lines that are difficult to modify. Different ways to incorporate the SPIONs onto the OM-pBAE polyplexes will be explored, a selection of effectively transfected cells will be tested and a platform for designing and tuning further transfection experiments will be proposed.

3.6 References

163. Xia, T., Kovochich, M., Liong, M., Zink, J. I. & Nel, A. E. Cationic polystyrene nanosphere toxicity depends on cell-specific endocytic and mitochondrial injury pathways. *ACS Nano* **2**, 85–96 (2008).

164. Xia, T. *et al.* Polyethyleneimine coating enhances the cellular uptake of mesoporous silica nanoparticles and allows safe delivery of siRNA and DNA constructs. *ACS Nano* **3**, 3273–3286 (2009).

165. Qiu, Y. *et al.* Surface chemistry and aspect ratio mediated cellular uptake of Au nanorods. *Biomaterials* **31**, 7606–7619 (2010).

166. Meng, H. *et al.* Engineered design of mesoporous silica nanoparticles to deliver doxorubicin and p-glycoprotein siRNA to overcome drug resistance in a cancer cell line. *ACS Nano* **4**, 4539–4550 (2010).

167. Meng, H. *et al.* Aspect ratio determines the quantity of mesoporous silica nanoparticle uptake by a small gtpase-dependent macropinocytosis mechanism. *ACS Nano* **5**, 4434–4447 (2011).

168. Zhao, F. *et al.* Cellular uptake, intracellular trafficking, and cytotoxicity of nanomaterials. *Small* **7**, 1322–1337 (2011).

169. Nel, A. E. *et al.* Understanding biophysicochemical interactions at the nano-bio interface. *Nat. Mater.* **8**, 543–557 (2009).

170. Foroozandeh, P. & Aziz, A. A. Insight into Cellular Uptake and Intracellular Trafficking of Nanoparticles. *Nanoscale Res. Lett.* **13**, (2018).

171. Chithrani, B. D., Ghazani, A. A. & Chan, W. C. W. Determining the size and shape dependence of gold nanoparticle uptake into mammalian cells. *Nano Lett.* **6**, 662–668 (2006).

172. Huang, X., Teng, X., Chen, D., Tang, F. & He, J. The effect of the shape of mesoporous silica nanoparticles on cellular uptake and cell function. *Biomaterials* **31**, 438–448 (2010).

173. Vivo, B. *et al.* The Shape Effect of Mesoporous Silica Nanoparticles on

Biodistribution ,. *ACS Appl. Nano Mater.* **5**, 5390–5399 (2011).

174. Pinals, R. L. *et al.* Protein Corona Composition and Dynamics on Carbon Nanotubes in Blood Plasma and Cerebrospinal Fluid. *bioRxiv Bioeng.* 1–32 (2020). doi:10.1101/2020.01.13.905356

175. Lundqvist, M. *et al.* The nanoparticle protein corona formed in human blood or human blood fractions. *PLoS One* **12**, 1–15 (2017).

176. Cedervall, T. *et al.* Understanding the nanoparticle-protein corona using methods to quantify exchange rates and affinities of proteins for nanoparticles. *Proc. Natl. Acad. Sci.* **104**, 2050–2055 (2007).

177. Ge, C. *et al.* Binding of blood proteins to carbon nanotubes reduces cytotoxicity. *Proc. Natl. Acad. Sci. U. S. A.* **108**, 16968–16973 (2011).

178. Wang, X. *et al.* Dispersal state of multiwalled carbon nanotubes elicits profibrogenic cellular responses that correlate with fibrogenesis biomarkers and fibrosis in the murine lung. *ACS Nano* **5**, 9772–9787 (2011).

179. Wang, X. *et al.* Quantitative techniques for assessing and controlling the dispersion and biological effects of multiwalled carbon nanotubes in mammalian tissue culture cells. *ACS Nano* **4**, 7241–7252 (2010).

180. Zhu, M. T. *et al.* Endothelial dysfunction and inflammation induced by iron oxide nanoparticle exposure: Risk factors for early atherosclerosis. *Toxicol. Lett.* **203**, 162–171 (2011).

181. Zhu, M. T. *et al.* Particokinetics and extrapulmonary translocation of intratracheally instilled ferric oxide nanoparticles in rats and the potential health risk assessment. *Toxicol. Sci.* **107**, 342–351 (2009).

182. Meng, H. *et al.* Ultrahigh reactivity provokes nanotoxicity: Explanation of oral toxicity of nano-copper particles. *Toxicol. Lett.* **175**, 102–110 (2007).

183. Hadjidemetriou, M. *et al.* In Vivo Biomolecule Corona around Blood-Circulating, Clinically Used and Antibody-Targeted Lipid Bilayer Nanoscale Vesicles. *ACS Nano* **9**, 8142–8156 (2015).

184. An, F. F. & Zhang, X. H. Strategies for preparing albumin-based nanoparticles for multifunctional bioimaging and drug delivery. *Theranostics* **7**, 3667–3689

(2017).

185. Wang, J., Byrne, J. D., Napier, M. E. & Desimone, J. M. More effective nanomedicines through particle design. *Small* **7**, 1919–1931 (2011).

186. Rappoport, J. Z. Focusing on clathrin-mediated endocytosis. *Biochem. J.* **412**, 415–423 (2008).

187. Wang, Z., Tiruppathi, C., Minshall, R. D. & Malik, A. B. Size and dynamics of caveolae studied using nanoparticles in living endothelial cells. *ACS Nano* **3**, 4110–4116 (2009).

188. Pelkmans, L., Kartenbeck, J. & Helenius, A. Caveolar endocytosis of simian virus 40 reveals a new two-step vesicular-transport pathway to the ER. *Nat. Cell Biol.* **3**, 473–483 (2001).

189. Tomatis, M. *et al.* High aspect ratio materials: Role of surface chemistry vs. length in the historical 'long and short amosite asbestos fibers'. *Inhal. Toxicol.* **22**, 984–998 (2010).

190. Conner, S. D. & Schmid, S. L. Regulated portals of entry into the cell. *Nature* **422**, 37–44 (2003).

191. Grant, B. D. & Donaldson, J. G. Pathways and mechanisms of endocytic recycling. *Nat. Rev. Mol. Cell Biol.* **10**, 597–608 (2009).

192. Luzio, J. P., Parkinson, M. D. J., Gray, S. R. & Bright, N. A. The delivery of endocytosed cargo to lysosomes. *Biochem. Soc. Trans.* **37**, 1019–1021 (2009).

193. Akinc, A., Thomas, M., Klibanov, A. M. & Langer, R. Exploring polyethylenimine-mediated DNA transfection and the proton sponge hypothesis. *J. Gene Med.* **7**, 657–663 (2005).

194. Sonawane, N. D., Szoka, F. C. & Verkman, A. S. Chloride Accumulation and Swelling in Endosomes Enhances DNA Transfer by Polyamine-DNA Polyplexes. *J. Biol. Chem.* **278**, 44826–44831 (2003).

195. Schaffer, D. V. & Lauffenburger, D. A. Optimization of cell surface binding enhances efficiency and specificity of molecular conjugate gene delivery. *J. Biol. Chem.* **273**, 28004–28009 (1998).

196. Huang, X., Neretina, S. & El-Sayed, M. A. Gold nanorods: From synthesis and properties to biological and biomedical applications. *Adv. Mater.* **21**, 4880–4910 (2009).

197. Putnam, D., Gentry, C. A., Pack, D. W. & Langer, R. Polymer-based gene delivery with low cytotoxicity by a unique balance of side-chain termini. *Proc. Natl. Acad. Sci. U. S. A.* **98**, 1200–1205 (2001).

198. Walkey, C. D. *et al.* Protein corona fingerprinting predicts the cellular interaction of gold and silver nanoparticles. *ACS Nano* **8**, 2439–2455 (2014).

199. Ishihama, Y. *et al.* Exponentially modified protein abundance index (emPAI) for estimation of absolute protein amount in proteomics by the number of sequenced peptides per protein. *Mol. Cell. Proteomics* **4**, 1265–1272 (2005).

200. Kudlicki, A. The optimal exponent base for emPAI is 6.5. *PLoS One* **7**, 6–9 (2012).

201. Calero, M. *et al.* Characterization of interaction of magnetic nanoparticles with breast cancer cells. *J. Nanobiotechnology* **13**, 16 (2015).

202. Shevtsov, M. a. *et al.* Tumor targeting using magnetic nanoparticle Hsp70 conjugate in a model of C6 glioma. *Neuro. Oncol.* **16**, 38–49 (2014).

203. Singh, N., Jenkins, G. J. S. S., Asadi, R. & Doak, S. H. Potential toxicity of superparamagnetic iron oxide nanoparticles (SPION). *Nano Rev.* **1**, 1–15 (2010).

204. Frank, J. A. *et al.* Magnetic intracellular labeling of mammalian cells by combining (FDA-approved) superparamagnetic iron oxide MR contrast agents and commonly used transfection agents. *Acad. Radiol.* **9**, 484–487 (2002).

205. Arbab, A. S. *et al.* Intracytoplasmic tagging of cells with ferumoxides and transfection agent for cellular magnetic resonance imaging after cell transplantation: Methods and techniques. *Transplantation* **76**, 1123–1130 (2003).

206. Mailänder, V. & Landfester, K. Interaction of Nanoparticles with Cells. *Biomacromolecules* 2379–2400 (2009).

207. Gu, J. L. *et al.* The internalization pathway, metabolic fate and biological effect of

superparamagnetic iron oxide nanoparticles in the macrophage-like RAW264.7 cell. *Sci. China Life Sci.* **54**, 793–805 (2011).

208. Haynes, C. L. *et al.* Nanoparticle optics: The importance of radiative dipole coupling in two-dimensional nanoparticle arrays. *J. Phys. Chem. B* **107**, 7337–7342 (2003).

209. Shibu Joseph, S. T., Ipe, B. I., Pramod, P. & George Thomas, K. Gold nanorods to nanochains: Mechanistic investigations on their longitudinal assembly using α,ω-alkanedithiols and interplasmon coupling. *J. Phys. Chem. B* **110**, 150–157 (2006).

210. Montaño, M. D., Olesik, J. W., Barber, A. G., Challis, K. & Ranville, J. F. Single Particle ICP-MS: Advances toward routine analysis of nanomaterials. *Anal. Bioanal. Chem.* **408**, 5053–5074 (2016).

211. Dan, Y., Shi, H., Liang, X. & Stephan, C. ICP - Mass Spectrometry Measurement of Titanium Dioxide Nanoparticles in Sunscreen using Single Particle ICP-MS. 4 (2015).

212. Neubauer, K. & Stephan, C. Determination of Gold and Silver Nanoparticles in Blood Using Single Particle ICP-MS. 3 (2014).

213. Bao, D., Oh, Z. G. & Chen, Z. Characterization of silver nanoparticles internalized by arabidopsis plants using single particle ICP-MS analysis. *Front. Plant Sci.* **7**, 1–8 (2016).

214. Amable, L., Stephan, C., Smith, S. & Merrifield, R. An Introduction to Single Cell ICP-MS Analysis. *White Pap.* 1–5 (2017).

215. Chithrani, B. D. & Chan, W. C. W. Elucidating the mechanism of cellular uptake and removal of protein-coated gold nanoparticles of different sizes and shapes. *Nano Lett.* **7**, 1542–1550 (2007).

216. Kah, J. C. Y., Chen, J., Zubieta, A. & Hamad-Schifferli, K. Exploiting the protein corona around gold nanorods for loading and triggered release. *ACS Nano* **6**, 6730–6740 (2012).

217. Zabner, J., Fasbender, A. J., Moninger, T., Poellinger, K. A. & Welsh, M. J. Cellular and Molecular Barriers to Gene Transfer by a Cationic Lipid. *J. Biol.*

Chem. **270**, 18997–29007 (1995).

218. Koltover, I., Salditt, T., Rädler, J. O. & Safinya, C. R. An Inverted Hexagonal Phase of Cationic Liposome – DNA Complexes Related to DNA Release and Delivery. *Science (80-.).* **281**, (1998).

219. Caracciolo, G. *et al.* Self-assembly of cationic liposomes – DNA complexes : a structural and thermodynamic study by EDXD. **351**, 222–228 (2002).

220. Yamada, Y., Kogure, K., Nakamura, Y., Inoue, K. & Akita, H. Development of Efficient Packaging Method of Oligodeoxynucleotides by a Condensed Nano Particle in Lipid Envelope Structure. *Biol. Pharm. Bull.* **28**, 1939–1942 (2005).

221. Simoes, S., Slepushkin, V., Pires, P., Gaspar, R. & Du, N. Mechanisms of gene transfer mediated by lipoplexes associated with targeting ligands or pH-sensitive peptides. *Gene Ther.* **6**, 1798–1807 (1999).

222. Simoes, S. *et al.* Transfection of human macrophages by lipoplexes via the combined use of transferrin and pH-sensitive peptides Abstract : The crucial function of macrophages in a variety of biological processes and pathologies. *J. Leukoc. Biol.* **65**, (1999).

223. Rodriguez-Quijada, C., Sánchez-Purrà, M., De Puig, H. & Hamad-Schifferli, K. Physical Properties of Biomolecules at the Nanomaterial Interface. *J. Phys. Chem. B* **122**, 2827–2840 (2018).

224. Ferrari, M. Frontiers in cancer nanomedicine: Directing mass transport through biological barriers. *Trends Biotechnol.* **28**, 181–188 (2010).

225. Winzen, S. *et al.* Complementary analysis of the hard and soft protein corona: Sample preparation critically effects corona composition. *Nanoscale* **7**, 2992–3001 (2015).

226. Baumann, R., Bodard, G., Cayless, H., Sosin, J. & Viglianti, R. Integrating Digital Papyrology. *Digit. Humanit. 2011* 2011–2020 (2010).

227. Ebert, D. D. *et al.* The 6-month effectiveness of Internet-based guided self-help for depression in adults with Type 1 and 2 diabetes mellitus. *Diabet. Med.* **34**, 99–107 (2017).

228. Bunjes, H. & Unruh, T. Characterization of lipid nanoparticles by differential

scanning calorimetry, X-ray and neutron scattering. *Adv. Drug Deliv. Rev.* **59**, 379–402 (2007).

229. Calorimetry, D. S. Differential Scanning Calorimetry; First and Second OrderTransitions in Polymers Purpose. *DSC Polym.* 1–7

230. Gill, P., Moghadam, T. & Ranjbar, B. Differential Scanning Calorimetry Techniques: Applications in Biology and Nanoscience. *J. Biomol. Tech.* **21**, 167–193 (2010).

231. Walkey, C. D. & Chan, W. C. W. Understanding and controlling the interaction of nanomaterials with proteins in a physiological environment. *Chem. Soc. Rev.* **41**, 2780–2799 (2012).

232. Michnik, A. Thermal stability of bovine serum albumin DSC study. *J. Therm. Anal. Calorim.* **71**, 509–519 (2003).

233. Lang, B. E. & Cole, K. D. Unfolding properties of recombinant human serum albumin products are due to bioprocessing steps. *Biotechnol. Prog.* **31**, 62–69 (2015).

234. Nagayama, S., Ogawara, K., Fukuoka, Y., Higaki, K. & Kimura, T. Time-dependent changes in opsonin amount associated on nanoparticles alter their hepatic uptake characteristics. **342**, 215–221 (2007).

235. Alexis, F., Pridgen, E., Molnar, L. K. & Farokhzad, O. C. Factors Affecting the Clearance and Biodistribution of Polymeric Nanoparticles. *Mol. Pharm.* **5**, 505–515 (2008).

236. Simoes, S. *et al.* Human serum albumin enhances DNA transfection by lipoplexes and confers resistance to inhibition by serum. **1463**, 459–469 (2000).

237. Akinc, A. *et al.* Targeted Delivery of RNAi Therapeutics With Endogenous and Exogenous Ligand-Based Mechanisms. *Mol. Ther.* **18**, 1357–1364 (2010).

238. Lundqvist, M. *et al.* Nanoparticle size and surface properties determine the protein corona with possible implications for biological impacts. **105**, 14265–14270 (2008).

239. Reed, R. G. & Burrington, C. M. The Albumin Receptor Effect May Be Due to a Surface-induced Conformational Change in Albumin *. (1989).

240. Schenkman, S., Araujo, P. S., Dijkman, R., Quina, F. H. & Chaimovich, H. Effects of Temperature and Lipid Composition on the Serum Albumin-induced Aggregation and Fusion of Small Unilamellar Vesicles. *Biochim. Biophys. Acta* **649**, 633–641 (1981).

241. Li, C. *et al.* Secreted phosphoprotein 24 kD (Spp24) inhibits growth of human pancreatic cancer cells caused by BMP-2. *Biochem. Biophys. Res. Commun.* **466**, 167–172 (2015).

242. Choi-Miura, N., Yoda, M., Saito, K., Takahashi, K. & Tomita, M. Identification of the Substrates for Plasma Hyaluronan Binding Protein. *Biol. Pharm. Bull.* **24**, 140–143 (2001).

243. Gara, S. K. *et al.* Germline HABP2 Mutation Causing Familial Nonmedullary Tyroid Cancer. *N. Engl. J. Med.* **373**, 448–455 (2015).

244. Camp, E. R. *et al.* Transferrin receptor targeting nanomedicine delivering wild-type p53 gene sensitizes pancreatic cancer to gemcitabine therapy. *Cancer Gene Ther.* **20**, 222–228 (2013).

245. Wagner, E., Curiel, D. & Cotten, M. Delivery of drugs , proteins and genes into cells using transferrin as a ligand for receptor-mediated endocytosis. **14**, 113–135 (1994).

246. Cheng, P. Receptor Ligand-Facilitated Gene Transfer: Enhancement of Liposome-Mediated Gene Transfer by Transferrin. **7**, 275–282 (1996).

247. Gatter, K. C., Brownt, G., Trowbridget, I. A. N. S. & Mason, D. Y. Transferrin receptors in human tissues : their distribution and possible clinical relevance. 539–545 (1983).

Chapter IV. Designing an enhanced transfection system for mesenchymal stem cells

Originally published as:

Balcells, L. *et al*. SPIONs' Enhancer Effect on Cell Transfection: An Unexpected Advantage for an Improved Gene Delivery System. *ACS Omega* 4, 2728-2740 (2019).

Patent: Multicomponent nanoparticles and use thereof (P201830507)

This page left blank intentionally

4.1 Introduction

In the previous chapters we have detailed a profound view into the cell mechanisms that rule the overall fate of gene delivery systems, so that genetic modification of cells could be better understood. In this chapter, this knowledge is applied and additional features from our gene delivery systems will be exploited to amplify their applicability. In other words, taking into account the cellular mechanisms behind cell transfection, discussed in chapter II, and the effect of protein corona on the cell uptake profiles of different nanoparticles, reviewed in chapter III, it is here proposed the application of our gene delivery systems to a more challenging purpose: the modification of mesenchymal stem cells for further use as cell therapy strategies. To do so, research on improved gene delivery vectors will be first approached.

As discussed earlier in this thesis, the success of gene therapy is largely dependent on the development of a vector or vehicle that can selectively and efficiently deliver a gene to target cells with minimal toxicity[248]. Also, substantial efforts have been devoted to the development of new Magnetic Nanoparticles (MNPs), the understanding of their behaviour, and the improvement of their applicability in many different areas. Magnetic cell labelling, hyperthermia, magnetic resonance imaging (MRI), tissue engineering and repair and biochemical separations are some of the applications for which MNPs have been extensively investigated[249–251]. Moreover, they have become key players in what is called *theranostics*, which consists on the combination of diagnostic and therapeutic entities into one drug delivery vehicle[252]. These new tools will have a profound impact on disease prevention, diagnosis and treatment, and, in the end, on the development of personalized medicine[253]. In fact, magnetic nanoparticles in combination with polyplexes were employed in previous chapters of this thesis. The biocompatibility of these systems, their modification of the interaction of gene delivery systems with proteins present in the medium, and the alteration of their cellular internalization and intracellular fate were proven.

Superparamagnetic Iron Oxide Nanoparticles (SPIONs) are a type of magnetic nanoparticles that consist of a magnetic core, surrounded by a hydrophilic and biocompatible coating to prevent agglomeration and ensure stability. These MNPs stand out due to their magnetic core that generally involves either magnetite (Fe_3O_4) or maghemite (γ-Fe_2O_3) and provides superparamagnetic properties. In addition, they can be functionalized with ligand molecules to achieve a certain function (e.g., targeting, membrane crossing or endosomal escape) and can also transport different substances

and molecules, such as chemotherapeutic agents, antibodies, nucleic acids, radionuclides, etc. To date, they have been used: (a) as contrast agents for MRI and magnetic cell labelled tracking in diagnostic applications[249,250,254] and (b) for magnetofection, which is a transfection technique that uses magnetic fields to attract particles containing magnetic nanoparticles into cells[66–68]. SPIONs are, by far, the most commonly MNP employed for medical applications[255]. Also, in the previous chapters, it has been demonstrated that the presence of SPIONs alters the autophagy process in HeLa cells, increases cell uptake of OM-pBAE polyplexes in HeLa and PANC-1 cells and results suggest that they also improve the transfection efficiency of such systems in PANC-1 cells.

Considering that such SPIONs are biocompatible, have been already used as part of gene delivery systems, and have shown to play a role in the cellular mechanisms behind cell transfection, their expanded use in combination with OM-pBAEs and genetic material was proposed. A broad transfection study comprising different carriers and cell lines ranging from more permissive to highly restrictive cells was carried out in order to find the best performing systems that could be further used to transfect stem cells.

In the present work, 2,3-dimercaptosuccinic acid (DMSA)-coated SPIONs were employed. Since surface coating is the most important parameter affecting cell interaction and *in vivo* distribution[68], magnetite-based ferrofluids need a surface coating in order to stabilize them and avoid their reactivity with non-desired molecules or their aggregation at a physiological pH. Due to its chemical properties as chelating agent, the FDA approved the use of DMSA for treatment of heavy metal poisoning in humans in 1989. This fact has been used to support its application as a biocompatible stabilizing coating for MNPs, since DMSA alone shows low-toxicity in various biological systems already studied[252]. In iron oxide nanoparticles, DMSA molecules are bound symmetrically to the magnetite nanoparticle surface through oxygen atoms, and the Fe–O–C linkage is similar to a polar covalent bond. These SPIONs have been proved to have excellent properties in terms of efficiency and biocompatibility for application to target cancer cells such as MCF-7 breast cancer cells[201], and have been already used for nanothermometry, magnetic separation, and bioremediation[252].

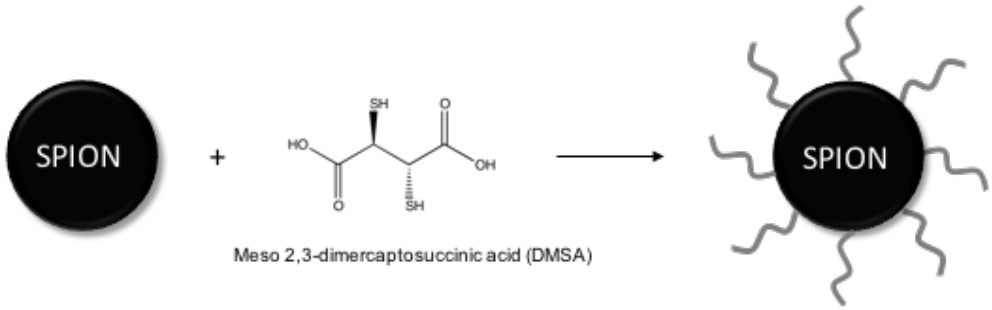

Figure 30. DMSA coating of SPIONs

Thus, we have here explored different strategies to form OM-pBAE nanoparticles containing both pDNA and SPIONs to transfect a variety of cell lines, aiming to determine whether SPION-containing OM-pBAE nanoparticles were able to enhance the efficiency of transfection of pDNA/pBAE polyplexes. Additionally, the magnetic feature of SPIONs, will allow the separation of efficiently transfected cells through the application of a magnetic field.

When cells are genetically modified, they can next be employed for several further purposes including immunotherapy, stable transgene expression in eukaryotic cells, theranostics, ex vivo models for clinical applications, and cell therapy strategies[256–263]. Most of these applications, especially the ones related to cell therapy, require a selection of successfully modified cells to increase the probabilities of achieving a final beneficial effect, and, therefore, the enrichment and selection of genetically modified cells become a key matter[81]. At this point and given the current growing interest in the combination of both gene and cell therapy strategies, a system allowing simultaneously the genetic modification of cells and their subsequent selection for *in vivo* implantation would be of great interest.

Taking advantage of the fact that we have a well-performing gene delivery system with the possibility to perform cell selection after cell modification, the work presented here could help improve current stem cells therapies. There is a great difficulty of efficiently deliver genetic material to stem cells due to their reluctance to be transfected, and clinical application of these strategies is hindered by expensive and complex regulatory requirements. Also, the lack of successfully modified cells can lead to counterproductive therapies. Putting together the knowledge of our gene delivery systems in terms of uptake and cell trafficking and the possibility to perform magnetic selection, the work presented here could be of great interest for further use of stem cells in cell therapy strategies.

It has been discussed that OM-pBAE polyplexes are valid and well-known gene delivery vectors and that they are able to enter cells efficiently and cause an effect. These polymers will be the basis of the delivery systems that will be used in the present chapter. As reported in chapters II and III, multicomponent nanoparticles composed of OM-pBAE polyplexes and a metallic component will be employed. Moreover, new ways to incorporate the metallic nanoparticles to the polyplexes will be also explored. Considerable attention will be devoted to the metallic component of the particles, including gold and iron-based MNPs, with a special focus on the SPIONs because of their high impact on cellular mechanisms shown in chapter II.

So, in the present chapter a wide range of transfections will be performed, and results will be analyzed according to what has been exposed in the previous chapters. Also, the magnetic selection of cells will be employed as a complement to the gene delivery systems allowing for clinical implantation of such systems. Finally, a platform for cell modification applicable to more challenging cell lines will be proposed. In conclusion, the overall results of this thesis will allow for the design and application of gene delivery systems with enhanced cell transfection efficacies. Through the understanding of the cellular responses behind cell transfection, it will be possible to customize new cell therapies thus improving their efficiency.

4.2 Aims

In order to achieve the main objective of the present chapter, the following tasks were proposed:

- Explore different ways to complex SPIONs and OM-pBAE polyplexes to form different types of nanoparticles and study the ability of such complexes to transfect different cell lines.

- Analyze the effect of the presence of SPIONs on the transfection efficiency of polyplexes made of OM-pBAE and GFP plasmid in both permissive and reluctant to transfection cell lines, and select the best performing systems.

- Perform an efficient sorting of magnetic labelled cells according to the internalization of SPIONs that allows the separation of cells containing the nanocomplexes formed by SPIONs, DNA and OM-pBAEs from the non-containing ones.

- Study the potential of the newly developed gene delivery systems as vectors for improved cell therapy applications in mesenchymal stem cells.

4.3 Materials and Methods

4.3.1 Materials

Reagents and solvents used in this chapter were purchased from Sigma-Aldrich. Plasmid pmaxGFP (3486 bp) was obtained from Amaxa. CR3 (NH2-Cys-Arg-Arg-Arg-COOH) peptide was obtained from GL Biochem Ltd (Shangai). DMSA-coated SPIONs (hydrodynamic size = 45 nm; surface charge = -12 mV; stock SPIONs dispersion, dispersed in water as the dispersant) were performed by Unit 9 of the Plataform of Production of Biomaterials and Nanoparticles of the NANBIOSIS ICTS, by the *Superfícies y Partículas Nanoestructuradas del Instituto de Nanociencia de Aragón* (PI J. Santamaría) group[143,144]. Cos-7, HeLa, U-87 MG and AMSC cells were obtained from ATCC (Manassas, VA). Products for cell culture (media, PBS, glutamine, penicillin-streptomycin solution, Lipofectamine® 2000) were obtained from Gibco, Hyclone and Invitrogen. SYBR™ Safe was obtained from Invitrogen (CA, USA). Magnetic and sterile-stored MS Columns were purchased from Miltenyi Biotec S.L., (Bergisch Gladbach, Germany).

4.3.2 pBAE synthesis and modification with oligopeptides

One of the best performing poly(β-amino ester) basic structures is C32 polymer, which is obtained by addition of 5-amino-1-pentanol to 1,4-butanediol diacrylate, as described in literature[264–266]. However, the positive charge provided by the tertiary amine of the C32 structure was proved to be inefficient for DNA encapsulation. To overcome this issue, the modification of C32 ends with short and positively charged oligopeptides, as described by Dosta *et al.*[147] was proposed. In particular, R3 oligopeptide (Cys-Arg-Arg-Arg) was used. Tri-arginine end-modified pBAE C32-CR3, was obtained by end-modification of acrylate-terminated C32 polymer with thiol-terminated tri-arginine oligopeptide. Although good DNA complexation and cell transfection results were obtained with oligopeptide-modified C32, the hydrophilic nature of this polymer leads to unstable nanoparticles. Therefore, the addition of a partially hydrophobic chain was suggested. 1-hexylamine, which is more hydrophobic than 5-amino-1-pentanol, was used. Nanoparticles synthesized at a ratio of 1.2:0.5:0.5 1,4-butanediol diacrylate:hexylamine:5-amino-1-pentanol were found to be more stable and to transfect cells with higher efficiency[147]. The modification of C6 ends with short and positively charged oligopeptides (C6-CR3), follows the same scheme as for C32.

4.3.3 SPION-containing nanoparticles manufacturing

Three types of nanoparticles were formed and tested: (a) Nanoparticles where the SPIONs and DNA are encapsulated by the polymer, named “T” (together); (b) Nanoparticles where the DNA is encapsulated by the polymer and then SPIONs are added to the solution, named “S” (separated); (c) Multicoating nanoparticles consisting of 4 layers: a nucleus formed by SPIONs; a polymer layer encapsulating the nucleus; a plasmid DNA layer and another polymer layer to ensure the DNA encapsulation, named “M” (Figure 31).

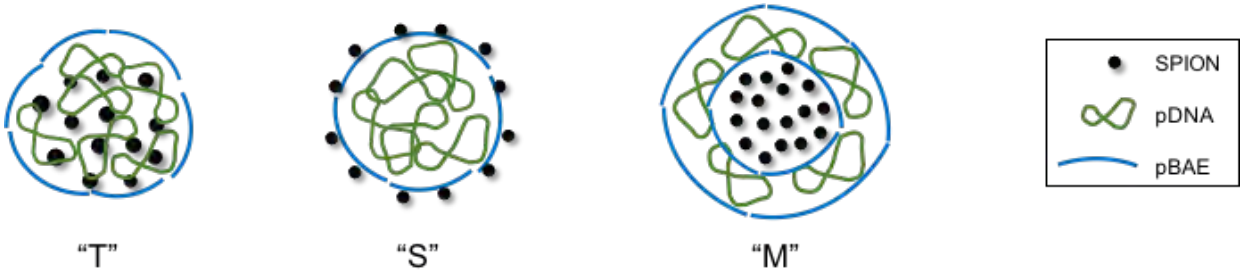

Figure 31. Scheme of the different structures hypothesized for SPION-containing nanoparticles

All these nanoparticles were freshly prepared in sodium acetate buffer solution (25 mM, pH = 5.5) and incubated for 30 min at 37 ºC. Then they were nanoprecipitated in serum-free DMEM (4.5 g glucose mL^{-1} without glutamine, pH = 7.2) prior to each transfection or in PBS (1X, pH = 7.4) prior to its DLS analysis. The complexes polymer:DNA:SPIONs were synthetized mixing equal volumes of polymer solution with DNA and/or SPIONs solution at different ratios.

The synthesis of 50 µL of S-type C32-CR3:pGFP (50:1) SPION-containing nanoparticles at 5 µg of SPIONs mL^{-1} is described in detail as an example: One Eppendorf was prepared with 25 µL of pGFP DNA solution in Sodium Acetate buffer 25 mM to get a concentration of $3x10^{-2}$ µg of DNA $µL^{-1}$. Another Eppendorf was prepared using 0.75 µL of C32-CR3 at 100 mg mL^{-1} diluted in Sodium Acetate buffer 25mM at 25 µL final volume. The Eppendorf containing the DNA solution was homogenized with a micropipette and its whole volume (25 µL) was added to the polymer solution Eppendorf, which had just been vortexed for 10 seconds. This mixture was incubated at 37 ºC for 30 min. Then, nanoparticles were further diluted 10 fold in PBS or DMEM and the necessary volume of SPIONs was added in order to have a final concentration of 5 µg of SPIONs mL^{-1}.

4.3.4 Gel retardation assays

Gel retardation assays or electrophoretic mobility shift assays (EMSA) were performed to confirm the complexation of plasmids with polymers and SPIONs. T,S and M-type nanoparticles were used. The polymer to pDNA ratio was fixed to 50:1 (w/w) with 2.5 or 5 μg mL^{-1} SPIONs. pBAE–pDNA complexes were freshly prepared and added to wells of agarose gel (0.8%, SYBR™ Safe used as staining agent). Samples were run at 80 V for 30 min (Apelex PS 305, France) and visualized by UV illumination.

4.3.5 Biophysical characterization of SPION-containing nanoparticles

4.3.5.1 *Dynamic Light Scattering*

The particle average hydrodynamic diameter (size) of the nanoparticles was determined by Dynamic Light Scattering (DLS) using a Zetasizer nano ZS (Malvern Instruments Ltd., United Kingdom, 4-mW laser). All the measurements were performed at 25 ºC with 30 seconds equilibrium time using a wavelength of 633 nm. Correlation functions were collected at a scattering angle of 90 º, and the Malvern particle sizing software (DTS version 5.03) was used to determine the particle size. The equipment was set to perform 3 measures each of which consisting of 10 cycles of measurements. The final size value of each sample was equivalent to the mean of these 3 measures. The size distribution was given by the polydispersity index (PDI). This is a value between 0 and 1 that indicates how does the size of the nanoparticles in the sample differ among them; a value of 1 indicates a lot of variability in sizes and thereby that the sample is not homogeneous; a value close to 0 means that the nanoparticles of the sample are very uniform in size. The samples to analyze by DLS were prepared diluting 100 μL of nanoparticles solution (in acetate buffer) in 1 mL final volume of PBS 1X previously filtered (0.22 μm) to simulate cellular environment.

The surface charge of the SPIONs:pBAE:DNA polyplexes (ζ potential) was determined from the electrophoretic mobility by means of the Smoluchowski equation[267]. The ζ potential measurements for each sample were performed in triplicates and every measurement consisted in 10 cycles of an applied electric field. The difference in potential when applying a constant voltage of 20 mV was determined by the DLS equipment. For this measures, 700 μL of the previously diluted nanoparticles were added into a ζ potential cuvette.

4.3.6 In vitro experiments

4.3.6.1 Cell lines

Different cell lines were used in the present chapter, all of them obtained from ATCC:

- Cos-7 cells (ATCC CRL-1651) are fibroblasts derived from African green monkey kidney tissue.
- HeLa cells (ATCC CCL-2) are derived from a cervical cancer taken from a 31-years-old patient.
- U-87 MG cells (ATCC HTB-14) are human primary glioblastoma cells with epithelial morphology. This cell line was obtained from a stage IV 44-year-old cancer patient.
- AMSCs (ATCC PCS-500-011) are adipose-derived mesenchymal stem cells from healthy human adults.

All cell lines were thawed and cultured in cell culture dishes. Culture media of these 3 cell lines was DMEM (4.5 g glucose mL^{-1} without glutamine, pH = 7.2) supplemented with 10% Fetal Bovine Serum (FBS, Hyclone, Utah USA), 1% penicillin/streptomycin mixture and the amino acid glutamine. Cells were grown on incubators at 37 ºC with 5% CO_2 atmosphere during successive passages, most of the times at ratio 1:5 every 2 or 3 days. Depending on the experiment, cells were cultured in 6, 12, 24 or 96-well plates, being this last one the most frequently used. Maintenance cell passages were done in 100x20mm polystyrene cell culture dishes (Thermo Fisher Scientific, Waltham, MA USA).

4.3.6.2 Cell transfection

For a 96-well plate, the detailed procedure of transfection was as follows. Cells were seeded on the plate at a concentration of $4x10^4$ cells/cm^2. Seeded cells were incubated at 37 ºC in 5% CO_2 atmosphere for 24 h before transfection. SPION-containing pBAEs/DNA nanoparticles were prepared as described above using pGFP. Polyplexes were nanoprecipitated and diluted in serum-free DMEM at a final concentration of 1.5 µg pGFP mL^{-1}. Then, cells were washed with PBS and 200 µL of the nanoparticles solution were added to each well at a final pGFP concentration of 0.3 µg/well. Cells were incubated for 2 h at 37 ºC in 5% CO_2 atmosphere. Subsequently, transfection media was removed and fresh supplemented media was added to the cells. Twenty-four hours later, GFP expression was observed by fluorescence microscopy and 48 h after transfection,

cells were incubated for 5 min with trypsin-EDTA at 37 ºC in 5% CO_2 atmosphere and fixed with previously filtered paraformaldehyde (PFA, 0.22 µm, 2% in PBS). GFP expression was quantified by flow cytometry (BD LSRFortessa cell analyzer) and compared against a negative control of untreated cells and a positive control of Lipofectamine® 2000 (Invitrogen by Life technologies, Thermo Fisher Scientific).

4.3.7 Magnetic cell sorting

HeLa cells, were transfected with different transfection agents: C6CR3-based nanoparticles without SPIONS (NP), S- and M-type nanoparticles at 5 µg of SPIONS mL^{-1} (S and M), and lipofectamine 2000 (C+). After that, they were trypsinized and fixed and further sorted using MS columns. For these sorting experiments, 24-well plates were employed. For each sample, a new column was used. First, the column was placed in direct contact with strong magnets and it was equilibrated by loading 1 mL of previously filtered PBS. The sample was then loaded, and the eluted fraction (nonmagnetic cells) was collected. Then, the magnet was removed, the column was placed on another Falcon tube, and the retained fraction (magnetic cells) was eluted by adding 2 mL of PBS and pressing the plunger. Thus, two fractions were obtained from each sorted sample. Apart from the sorted samples, replicates that were not sorted were also prepared. Then, these non-sorted samples together with the magnetic and nonmagnetic fractions of each sorted sample were centrifuged at 1000 rpm for 5 min. The supernatant was discarded until only 200 µL of media or PBS was left, and the pellet was resuspended. This was analyzed by flow cytometry (FACS) in terms of GFP expression and number of cells, and it was possible to determine whether the SPIONs and the DNA/pBAE complexes entered together in the cells or not.

4.3.8 Statistical analysis

GraphPad Prism software was used for the statistical analysis. Two-way ANOVA and t-test were applied to find out statistical differences between groups or between each condition as compared to the control group, respectively. The significance of the difference in the data is $*p < 0.05$, $**p < 0.01$, $***p < 0.001$, and $****p < 0.0001$ regarding controls of untreated cells (C−) or cells treated with DNA/OM-pBAE nanoparticles without SPIONs (NPs), depending on the experiment.

4.4 Results and Discussion

In the previous chapters, the characterization of the gene delivery systems used hereinafter was performed. These complexes were used to study both their interaction with proteins modulating their cellular uptake and the intracellular mechanisms affecting overall transfection results. Also, their locations within the cells were assessed. Here, besides the addition of SPIONs to the pre-formed OM-pBAE/DNA polyplexes, other ways to complex SPIONs to these polyplexes were exploited with the aim of finding possible better performing systems. Then, these multicomponent nanoparticles were employed to transfect different cell lines and to select effectively transfected cells. Finally, the overall results of this thesis altogether will open the door to the design of improved stem cell modifications for use in cell therapy strategies.

4.4.1 Manufacturing of multicomponent nanoparticles

Considering previous results from our group and results disclosed in previous chapters in this thesis, it has been demonstrated that DNA can be encapsulated by means of cationic OM-pBAEs[161] and that SPIONs can be incorporated in such polyplexes, respectively. Aimed at finding SPION-containing nanoparticles with high efficacies in cell transfection, different ways to form DNA-loaded SPION-containing nanocarriers were explored. In particular, the three types of nanoparticles explained in the Materials and Methods section were formed and tested: (a) Nanoparticles where the SPIONs and DNA were encapsulated by the polymer, named “T” (together); (b) Nanoparticles where the DNA was encapsulated by the polymer and then SPIONs were added to the solution, named “S” (separated); (c) Multicoating nanoparticles consisting of 4 layers: a nucleus formed by SPIONs; a polymer layer encapsulating this nucleus; a plasmid DNA layer; and another polymer layer to ensure the DNA encapsulation, named “M”.

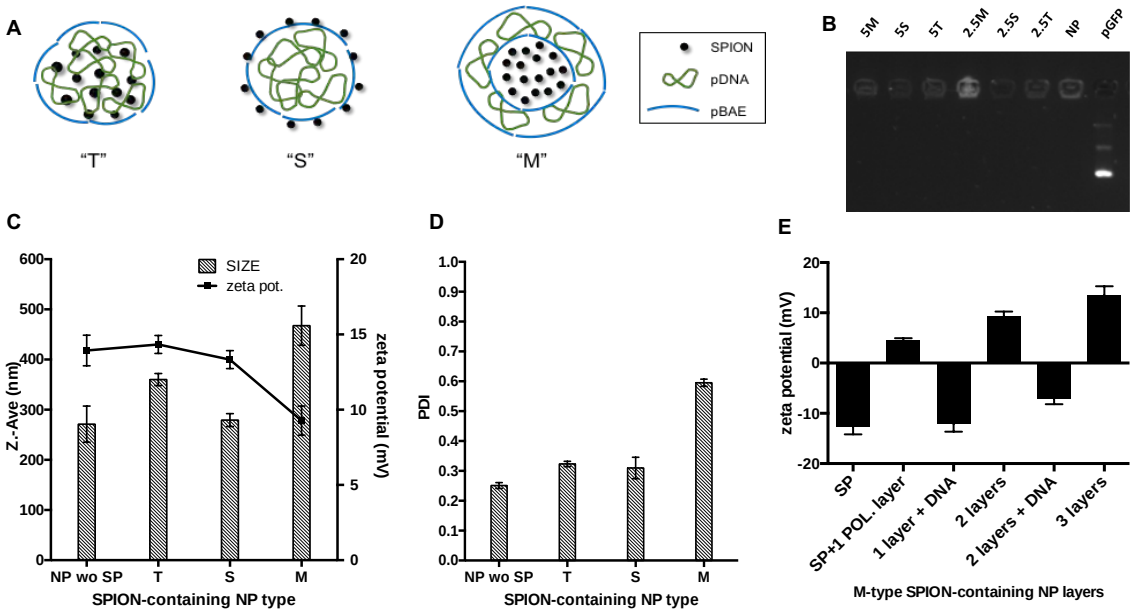

Figure 32. Manufacturing and characterization of SPION-containing nanoparticles. (A) Scheme of the different structures hypothesized for SPION-containing nanoparticles (T = together nanoparticles; S = separate nanoparticles; and M = multicoating nanoparticles); (B) EMSA of naked pGFP (pGFP) and the plasmid complexes with only pBAE (NP) and with pBAE + SPIONs, at the indicated concentrations, with the different type of structures (T, S or M); (C) Hydrodynamic diameter (in nm) and zeta potential (in mV), by DLS analysis, of nanoparticles without SPIONs and different SPION-containing nanoparticles at a fixed SPIONs' concentration; (D) Polidispersity Index (PDI) of the same nanoparticles; (E) Layer by layer zeta potential analysis of M-type SPION-containing nanoparticles. All data correspond to mean +/s SD values of, at least, three replicates.

"T" type of SPION-containing nanoparticles was formed following the most similar procedure to the SPION-free nanoparticles (NP without SP). First, a gel retardation assay confirmed the complexation of the plasmid with the pBAE polymer, without and with the presence of SPIONs (Figure 32B). As shown in Figure 32C, these nanoparticles showed a bigger hydrodynamic diameter than nanoparticles without SPIONs (NP wo SP) but in the acceptable size range and a positive surface potential. "S"-type nanoparticles are equally formed as the NPs with the exception that just when they precipitate, SPIONs are added to the solution. Thus, SPIONs are thought to be attached to the nanoparticle surface. These NPs showed almost the same size and zeta potential than nanoparticles without SP (NP wo SP). Although it could be expected a negative surface charge due to the hypothesized presence of the SPIONs at the external part of the nanoparticle, these nanoparticles remain cationic because we did not add enough SPIONs to form a continuous layer surrounding the whole nanoparticle surface. This was made in order to maintain the cationic character of the nanoparticles, required to enhance cell transfection. Finally, "M"-type SPION-containing NPs are the most differently formed from conventional DNA/OM-pBAE NPs, as they imply a layer by layer (LbL) deposition

of the different elements. The LbL deposition of oppositely charged polyelectrolytes on the surface of condensed DNA or viral particles has been largely employed[268–270]. However, LbL on the surface of inorganic nanoparticles, such as the SPIONs employed here or the gold nanoparticles, has recently attracted attention from researchers because of their capability to deliver therapeutic genes to human cells[257]. The higher hydrodynamic diameter and PDI (Figure 32C and D) of these particles was expected because of the LbL procedure[99,271].

Evidence of the LbL deposition could be observed analyzing the zeta (ζ) potential of multicoating nanoparticles of C32-CR3 pBAE at a weight ratio of 50:1 with the pGFP and at a SPIONs concentration of 5 μg mL^{-1} (Figure 32E). As previously mentioned, a nucleus of SPIONs, which are negatively charged due to its DMSA coating, was covered with an initial layer of polymer, which was positively charged, inducing a drastic change of the ζ potential of the nanoparticles formed, from clearly negative to positive values. Subsequent addition of DNA produced a change of the ζ potential from positive to negative, thus demonstrating that it was interacting with the positive nanoparticles previously formed. Similarly, further additions of either polymer or DNA layers switched the ζ potential of the polyplexes. The plot on Figure 32E shows the ζ potential switches derived from three polymer layers. However, because of their excessive size (data not shown), M nanoparticles with three polymeric layers were not employed. Further experiments were carried out with two polymer layers M-type nanoparticles, which are formed by a total of 4 layers including the SPIONs nucleus, the 2 polymeric layers and the DNA layer.

4.4.2 SPIONs' optimal concentration for transfection assays

Once these three approaches to form SPION-containing nanoparticles were characterized in terms of size and polydispersity, their transfection efficiency was next analyzed. We first determined the optimal SPIONs concentrations to work with and then which type of SPION-containing nanoparticles should be chosen for further experiments.

First, a screening of different SPIONs concentrations into DNA/OM-pBAEs polyplexes was conducted with the aim to choose the ones showing more transfection efficiency. Considering the cell compatibility results obtained with the SPIONs (chapter III), a range between 0 and 20 μg of SPIONs mL^{-1} was chosen. This experiment was performed with Cos-7 cells, since they are considered a permissive cell line, and with one common type of nanoparticles (T-type) for all the SPIONs concentrations. The other types of SPION-

containing nanoparticles would be latter deeply analyzed in terms of transfection efficiency.

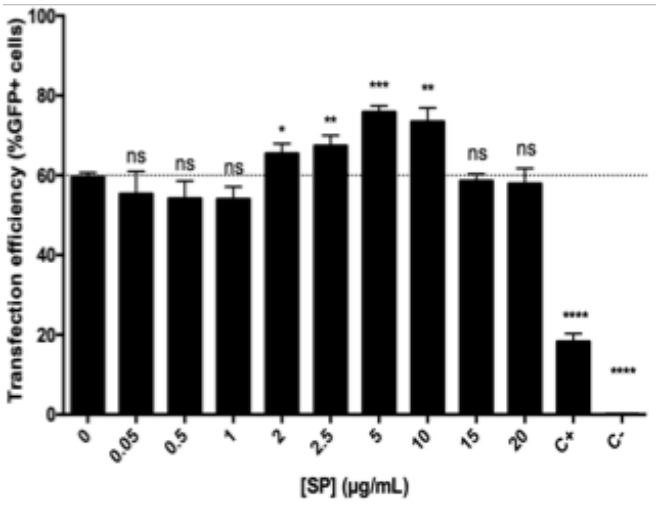

Figure 33. FACS analysis regarding the transfection efficiency screening of different SPIONs concentrations into C32-CR3:pGFP(50:1) T nanoparticles. Their percentage of GFP expression was measured by FACS. The values are the mean ± SD of experiments carried out in triplicate. The significance of the difference in the data is *p<0.05, **p<0.005, ***p<0.0005 and ****p<0.0001 regarding cells treated with DNA/OM-pBAE nanoparticles without SPIONs (0). "ns" means no significance. C+ are cells treated with Lipofectamine® and 0.1 µg of pGFP/well and C- are untreated cells.

The expression of the reporter gene GFP was used to evaluate the transfection efficiency. FACS analysis allowed for the quantification of transfection efficiency as detailed in Figure 33. Remarkably, this figure indicates that at a SPIONs concentration ranged between 2 and 10 µg mL^{-1} the transfection efficiency significantly increased in comparison to nanoparticles that did not contain SPIONs (NPs), indicating that probably, below 2 µg of SPIONs mL^{-1} the amount of these magnetic nanoparticles might not be enough to cause any effect on the cells. On the other hand, at concentrations higher than 10 µg of SPIONs mL^{-1}, these magnetic nanoparticles (MNP) may agglomerate leading to inefficient uptake of polyplexes. This plot also reveals that the highest percentage of transfected cells was observed around 5 µg mL^{-1} of SPIONs. From concentrations higher than 5 µg SPIONs mL^{-1}, transfection ratios decreased. Thereby, 0.5, 2.5 and 5 µg of SPIONs mL^{-1} were the chosen concentrations to work with in further experiments. Interestingly, these working concentrations are far from the toxicity range of SPIONs showed in chapter III. Also, this is in accordance with previous results where S-type NPs at 5 µg of SPIONs mL^{-1} showed increased transfection efficiency in PANC-1 cells.

4.4.3 Transfection screening of the different SPION-containing nanoparticles

Once the SPIONs concentrations were established, the most efficient type of nanoparticle had to be chosen. In order to do so, Cos-7 cells were treated with the three types of nanoparticles formed (T, S and M) at 0.5, 2.5 and 5 µg of SPIONs mL^{-1}. The transfection efficiency of all the different conditions was first observed by fluorescence microscopy (Figure 34A) and then quantified by FACS (Figure 34B).

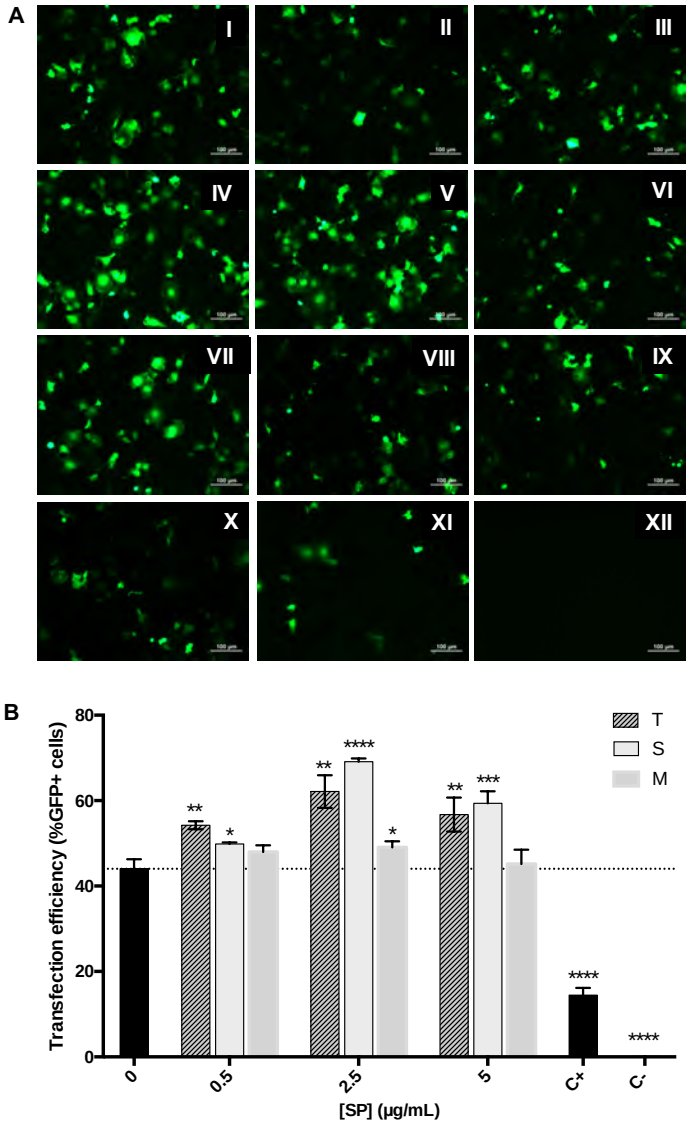

Figure 34. Transfection screenings of the different nanoparticles. (A) Fluorescence microscopy images of the T, S and M C32-CR3:pGFP (50:1) nanoparticles transfections on Cos-7 cells at different SPIONs concentrations. (I): 0.5 T; (II): 0.5 S; (III): 0.5 M; (IV): 2.5 T; (V): 2.5 S; (VI): 2.5 M; (VII): 5 T; (VIII): 5 S; (IX): 5 M; (X) NPs without SPIONs; (XI): Positive control of Lipofectamine®; (XII): Negative control of untreated cells and (B) Screening of T, S and M C32-CR3:pGFP (50:1) nanoparticles transfections on Cos-7 cells at different SPIONs concentrations.

Given the results showed in Figure 34, S nanoparticles were chosen because of their higher transfection results at the two largest concentrations of SPIONs. In addition, S nanoparticles' transfection results showed lower variability in comparison to T nanoparticles. Moreover, the presence of SPIONs improved cell transfection of S nanoparticles at all the concentrations tested, as compared to non-loaded NPs. Therefore, in further cell transfections this type of nanoparticles was selected.

On the other hand, despite not showing significant differences with NPs in two of the three concentrations of SPIONs tested, M nanoparticles were also chosen for further *in vitro* studies because of their singularity due to their LbL structure. In many applications, this kind of structures could be very useful, for the possibility to load different types of active principles in the different layers of the complex.

4.4.4 SPIONs improve cell transfection of OM-pBAE/pDNA polyplexes

Experiments detailed in chapter II showed that the presence of SPIONs altered autophagy and exosomes production, suggesting the modification of the fate of gene delivery systems. Also, results from chapter III and above in this chapter suggested a positive effect of SPIONs on cell transfection. In order to confirm it and to determine if the results obtained so far were applicable to different types of cells, transfection efficiency of S and M nanoparticles, prepared at 0.5, 2.5 and 5 μg of SPIONs mL^{-1} was studied in three different cell lines (Cos-7, HeLa and U-87 MG). In particular, the expression of the reporter gene GFP was analyzed through flow cytometry analysis. These experiments were performed using two different polymers: C32-CR3, abbreviated as C32-R and C6-CR3, named C6-R. The latter was used because of its capability to form more stable nanoparticles, due to its hydrophobic moiety[147], able to be lyophilized without changing their physicochemical properties[94]. The balance between stability of the polyplexes and cytotoxicity would determine the best performing polymer for each cell line.

As mentioned before, Cos-7 is considered as a quite permissive to transfection cell line. Then, cells from a cervical cancer (HeLa), which are more difficult to transfect[91], were analyzed. Finally, the glioblastoma cell line U-87 MG was employed as a model of cells that are highly difficult to modify using non-viral vectors[272]. This growing complexity in cell modification was designed in order to optimize the nanoparticles' formulations and solve the large issue of modifying mesenchymal stem cells.

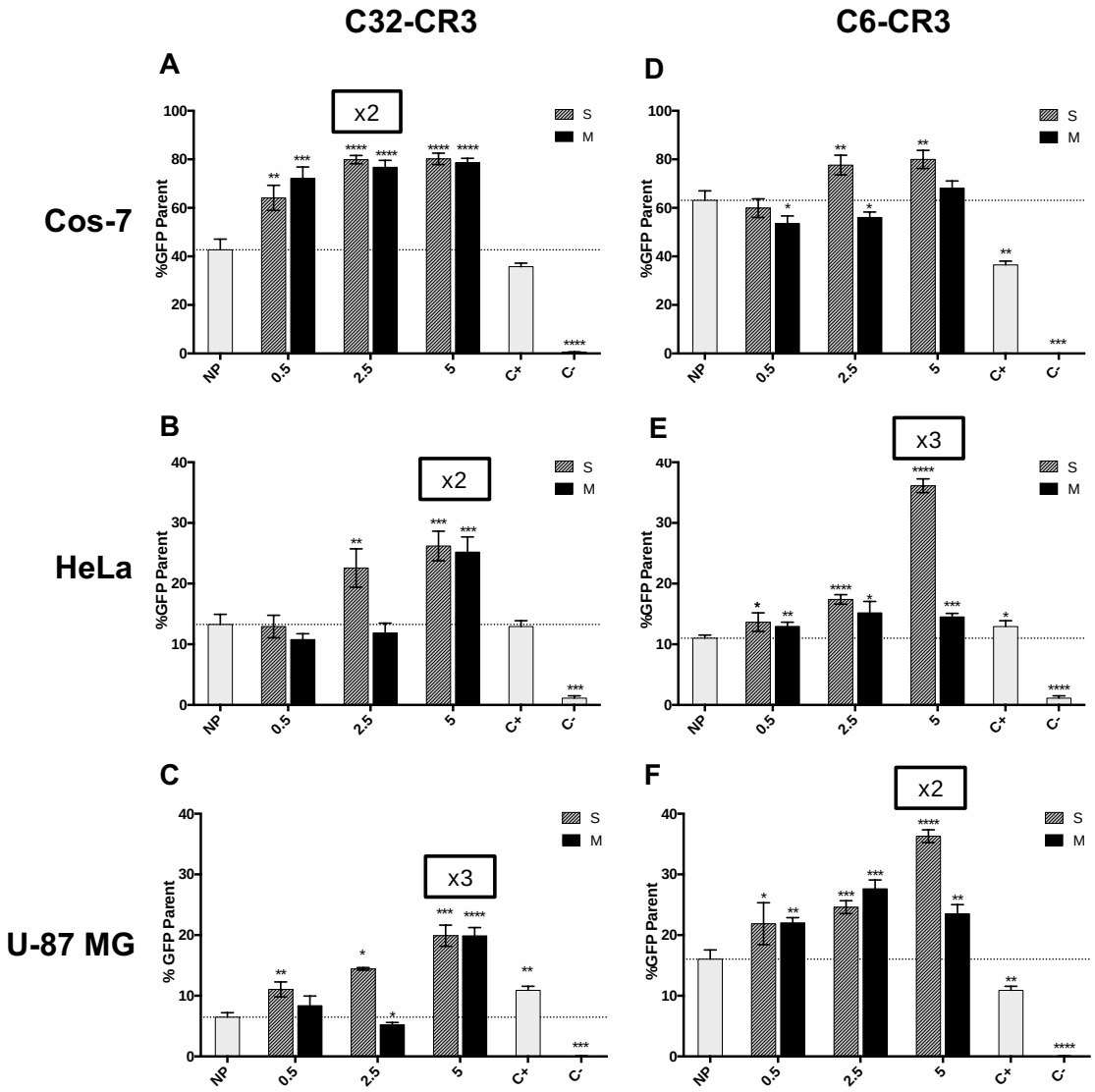

Figure 35. Transfection efficiency results of S and M-type C32-CR3:pGFP (50:1) (A to C) and C6-CR3:pGFP (25:1) (D to E) SPION-containing nanoparticles into Cos-7 (A and D), HeLa (B and E) and U-87 MG cells (C and F). Values correspond to the mean ± SD of triplicates of a same experiment. t-test was applied to find out statistical differences. S = separate nanoparticles; and M = multicoating nanoparticles. C+ = Lipofectamine transfection reagent; C- = cells incubated with only media. Scale bars are different depending on cell line to facilitate the reading.

As previously shown, SPIONs remarkably increased transfection efficiency of C32-CR3 polylpexes in Cos-7 cells (Figure 33 and Figure 35A). The transfection efficiency of these polyplexes was almost doubled when 2.5 or 5 µg of SPIONs mL^{-1} were added to the NPs, and for any of the three SPIONs concentrations tested it was higher than when using NPs. No significant differences were observed between the two highest concentrations of SPIONs or between S and M nanoparticles. On the other hand, we

also tested C6-CR3 polymer. This polymer is very similar to C32, although due to modifications on its lateral chains, it is more hydrophobic. This small change did not induce changes in the physicochemical properties of nanoparticles (data not shown). In the case of C6-CR3-based polyplexes (Figure 35D), differences were observed between the types of nanoparticles used: not all the nanoparticles tested increased the transfection efficiency of the nanoparticles without SPIONs. This only happened with 2.5 and 5 μg of SPIONs mL^{-1} for S nanoparticles and 5 μg of SPIONs mL^{-1} for M ones. Therefore, for C6-CR3 based polyplexes 5 μg of SPIONs mL^{-1} was the best performing concentration of the three evaluated, and S NPs were the best type of nanoparticles. According to the absence of cytotoxicity at both 2.5 and 5 μg of SPIONs mL^{-1} concentrations, and given that both concentrations showed similar transfection efficiency results, we selected the one with the higher SPIONs loading to facilitate magnetic sorting in future experiments.

Regarding HeLa cells (Figure 35B and E), the transfection efficiency of C32-CR3 polyplexes was remarkably increased when 2.5 or 5 μg of SPIONs mL^{-1} were added to the S nanoparticles or when 5 μg of SPIONs mL^{-1} were added to the M ones. At this SPIONs concentration, S and M showed the same transfection efficiency and, at lower concentrations, the transfection was higher in S ones. In the case of C6-CR3 polyplexes the transfection efficiency was only clearly increased with the S NPs at 5 μg of SPIONs mL^{-1} (Figure 35E).

Finally, the percentages of GFP expression in U-87 MG cells gave evidence of their reluctance to transfection (Figure 35C and F). However, the transfection efficiency of C32-CR3-based polyplexes on these cells was significantly enhanced by the presence of SPIONs at their highest concentration (5 μg mL^{-1}) on M nanoparticles, and at any of the concentrations tested for S nanoparticles. The best performing SPIONs concentration was clearly 5 μg mL^{-1} and at this concentration S and M nanoparticles showed 3-fold enhanced transfection efficiency. The transfection efficiency of C6-CR3-based polyplexes without SPIONs (NP) was higher than that of C32-CR3 ones on U-87 MG cells. Regarding SPIONs, they had a positive effect on transfection efficiency on this cell line for any concentration and any type of C6-CR3-based SPIONs-containing nanoparticles tested. Interestingly, S nanoparticles with 5 μg of SPIONs mL^{-1} showed the best result, doubling the transfection efficiency of NP. In conclusion, SPIONs show a clear enhancer effect on the transfection of U-87 MG cells.

The fact that in the three cell lines tested C6-CR3 polyplexes without SPIONs (NPs) showed higher or at least the same transfection efficiencies than C32-CR3s was not

surprising because C6 polymers were designed to improve the stability, packaging capacity and transfection efficiency of their C32 counterparts[147]. Also, C6-based polyplexes in general needed higher amounts of SPIONs to show significantly increased transfection efficacy. It has been discussed that although not all the combinations between DNA, OM-pBAEs and SPIONs tested were able to significantly enhance cellular transfection, the clear majority of them did show higher transfection efficiency than the same NPs only combining OM-pBAE with DNA (NP). This assertion applies to the two types of nanoparticles tested (S and M) although better results were obtained with the S ones. Thereby, the transfection efficiency enhancer effect of SPIONs in Cos-7, HeLa and U-87 MG cell lines was clearly proven.

Taking an overview of the three cell lines tested, it is possible to assert that in the case of a permissive cell line as Cos-7, the best performing SPION-containing nanoparticle tested (C32 5S) can duplicate the transfection capability of C32-CR3-NP. However, in cells that are more difficult to transfect, such as U-87 MG or HeLa, which show a transfection efficiency of around 10% when using NPs without SPIONs, the effect of the presence of SPIONs in the polyplexes can achieve 3-fold higher values of transfection efficiency. Thereby, although the absolute values of transfection on such cell lines are much lower than in Cos-7 cells, the increase in cell transfection efficiency due to the presence of SPIONs is higher. These are encouraging results regarding cell therapy strategies, since the cells that are used for these purposes usually show high reluctance to genetic modification.

It is worth remarking that transfection efficiency could be further improved by adding a magnetic field when performing the transfection, to facilitate the movement of the SPIONs. However, in the present study it was not used, since the capacity of the whole complexes to transfect cells without external forces was the issue to study, with the aim to compare with particles without SPIONs loading.

4.4.5 SPIONs allow the selection of effectively transfected cells

As mentioned before, the second major point of this chapter was to select those genetically modified cells benefiting from the magnetism of SPIONS-containing NPs. To do so, magnetic columns were used due to their ability to recover the magnetic fraction, ease of preparation, capacity to work with high number of cells and allowance of a rapid

and efficient cell separation. The first parameter evaluated was the expression of GFP before performing the sorting in both fractions (magnetic and non-magnetic) obtained after the sorting (Figure 36A).

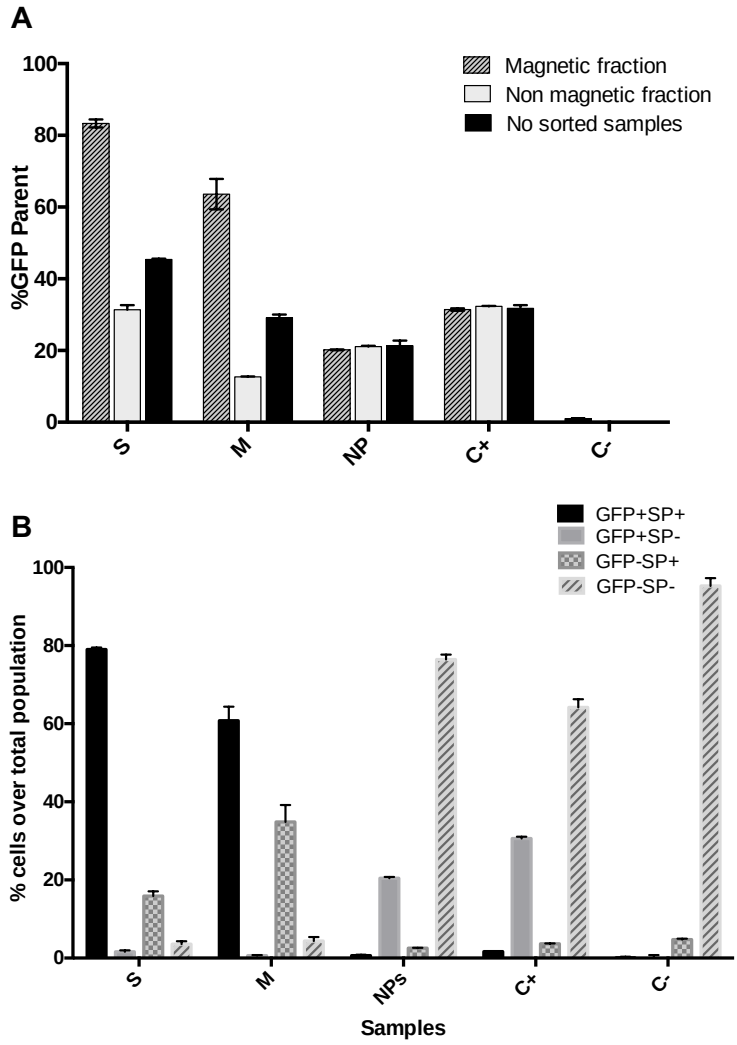

Figure 36. Magnetic cell sorting. FACS analysis regarding (A) the transfection efficiency of C6-CR3 S and M nanoparticles on both magnetically sorted and no sorted HeLa cells and (B) each fraction of sorted HeLa cells treated with S and M nanoparticles. Results are presented as mean +/s SD of triplicates. S = separate nanoparticles; and M = multicoating nanoparticles; C+ = Lipofectamine transfection reagent; C- = cells incubated with only medium.

As Figure 36A shows, S nanoparticles, as well as the M ones, showed significantly increased levels of GFP expression on their magnetic fractions as compared to their non-sorted samples. Accordingly, the eluted or non-magnetic fraction showed lower transfection efficiency. By contrast, negative and positive controls and NPs (samples

without SPIONs) maintained their GFP expression level in both sorted and non-sorted cells, thus demonstrating that sorting did not negatively affect cell transfection.

Next, the magnetic labelling of cells was evaluated. To do so, the number of cells was normalized between the magnetic and the non-magnetic fraction of the different conditions and the percentage of each fraction was determined. The magnetic labelling of HeLa cells treated with both S and M nanoparticles was around 95%. As expected, the samples without SPIONs (NP, C+ and C-) showed a clear majority of cells that are not magnetic (95-99%). The low percentages of their magnetic cells can be considered as default error of the sorting system.

Once the transfection efficiency and the magnetic labelling was analyzed, we next evaluated what percentage from the total number of cells did represent every category (Figure 36B), namely: (a) cells expressing GFP and magnetically labelled (GFP+SP+); (b) cells expressing GFP but no magnetically labelled (GFP+SP-); (c) cells not expressing GFP but magnetically labelled (GFP-SP+); and (d) cells that neither express GFP nor were magnetic (GFP-SP-). The first fraction (GFP+SP+) would contain the desired cells, being both magnetic (have internalized SPIONs) and genetically modified (express GFP coded by the pDNA). For further clinical applications, enriching this fraction might be very important to ensure that all the cells re-implanted in a patient are carrying the therapeutic gene and therefore increase the success' probability of the therapy. Collecting these four fractions from the total number of cells, allowed us to discard false positive and negative events.

Figure 36B shows that the fraction of cells expressing GFP and being magnetically labelled (GFP+SP+) represented almost the 80% in the case of cells treated with S nanoparticles. Cells treated with M nanoparticles showed around 60% of this "desired fraction", where both transfection and magnetic labelling had occurred. These results confirm the efficacy of our system. On the other hand, the fraction of cells that were magnetic but not transfected (GFP-SP+) represents the false positive events. Since previous studies report that, in cell therapy applications, stem cells could favor tumor self-growth *in vivo*[273], the percentage of cells in this fraction should be reduced. To this purpose, an appealing strategy could be the covalent attachment of the magnetic nanoparticles to the polymer.

On the other hand, as shown in Figure 36B, the non-magnetic fraction of samples without SPIONs (NPs, C+ and C-) represented most of the cells. In the case of NPs and C+, these non-magnetic cells were distributed between the GFP+ and the GFP-

fractions, according to their transfection efficiency, while in the case of C-, the cells were GFP- in large majority. To sum up, this magnetic sorting has allowed the massive separation of each sample into four fractions according to transfection efficiency and magnetic labelling of cells, showing promising results.

Overall, the obtained results have revealed the enhancer effect of SPIONs on the transfection of both permissive and reluctant to transfection cell lines. Furthermore, the presence of SPIONs in the polyplexes allowed not only such unexpected increase of cell transfection but also the selective magnetic separation of genetically modified cells. The enrichment of the transfected cells fraction might be crucial for further clinical cell therapy applications and therefore, the results presented here open the door to SPION-containing nanoparticles as promising tools for stem cell-based therapies.

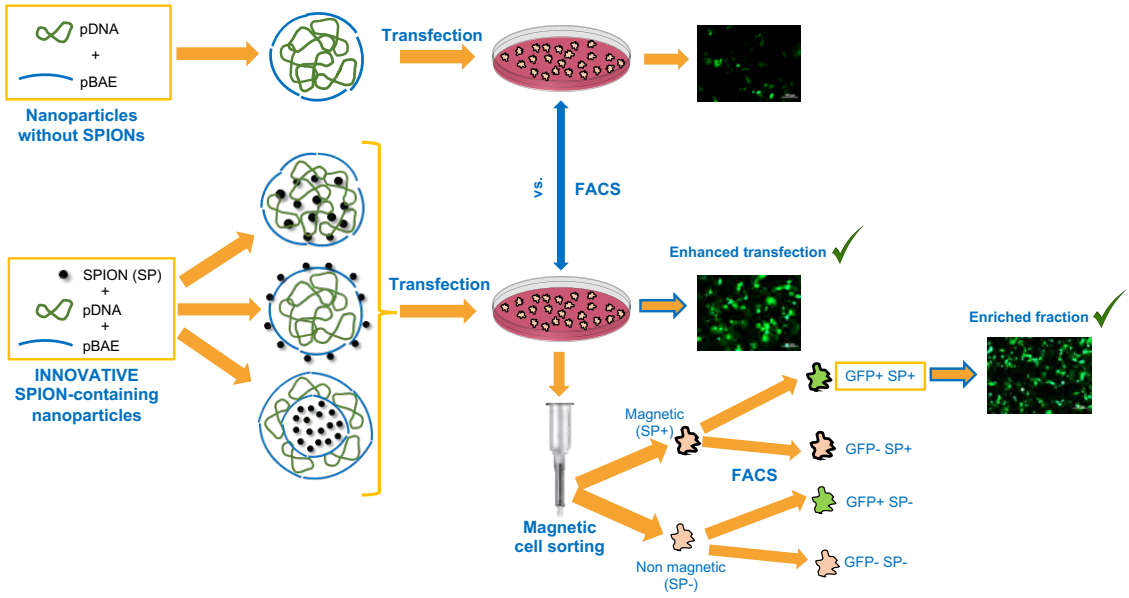

Figure 37. Schematic summary of transfection and magnetic sorting results[149].

4.4.6 AMSCs transfection with multicomponent nanoparticles

Finally, considering the results of this and the previous chapters, the systems here developed were transferred to stem cells. The goal was to benefit from the advantages of such gene delivery systems, namely the high transfection efficacy, the ability to modify intracellular processes, and the possibility to perform a magnetic cell sorting, to try to modify stem cells. These cells are usually employed for cell therapy applications and

present high reluctance to be modified by means of non-viral gene delivery systems. Thus, the challenge for out multicomponent nanoparticles was substantial.

Adipose-derived mesenchymal stem cells (AMSCs) were employed. Instead of transfecting these cells and try to understand the obtained results, the strategy used hereinafter was the following: an intracellular study similar to the one presented in chapter II was designed aimed at then helping understand, predict and try to further improve the low transfection efficiencies that these cells present.

4.4.6.1 Basal autophagy and exosomes production levels in AMSC cells

Same as with HeLa cells, AMSCs were incubated with the different complexes made of polymeric nanoparticles (OM-pBAE and pDNA) with or without metallic components (AuNPs or SPIONs) in order to study alterations on autophagy and exosomes production cellular mechanisms. First, the basal levels of these mechanisms had to be assessed. To do so, AMSCs cells were seeded and 24 h later, they were incubated for different exposure times with regular cell medium. Afterwards, the immunostaining procedure was performed, and their autophagy and exosomes production basal levels were assessed. These samples were used as negative controls of untreated cells. CD9 and LC3 were labelled to monitor exosomes production and autophagy, respectively.

As shown in Figure 38, AMSCs untreated cells showed very low levels of CD9 signal intensity over the tested timepoints (0.5 to 48 h). Similarly, the autophagy marker (LC3) showed a slight increase at t = 8h kept until 48 h time. In conclusion, the basal levels of CD9 and LC3 expression in AMSCs are much lower than the basal levels observed in HeLa cells (chapter II).

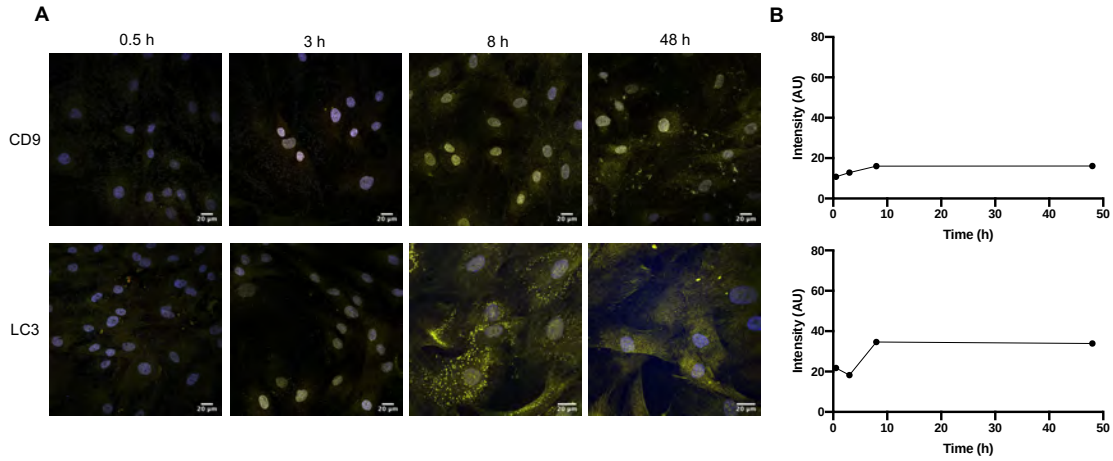

Figure 38. Basal levels of exosomes production and autophagy in AMSC cells at different timepoints. (A) Confocal images are the merge of DAPI staining channel (blue) and CD9 or LC3 channel (yellow). (B) Quantification of the CD9 or LC3 intensity. Scalebars = 20 μm

4.4.6.2 Assessing exosomes production and autophagy in AMSC cells transfected with OM-PBAEs-based gene delivery systems

After studying the basal levels in untreated AMSCs of CD9 and LC3 as markers of exosomes and autophagosomes, respectively, cells were incubated with different complexes in order to study variations on the expression of such markers.

Same as with HeLa cells in chapter II, AMSCs were seeded and exposed to the samples detailed in Table 4 for different timepoints. Here, besides SPIONs, spherical gold nanoparticles (AuNPs) were also employed. Although these nanoparticles showed to have a lesser impact on cellular mechanisms as compared to SPIONs on HeLa cells (see chapter II), they showed to modify cell uptake of bare OM-pBAE polyplexes in both HeLa and PANC-1 cells (see chapter III).

Then, after the immunohistochemistry procedure, samples were observed under the confocal fluorescent microscope and the intensity of the CD9 or LC3 markers was quantified (Figure 39 and Figure 40).

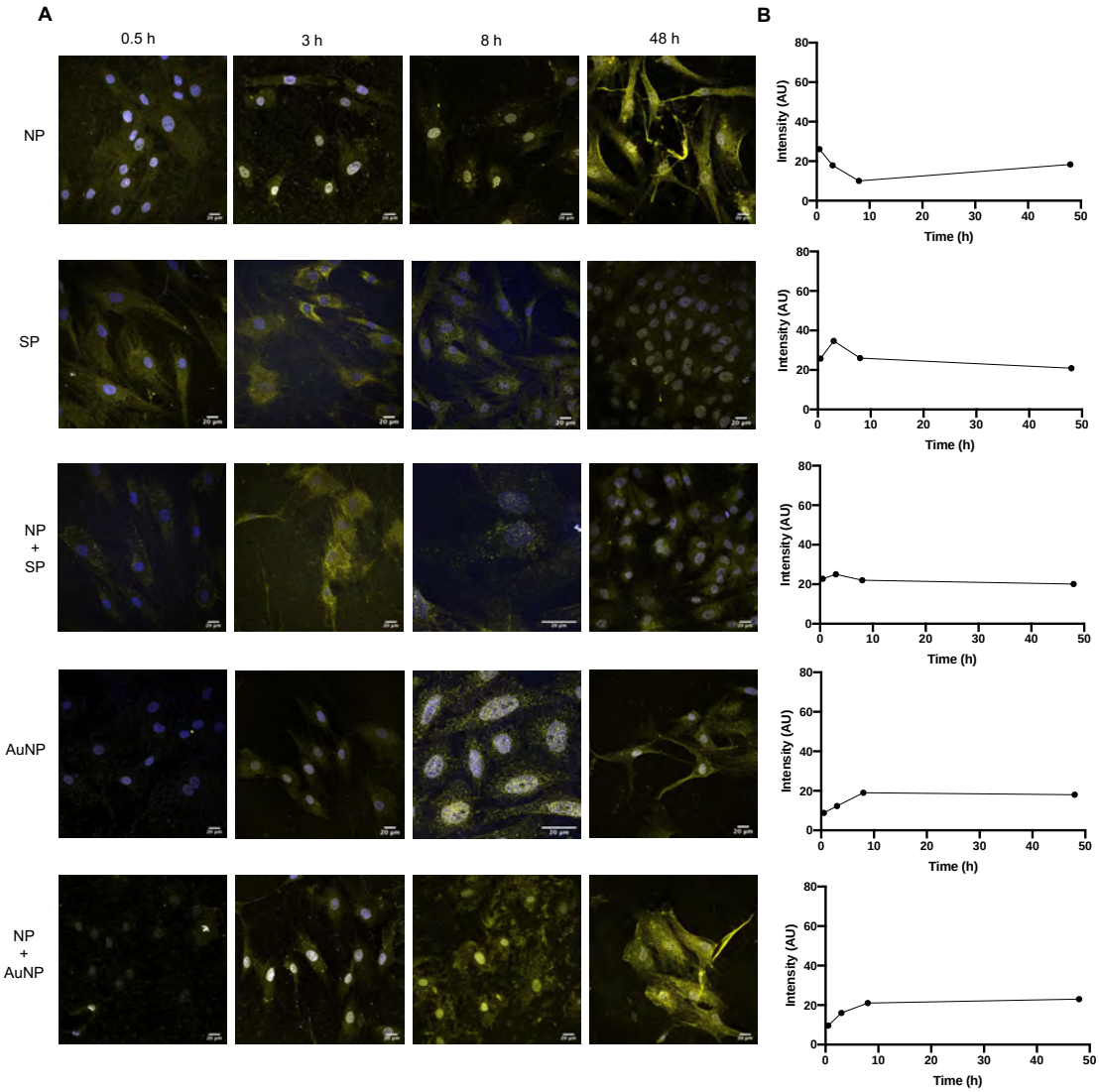

Figure 39. Exosomes production in AMSCs in response to different nanoparticles at different timepoints. (A) Confocal images are the merge of DAPI staining channel (blue) and CD9 channel (yellow). (B) Quantifications of the CD9 intensity. Scalebars = 20 μm

Figure 39 shows, in general, low levels of CD9 in all the samples and timepoints tested. No significant differences can be appreciated between the negative control of untreated cells (Figure 38) and the cells treated with OM-pBAE-NPs in terms of exosomes production. The samples that contain SPIONs (SP and NP+SP) seem to slightly increase the production of exosomes from t = 3h, whereas gold nanoparticles samples (AuNP and NP+AuNP) showed their maximum CD9 signals at t = 8 and 48 h exposure times.

At the timepoints tested, AMSCs appear to be less sensitive to polyplexes and metallic particles in terms of exosomes production than HeLa cells (chapter II). Although no significant differences appeared, HeLa cells treated with bare SPIONs and SPIONs

complexed with OM-pBAE NPs showed increases in CD9 signal as compared to untreated cells (Figure 12)).

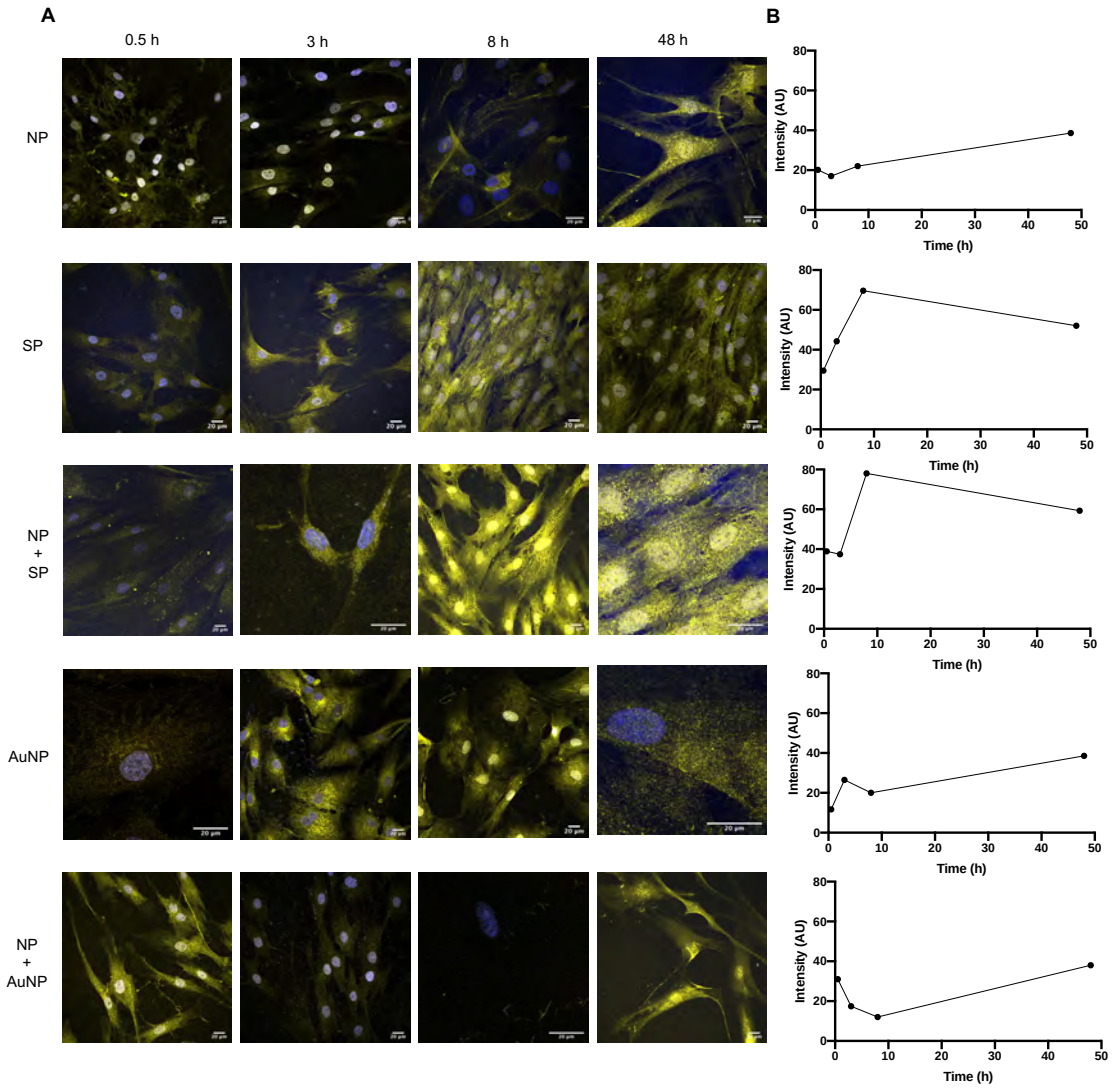

Figure 40. Autophagy in AMSCs in response to different nanoparticles at different timepoints. (A) Confocal images are the merge of DAPI staining channel (blue) and LC3 channel (yellow). (B) Quantifications of the LC3 intensity. Scalebars = 20 µm

Regarding autophagy, Figure 40 shows that the presence of OM-pBAE NPs did not increase the LC3 expression as compared to the control of untreated cells (Figure 38). Similarly, the samples that contained gold nanoparticles, either alone (AuNPs) or complexed with OM-pBAE NPs (NP+AuNP), showed no gain in LC3 signal at any timepoint tested compared to the negative control. By contrast, the presence of SPIONs doubled the AMSCs autophagosome signal from t = 3h in the case of bare SPIONs (SP) and even earlier, at t= 0.5 h, in the case of complexed SPIONs (NP+SP). The peak of LC3 expression in these two samples was found after 8 h of incubation.

These results are comparable to the ones obtained with HeLa cells (chapter II), where the process of ferritinophagy was described as a cell clearing mechanism to eliminate the excess of Fe caused by the presence of SPIONs. Also, SPIONs increased the LC3 levels in HeLa cells already after 30 minutes of incubation.

The differences between HeLa cells and AMSCs in terms of exosomes production and autophagy in response to our different nanoparticles could tentatively help explain the difficulty to genetically modify stem cells using non-viral vectors[77]. The hypothesis that we posed in chapter II was summarized as follows:

$$\boldsymbol{Cell\ uptake} \longrightarrow \uparrow \boldsymbol{Autophagy} \longrightarrow \downarrow \boldsymbol{Exosomes\ production}$$

$$\boldsymbol{Endosomal\ escape} > \boldsymbol{Autophagy} \longrightarrow \uparrow \boldsymbol{Transfection}$$

In brief, the cell internalization of nanoparticles would cause an increase in the endosomal escape process, damaging the endosomes and causing the triggering of autophagic mechanisms. However, if the endosomal escape is greater than the autophagy, the system will be efficient in terms of cell transfection although having the autophagy rate increased. In parallel, this triggering of autophagy and endosomal escape will be a handicap for exosomes production.

Since the NPs used for both HeLa and AMSCs were the same and the cell media too, the biological identity of the NPs (the one that the cells “see”) was the same. Therefore, the systems are comparable. The first process that could be distinguished between the two cell lines is the cellular uptake. It has to be kept in mind that the internalization route of cationic polyplexes or nano-carriers is highly cell type dependent and may vary between different cell lines[34]. In order to study if the uptake is indeed very different in AMSCs as compared to HeLa cells, ICP studies of OM-pBAE nanoparticles containing metallic components could be designed. This way, if uptake was indeed deficient, the low transfection efficiency of AMSCs could be enhanced by designing and pre-forming protein coronas around the NPs enriched in proteins that favor cell uptake. Then, as it has been discussed earlier, the level of autophagosomes in AMSCs was rather low. This could be used in a favorable way: on the one hand, the gene delivery systems that were able to escape from endosomes, if not autophagocytosed, they could deliver their cargo and transfect cells. In the same vein, if the desired cell application was to produce stem cell-derived therapeutic exosomes, which is a new trend in nanomedicine[59,138–140], this low autophagic flux would be favorable and could be even more diminished using

autophagy inhibitors[35,274]. In fact, it has been reported that the blockade of autophagy increases transfection efficacy of polyplexes[275]. Finally, another key process to tackle when designing gene delivery systems for mesenchymal stem cells would be the endosomal escape. A study on the cell localization of the polyplexes, labelling endosomes would be of great interest. It has been reported that cationic nanoparticles are internalized by mesenchymal stem cells were located inside cellular compartments resembling endosomes[276], but a wider study with our gene delivery systems would be more conclusive. As detailed in the above formula, the endosomal escape needs to be greater than the autophagy flux in order to allow an effective cell transfection.

In conclusion, it has been here discussed the application of the knowledge disclosed throughout this thesis to MSCs-based cell therapies with the goal of improving their success rates. By having a deeper knowledge of the cellular mechanisms behind cell transfection, the interaction of nanoparticles with their environment, and the use of multicomponent nanoparticles, improved systems for cell therapy strategies can be designed and employed.

4.5 Concluding remarks

In this chapter, three types of SPION-containing nanoparticles with potential as gene delivery carriers have been successfully developed and characterized. (a) nanoparticles where both SPIONs and DNA are encapsulated by the polymer (T); (b) nanoparticles where the DNA is encapsulated by the polymer and then SPIONs are added (S); (c) multicoating nanoparticles consisting of 4 layers (M).

The SPIONs concentrations into DNA/pBAEs polyplexes showing more transfection efficiency have been stablished by screening transfection *in vitro* tests on Cos-7 cells. In addition, the influence of the type of nanoparticle on the transfection efficiency has been assessed. S and M nanoparticles have been selected for further transfection studies because of their higher transfection efficiency and their singularity in their LbL structure, respectively.

In vitro transfection experiments have demonstrated that the presence of SPIONs on the polyplexes formed by pDNA and C32-CR3 or C6-CR3 enhances their cell transfection efficiency both on a permissive cell line (Cos-7) and on highly reluctant cultured cells (HeLa and U-87 MG).

The best performing SPIONs concentration and type of SPION-containing nanoparticle, regarding both polymer backbone (C32-CR3 or C6-CR3) and structure (S or M nanoparticles) have been established for every cell line studied. In the case of a permissive cell line as Cos-7, the best performing SPION-containing nanoparticles tested (C32 5S) can duplicate the transfection capability of C32-NP, achieving around 80% of transfected cells. For cells more difficult to transfect, such as U-87 MG or HeLa, where the transfection efficiency of SPION-free nanoparticles (NP) is around 10%, the incorporation of SPIONs in the polyplexes can achieve 3-fold higher values of transfection efficiency.

A commercially available magnetic cell sorter has allowed an effective separation and the recovering of both magnetic and non-magnetic cell fractions. Therefore, the presence of SPIONs in these polyplexes has allowed not only this unanticipated increase of cell transfection but also the selective magnetic separation of genetically modified cells from the ones that do not contain the foreign DNA. Since the enrichment of the transfected cells fraction might be crucial for further clinical cell therapy applications, the results here presented open the door to SPION-containing nanoparticles as promising tools for cell therapy approaches. The results here presented might be of great value for further steps towards stem cell-based therapies.

Finally, the overall results of this thesis have been put together to help understand the rationale behind the difficulty to genetically modify mesenchymal stem cells. By comparing the autophagy and exosomes production levels in HeLa and AMSCs, and using the hypothesis formulated in chapter II, three key processes of AMSCs have been pointed out: endocytosis, autophagy and endosomal escape.

In order to improve further transfections in AMSCs, the protein corona engineering, the modulation of autophagy using inhibitors and the labelling of endosomes have been proposed as useful tools to overcome the limitations offered by endocytosis, autophagy and endosomal escape processes.

4.6 References

248. Li, S. & Huang, L. Nonviral gene therapy: Promises and challenges. *Gene Ther.* **7**, 31–34 (2000).

249. Chen, C. C. V *et al.* Simple SPION Incubation as an Efficient Intracellular Labeling Method for Tracking Neural Progenitor Cells Using MRI. *PLoS One* **8**, 1–11 (2013).

250. Petri-Fink, A., Chastellain, M., Juillerat-Jeanneret, L., Ferrari, A. & Hofmann, H. Development of functionalized superparamagnetic iron oxide nanoparticles for interaction with human cancer cells. *Biomaterials* **26**, 2685–2694 (2005).

251. Sun, C., Lee, J. & Zhang, M. Magnetic nanoparticles in MR imaging and drug delivery. *Adv. Drug Deliv. Rev.* **60**, 1252–1265 (2008).

252. Ruiz, A. *et al.* Magnetic nanoparticles coated with dimercaptosuccinic acid: development, characterization, and application in biomedicine. *J. Nanoparticle Res.* **16**, (2014).

253. Rahman, M. *et al.* Novel approach for the treatment of cancer: Theranostic nanomedicine. *Pharmacologia* **3**, (2012).

254. Gobbo, O. L., Sjaastad, K., Radomski, M. W., Volkov, Y. & Prina-Mello, A. Magnetic Nanoparticles in Cancer Theranostics. *Theranostics* **5**, 1249–63 (2015).

255. Tartaj, P., Morales, M. P., Gonzalez-Carreno, T., Veintemillas-Verdaguer, S. & Serna, C. J. The iron oxides strike back: From biomedical applications to energy storage devices and photoelectrochemical water splitting. *Adv. Mater.* **23**, 5243–5249 (2011).

256. Sharpe, M. & Mount, N. Genetically modified T cells in cancer therapy: opportunities and challenges. *Dis. Model. Mech.* **8**, 337–350 (2015).

257. Bishop, C. J., Tzeng, S. Y. & Green, J. J. *Degradable polymer-coated gold nanoparticles for co-delivery of DNA and siRNA*. *Acta Biomaterialia* **11**, (Acta Materialia Inc., 2015).

258. Pan, D., Lanza, G. M., Wickline, S. A. & Caruthers, S. D. Nanomedicine: Perspective and promises with ligand-directed molecular imaging. *Eur. J. Radiol.*

70, 274–285 (2009).

259. Lammers, T., Aime, S., Hennink, W. E., Storm, G. & Kiessling, F. Theranostic nanomedicine. *Acc. Chem. Res.* **44**, 1029–1038 (2011).

260. Gage, F. H., Kawaja, M. D. & Fisher, L. J. Genetically modified cells: applications for intracerebral grafting. *Trends Neurosci.* **14**, 328–333 (1991).

261. Hidai, C. & Kitano, H. Nonviral Gene Therapy for Cancer: A Review. *Diseases* **6**, 57 (2018).

262. Porada, C. D. & Almeida-porada, G. Mesenchymal Stem Cells as Gene Delivery Vehicles. *Adv. Drug Deliv. Rev.* (2013).

263. Calne, R. Y., Gan, S. U. & Lee, K. O. Stem cell and gene therapies for diabetes mellitus. *Nat. Rev. Endocrinol.* **6**, 173–177 (2010).

264. Lynn, D. M. & Langer, R. Degradable Poly (beta-amino esters): Synthesis , Characterization , and Self-Assembly with Plasmid DNA. *J Am Chem Soc* **122**, 10761–10768 (2000).

265. Akinc, A., Anderson, D. G., Lynn, D. M. & Langer, R. Synthesis of poly(ß-amino ester)s optimized for highly effective gene delivery. *Bioconjug. Chem.* **14**, 979–988 (2003).

266. Zugates, G. T. *et al.* Rapid optimization of gene delivery by parallel end-modification of poly(beta-amino ester)s. *Mol. Ther.* **15**, 1306–1312 (2007).

267. Diehl, A. & Levin, Y. Smoluchowski equation and the colloidal charge reversal. *J. Chem. Phys.* **125**, 1–5 (2006).

268. Lvov, Y. *et al.* Successive Deposition of Alternate Layers of Polyelectrolytes and a Charged Virus. *Langmuir* **10**, 4232–4236 (1994).

269. Decher, G. Fuzzy Nanoassemblies: Toward Layered Polymeric Multicomposites. *Science (80-.).* **277**, 1232–1237 (1997).

270. Trubetskoy, V. S., Loomis, A., Hagstrom, J. E., Budker, V. G. & Wolff, J. A. Layer-by-layer deposition of oppositely charged polyelectrolytes on the surface of condensed DNA particles. *Nucleic Acids Res.* **27**, 3090–3095 (1999).

271. Deng, Z. J. *et al.* Layer-by-layer nanoparticles for systemic codelivery of an

anticancer drug and siRNA for potential triple-negative breast cancer treatment. *ACS Nano* **7**, 9571–9584 (2013).

272. An, S. *et al.* Nonviral gene therapy in vivo with PAM-RG4/apoptin as a potential brain tumor therapeutic. *Int. J. Nanomedicine* **8**, 821–34 (2013).

273. Zhu, W. *et al.* Mesenchymal stem cells derived from bone marrow favor tumor cell growth in vivo. *Exp. Mol. Pathol.* **80**, 267–274 (2006).

274. Mauthe, M. *et al.* Chloroquine inhibits autophagic flux by decreasing autophagosome-lysosome fusion. *Autophagy* **14**, 1435–1455 (2018).

275. Zhong, X., Panus, D., Ji, W. & Wang, C. Modulating polyplex-mediated gene transfection by small-molecule regulators of autophagy. *Mol. Pharm.* **12**, 932–940 (2015).

276. Lorenz, M. R. *et al.* Uptake of functionalized, fluorescent-labeled polymeric particles in different cell lines and stem cells. *Biomaterials* **27**, 2820–2828 (2006).

Chapter V. Conclusions

This page left blank intentionally

Conclusions

In this thesis, multicomponent nanoparticles have been employed to perform a thorough study of the cellular mechanisms induced upon cell transfection. Gene delivery systems composed of polyplexes made of OM-pBAEs and pDNA and a metallic component being either gold nanoparticles or SPIONs have been used to (1) unbox cells and analyze the intracellular processes that dictate the fate of internalized vectors, (2) study their interaction with proteins and demonstrate that this phenomenon is key for their cellular uptake and finally (3) apply the knowledge of their properties and abilities to genetically modify reluctant to transfection cells that are used for cell therapy strategies.

Firstly, in order to gain insight into the cell processes of autophagy and exosomes production, a study using different nanoparticles was proposed. These NPs included bare OM-pBAE polyplexes, OM-pBAE polyplexes combined with SPIONs or gold nanoparticles and these metallic nanoparticles without the polyplexes.

- The addition of metallic particles onto OM-pBAE polyplexes was demonstrated to render particles suitable for cell usage.

- It has been validated the use of confocal microscopy as a technique to monitor the basal levels of exosomes production and autophagosomes in HeLa cells.

- The presence of SPIONs increased exosomes production in HeLa cells. They also triggered their autophagy probably through what is known as ferritinophagy or iron-related autophagy.

- However, the partial inhibition of exosomes release due to autophagy activation was proposed as an explanation to these results. That is, SPIONs increase both autophagy and exosomes production but this later process is partially hindered by autophagic redirecting of internalized nanoparticles. At the same time, the damage in endosomes caused by internalized nanoparticles trying to escape from them was pointed out as a triggering factor of autophagy.

- After two days, there were still C6R molecules remaining inside cells which were about to be eliminated via exosome release or autophagy degradation.

The characteristics of nanoparticles that affect their cellular internalization were next studied. Also, the cellular uptake of different metallic complexes was quantified and a proteomics study was carried out to analyze the different protein corona profiles.

- The cell biocompatibility of the different complexes employed in this work was assessed. OM-pBAE polyplexes, OM-polyplexes with AuNPs or SPIONs and these metallic particles alone showed no cytotoxicity in a broad range of concentrations tested.

- Cell uptake of the complexes increased at higher metallic NP concentrations, with AuNP exhibiting greater internalization compared to SPIONs.

- Rod-shaped gold nanoparticles have been also effectively synthetized and, as expected, they showed a less efficient cell uptake than spherical gold nanoparticles. Interestingly, cell uptake of both gold nanospheres and nanorods as well as of SPIONs was increased when the metallic particles were complexed to OM-pBAEs

- The addition of metallic particles to the OM-pBAE NPs enhanced the transfection efficacy on PANC-1 cells at any of the ratios tested. However, higher uptakes did not correlate completely with higher cell transfection rates.

- In order to understand the obtained differences in the uptake and transfection profiles among NPs, the protein corona of the different complexes was isolated and analyzed. Proteomic data identified protein candidates that correlate with this enhanced transfection.

- Specifically, albumin and transferrin have been previously linked with higher transfection efficacies and they have shown to trigger endosomal escape. These findings highlight the importance of understanding the biocorona composition and its correlation with transfection, which can be used to engineer pre-formed PC to enhance gene delivery efficacies.

Finally, considering the insights into the cell mechanisms that rule the overall fate of nanoparticles and the factors affecting cellular uptake and transfection, the application of our gene delivery systems to a more challenging purpose, such as the modification of mesenchymal stem cells for further cell therapy strategies, was proposed.

- Three types of SPION-containing nanoparticles with potential as gene delivery carriers have been successfully developed and characterized.

- The SPIONs concentrations into DNA/pBAEs polyplexes showing more transfection efficiency have been stablished by screening transfection *in vitro* tests on Cos-7 cells. In addition, the influence of the type of nanoparticle on the transfection efficiency has been assessed.

- The best performing SPIONs concentration and type of SPION-containing nanoparticle, regarding both polymer backbone and structure have been established for every cell line studied. In the case of a permissive cell line as Cos-7, the best performing SPION-containing nanoparticles tested can duplicate the transfection capability of their C32-NP counterpart (without SPIONs). For cells more difficult to transfect, such as U-87 MG or HeLa, the incorporation of SPIONs in the polyplexes can achieve 3-fold higher values of transfection efficiency.

- The presence of SPIONs in these polyplexes has allowed not only this unanticipated increase of cell transfection but also the selective magnetic separation of genetically modified cells from the ones that do not contain the foreign DNA.

- Finally, the overall results of this thesis have been put together to help understand the rationale behind the difficulty to genetically modify mesenchymal stem cells. By comparing the autophagy and exosomes production levels in HeLa and AMSCs, and using the hypothesis formulated in chapter II, three key processes of AMSCs have been pointed out: endocytosis, autophagy and endosomal escape.

- In order to improve further transfections in AMSCs, the protein corona engineering, the modulation of autophagy using inhibitors and the labelling of endosomes have been proposed as useful tools to overcome the limitations offered by endocytosis, autophagy and endosomal escape processes.

This page left blank intentionally